

SEISMIC ASSESSMENT OF REINFORCED CONCRETE BEAM-TO-COLUMN  
CONNECTIONS UNDER REVERSED CYCLIC LOADING

A THESIS SUBMITTED TO  
THE GRADUATE SCHOOL OF NATURAL AND APPLIED SCIENCES  
OF  
MIDDLE EAST TECHNICAL UNIVERSITY

BY

UMUT AKIN

IN PARTIAL FULFILLMENT OF THE REQUIREMENTS  
FOR  
THE DEGREE OF MASTER OF SCIENCE  
IN  
CIVIL ENGINEERING

APRIL 2011

Approval of the thesis:

**SEISMIC ASSESSMENT OF REINFORCED CONCRETE BEAM-TO  
COLUMN CONNECTIONS UNDER REVERSED CYCLIC LOADING**

submitted by **UMUT AKIN** in partial fulfillment of the requirements for the degree  
of **Master of Science in Civil Engineering Department, Middle East Technical  
University** by,

Prof. Dr. Canan Özgen  
Dean, Graduate School of **Natural and Applied Sciences**

\_\_\_\_\_

Prof. Dr. Güney Özcebe  
Head of Department, **Civil Engineering**

\_\_\_\_\_

Assist. Prof. Dr. Burcu Burak  
Supervisor, **Civil Engineering Dept., METU**

\_\_\_\_\_

**Examining Committee Members:**

Assoc. Prof. Dr. Murat Altuğ Erberik  
Civil Engineering Dept., METU

\_\_\_\_\_

Assist. Prof. Dr. Burcu Burak  
Civil Engineering Dept., METU

\_\_\_\_\_

Assoc. Prof. Dr. Erdem Canbay  
Civil Engineering Dept., METU

\_\_\_\_\_

Assist. Prof. Dr. Afşin Sarıtaş  
Civil Engineering Dept., METU

\_\_\_\_\_

Assist. Prof. Dr. Halit Cenan Mertol  
Civil Engineering Dept., Atılım University

\_\_\_\_\_

**Date:**

\_\_\_\_\_

**I hereby declare that all information in this document has been obtained and presented in accordance with academic rules and ethical conduct. I also declare that, as required by these rules and conduct, I have fully cited and referenced all material and results that are not original to this work.**

Name, Last name: Umut AKIN

Signature:

## **ABSTRACT**

### **SEISMIC ASSESSMENT OF REINFORCED CONCRETE BEAM-TO-COLUMN CONNECTIONS UNDER REVERSED CYCLIC LOADING**

Akın, Umut

M.Sc., Department of Civil Engineering

Supervisor: Assist. Prof. Dr. Burcu Burak

April 2011, 153 Pages

Prior experimental research clearly reveals that the performance of reinforced concrete frame structures under earthquake loading is closely related to the behavior of beam-to-column connection regions. In order for a reinforced concrete building to have an adequate response under high lateral deformations, beam-to-column connections should be able to preserve their integrity. However, even today beam-to-column connections are assumed to be rigid or elastic, leading to an incorrect estimation of the structural response under earthquake loading. One of the basic reasons for the assumption of rigid joints is the lack of analytical models that adequately represent the seismic behavior of the connection region. In this thesis, an analytical model that realistically represents the beam-to-column connection response is developed, in the light of prior experimental data. The experimental subassemblies used in the generation of the analytical model are later modeled in OpenSees environment in order to verify the accuracy of the model. Throughout the research, utmost attention is paid for the model to be simple enough to be used practically and also to cover a wide range of beam to column connection properties.

**Keywords:** Reinforced Concrete Moment Resisting Frames, Earthquake Loading, Beam-to-Column Connections, Reversed Cyclic Loading, OpenSees, Analytical Model.

## ÖZ

### BETONARME KOLON-KİRİŞ BİRLEŞİM BÖLGELERİNİN TERSİNİR TEKRARLANIR YÜKLER ALTINDAKİ DAVRANIŞININ DEĞERLENDİRİLMESİ

Akın, Umut

Yüksek Lisans, İnşaat Mühendisliği Bölümü

Tez Yöneticisi: Yrd. Doç. Dr. Burcu Burak

Nisan 2011, 153 Sayfa

Bugüne kadar yapılmış olan deneysel çalışmalar açıkça göstermektedir ki, betonarme çerçeve sistemlerinin deprem yükü altındaki performansı, kolon-kiriş bağlantı bölgelerinin davranışı ile yakından ilgilidir. Betonarme bir yapının yüksek deformasyonlar altında sağlam kalabilmesi, ancak kolon-kiriş bağlantılarının bütünlüğünü muhafaza edebilmesi ile mümkündür. Ancak bugün dahi betonarme yapıların tasarımında kolon-kiriş bağlantı bölgelerinin rijit ya da elastik olarak davranacağı varsayılmakta, bunun sonucunda da yapıların deprem yükü altındaki davranışları doğru biçimde öngörülememektedir. Bu durumun ana sebeplerinden biri kolon-kiriş bağlantı bölgelerinin davranışını gerçekçi bir şekilde yansıtacak analitik modellerin eksikliğidir. Bu araştırma sonucunda, kolon-kiriş bağlantılarının tersinir tekrarlanır yükler altındaki davranışı daha önceden tamamlanmış deneysel çalışmalardan elde edilen veriler ışığında incelenerek, bu davranışı başarılı bir biçimde yansıtan analitik bir model oluşturulmuştur. Modelin oluşturulmasında kullanılan deneysel çalışmalar daha sonra OpenSees programı aracılığıyla modellenerek, önerilen davranış özelliklerinin deneysel verilerle uyumluluğu ortaya konmuştur. Analitik çalışma süresince oluşturulan modelin pratik kullanıma uygun basitlikte ve farklı bağlantı türlerini de temsil edebilecek şekilde kapsamlı olmasına çaba gösterilmiştir.

Anahtar Kelimeler: Betonarme Çerçeve Sistemler, Deprem Yükü, Kolon-Kiriş Birleşim Bölgeleri, Tersinir Tekrarlanır Yük, OpenSees, Analitik Model.

*To My Lovely Family*

## ACKNOWLEDGEMENTS

I wish to express my sincerely gratitude to my thesis supervisor, Assist. Prof Dr. Burcu Burak for her invaluable guidance, encouragement and assistance through the study. Without her precious contributions, this thesis would not have been completed. I also wish to thank Assist. Prof Dr. Afşin Sarıtaş for his kind interest in this work and suggestions.

I would like to thank my family for their deep understanding, irreplaceable support and most of all, the endless motivation during the hard work days. In each page of this report and each day of my eight years' education time in the Middle East Technical University owes to the lovely environment provided by them.

Finally, I wish to thank my dear friends, Çağdaş Mutlu, Temuçin Som, Gürkan Eraslan, Eda Selin Akyol and Büşra Gizem Vayvay; from the first day to the last, I always felt their sincere support behind me.

## TABLE OF CONTENTS

ABSTRACT.....	iv
ÖZ.....	v
ACKNOWLEDGEMENTS.....	vii
LIST OF TABLES.....	xiii
LIST OF FIGURES.....	xiv
LIST OF SYMBOLS.....	xvii
1 INTRODUCTION.....	1
1.1 BEAM-TO-COLUMN CONNECTIONS.....	1
1.2 RESEARCH OBJECTIVE AND SCOPE.....	3
2 LITERATURE REVIEW.....	5
2.1 BACKGROUND INFORMATION.....	5
2.2 CLASSIFICATION OF BEAM-TO-COLUMN CONNECTIONS.....	6
2.2.1 ACI 318-R08.....	7
2.2.2 ACI 352R-02.....	8
2.2.3 Eurocode 8.....	14
2.2.4 TEC 2007.....	16
2.2.5 AIJ Guideline (1999).....	18

2.3	PARAMETERS AFFECTING BEAM-TO-COLUMN CONNECTIONS	20
2.3.1	Joint Transverse Reinforcement.....	20
2.3.2	Slab Participation .....	23
2.3.3	Bond .....	27
2.3.4	Moment Strength Ratio .....	30
2.3.5	Presence of Transverse Beams .....	32
2.3.6	Column Axial Load .....	33
2.4	ECCENTRIC BEAM-TO-COLUMN CONNECTIONS.....	33
2.5	WIDE BEAM-TO-COLUMN CONNECTIONS.....	36
2.6	ANALYTICAL MODELING OF CONNECTIONS.....	38
3	DATABASE CONSTRUCTION .....	46
3.1	OVERVIEW.....	46
3.1.1	Range of Specimen Properties .....	47
3.2	SELECTED SPECIMENS .....	48
3.3	LABELING OF SPECIMENS .....	52
3.4	FINAL DATABASE .....	53
4	ANALYTICAL MODEL.....	57
4.1	GENERAL DESCRIPTION.....	57
4.2	JOINT SHEAR STRENGTH PREDICTION .....	58
4.2.1	Basic Joint Shear Strength Prediction ( $V_{j0}$ ).....	58

4.2.2	Adjustment Factors .....	59
4.2.3	Axial Load Factor.....	60
4.2.4	Slab Factor.....	61
4.2.5	Surrounding Beam Factor .....	62
4.2.6	Shear Reinforcement Ratio Factor .....	64
4.2.7	Shear Reinforcement $f_{yield}$ Factor.....	65
4.2.8	Wide Beam Factor.....	66
4.2.9	Bond Factor .....	67
4.2.10	Eccentricity Factor.....	69
4.2.11	Summary of Joint Shear Strength Prediction.....	69
4.2.12	Evaluation of Joint Shear Strength Prediction.....	73
4.2.13	Efficiency of Shear Strength Adjustment Factors .....	81
4.3	DETERMINATION OF CONNECTION PERFORMANCE POINTS .	82
4.3.1	Definition of Performance Points.....	82
4.3.2	Prediction of Performance Point $P_{inel}$ .....	84
4.3.3	Construction of Joint Shear Stress vs. Strain Curve.....	86
4.4	SUMMARY OF THE ANALYTICAL MODEL.....	88
5	VERIFICATION OF THE JOINT MODEL .....	92
5.1	OVERVIEW.....	92
5.2	DESCRIPTION OF ELEMENTS .....	93

5.2.1	Beam and Column Elements .....	93
5.2.2	Beam-to-Column Connection Element .....	96
5.2.3	Loading Procedure and Generated Models .....	101
5.3	DETERMINATION OF JOINT MOMENT ARM .....	103
5.4	COMPARISON OF ANALYTICAL AND EXPERIMENTAL RESULTS .....	107
5.4.1	Specimens of Burak and Wight.....	107
5.4.2	Specimens of Raffaele and Wight.....	113
5.4.3	Specimens of Kurose et al.....	117
5.4.4	Specimens of Chen and Chen.....	122
5.4.5	Evaluation of Pinching Response.....	126
5.4.6	Contribution of Joint Shear Strain to the Total Story Drift.....	128
5.4.7	Comparison of Response with and without the Connection Model.....	130
6	SUMMARY AND CONCLUSIONS .....	133
6.1	SUMMARY .....	133
6.2	CONCLUSIONS .....	134
6.3	RECOMMENDATIONS FOR FUTURE RESEARCH .....	136
	REFERENCES .....	137
	APPENDICES .....	145
	APPENDIX A: SELECTED EXPERIMENTS .....	145
A.1	TEST SETUP.....	145

A.2	IMPOSED DISPLACEMENT HISTORIES .....	147
	APPENDIX B: COMPARISON OF GRAPHS .....	149
B.1	LATERAL LOAD vs. STORY DRIFT (or DEFORMATION).....	149
B.2	JOINT SHEAR FORCE vs. JOINT DEFORMATION.....	152

## LIST OF TABLES

### TABLES

Table 2.1: Joint Shear Strength Factors (ACI352R-02).....	12
Table 3.1: Selected Specimens .....	54
Table 3.2: Key Properties of Specimens Included in the Database .....	56
Table 4.1: Joint Shear Strength Prediction .....	71
Table 4.2: Comparison of Joint Shear Strength Accuracy, $V_{j,proposed}$ VS. $V_{j,TEC}$ .....	75
Table 4.3: Comparison of Joint Shear Strength Accuracy, $V_{j,proposed}$ VS. $V_{j,ACI,352}$ .....	78
Table 4.4: Efficiency of Shear Strength Adjustment Factors .....	82
Table 4.5: Summary Table for Joint Shear Force Proportions .....	86
Table 4.6: Summary Table for Joint Shear Strain Proportions .....	86
Table 4.7: Summary Table for Joint Shear Force Prediction Accuracy .....	87
Table 4.8: Summary Table for Joint Shear Strain Prediction Accuracy .....	87
Table 4.9: Accuracy of Joint Shear Strain Values .....	88
Table 5.1: Comparison of Story Drift Contributions at 2% Story Drift .....	129

## LIST OF FIGURES

### FIGURES

Figure 2.1: Effective Joint Area ( $A_j$ ) in ACI 318R-08.....	8
Figure 2.2: Types of Connections (ACI 352R-02) .....	9
Figure 2.3: Forces Acting on Connection Regions.....	10
Figure 2.4: Joint Shear Force Computation for Type 1 and Type 2 Connections .....	13
Figure 2.5: Definitions about Beam-to-Column Connections (TEC 2007).....	17
Figure 2.6: Effective Joint Width and Depth Definitions (AIJ Guideline).....	19
Figure 2.7: Effective Flange Widths (Eurocode 8).....	25
Figure 2.8: Effective Flange Widths (TS-500) .....	27
Figure 2.9: Idealized Bond Stress (ACI 352R-02).....	28
Figure 2.10: Eccentric Beam to Column Connection (Raffaella and Wight, 1992) ..	34
Figure 2.11: Forces on Eccentric Connections (Raffaella and Wight, 1992) .....	34
Figure 2.12: Scissors Model Proposed by Alath and Kunnath (1995) .....	39
Figure 2.13: Model of Elmorsi et al. (1998) .....	40
Figure 2.14: Model of Fleury et al. (2000) .....	40
Figure 2.15: Model of Lowes and Altoontash (2003).....	41
Figure 2.16: Model of Shin and LaFave (2004) .....	42
Figure 2.17: Connection Model Proposed by Burak (2008).....	44
Figure 2.18: Perform-3D Panel Zone Element .....	45
Figure 3.1: Labeling of Connections in the Database.....	53
Figure 4.1: Definition of Performance Points.....	83
Figure 4.2:: Joint Shear Force vs. Strain Curve for Exterior Connections .....	90
Figure 4.3: Joint Shear Force vs. Strain Curve for Interior Connections .....	90
Figure 5.1: Comparison of Stiffness Model with Experimental Data (Update to ASCE/SEI 41 Concrete Provisions, 2007).....	95
Figure 5.2: Scissors Connection Model (Alath and Kunnath, 1995).....	97
Figure 5.3: Pinching4 Material Definition (Lowes and Altoontash, 2003) .....	99

Figure 5.4: OpenSees Model for Interior Beam-to-Column Connections .....	101
Figure 5.5: OpenSees Model for Exterior Beam-to-Column Connections.....	102
Figure 5.6: OpenSees Model for Connections Loaded on Beam.....	102
Figure 5.7: (a) Free Body Diagram of an Exterior Joint Subassembly and.....	103
Figure 5.8: (a) Forces Acting on the Joint Region and (b) Horizontal Force Equilibrium at the Mid-Height of the Joint.....	104
Figure 5.9: The Free Body Diagram of the Scissors Model .....	105
Figure 5.10: Burak and Wight, Specimen 1-S .....	108
Figure 5.11: Burak and Wight, Specimen 2-S .....	109
Figure 5.12: Burak and Wight, Specimen 3-S .....	110
Figure 5.13: Burak and Wight, Specimen 1-N .....	111
Figure 5.14: Burak and Wight, Specimen 2-N .....	112
Figure 5.15: Burak and Wight, Specimen 3-N .....	113
Figure 5.16: Raffaele and Wight, Specimen 1 .....	114
Figure 5.17: Raffaele and Wight, Specimen 2.....	115
Figure 5.18: Raffaele and Wight, Specimen 3.....	116
Figure 5.19: Raffaele and Wight, Specimen 4.....	116
Figure 5.20: Kurose et al., Specimen J1 .....	118
Figure 5.21: Kurose et al., Specimen J2, E-W Direction.....	119
Figure 5.22: Kurose et al., Specimen J2, N-S Direction.....	120
Figure 5.23: Kurose et al., Specimen J3, E-W Direction.....	121
Figure 5.24: Kurose et al., Specimen J3, N-S Direction.....	121
Figure 5.25: Connection Detail of Spread Ended Beams, Chen and Chen [11] .....	122
Figure 5.26: Chen and Chen, Specimen JC .....	123
Figure 5.27: Chen and Chen, Specimen JE.....	124
Figure 5.28: Chen and Chen, Specimen JS1 .....	125
Figure 5.29: Chen and Chen, Specimen JS4.....	126
Figure 5.30: Joint Response of Specimens JC and JE, Chen and Chen [11].....	127
Figure 5.31: Joint Response of Specimens 1 and 2, Raffaele and Wight [45] .....	127
Figure 5.32: Joint Response of Specimen J1, Kurose et al. [32] .....	128
Figure 5.33: Rigid Connection vs. Connection Model, Burak and Wight, Sp. 1-S.	130
Figure 5.34: Rigid Connection vs. Connection Model, Burak and Wight, Sp. 2-S	131

Figure 5.35: Rigid Connection vs. Connection Model, Burak and Wight, Sp. 3-S.	131
Figure A1.1: Test Setup of Burak and Wight .....	145
Figure A1.2: Test Setup of Raffaele and Wight .....	145
Figure A1.3: Test Setup of Kurose et al. ....	146
Figure A1.4: Test Setup of Chen and Chen .....	146
Figure A2.1: Displacement History of Burak and Wight .....	147
Figure A2.2: Displacement History of Raffaele and Wight .....	147
Figure A2.3: Displacement History of Chen and Chen .....	148
Figure A2.4: Displacement Histories of Kurose et al. ....	148
Figure B1.1: Specimens of Burak and Wight .....	149
Figure B1.2: Specimens of Raffaele and Wight .....	150
Figure B1.3: Specimens of Kurose et al. ....	151
Figure B1.4: Specimens of Chen and Chen .....	152
Figure B2.1: Specimens of Burak and Wight .....	153
Figure B2.2: Specimens of Raffaele and Wight .....	153

## LIST OF SYMBOLS

- $A_c$  : core cross sectional area of column
- $A_g$  : gross cross sectional area of column
- $A_j$  : effective joint area
- $A_{sh}$  : total cross sectional area of hoop reinforcement
- $b_b$  : beam web width
- $b_c$  : column width
- $b_c''$  : core dimension of a column, length of the transverse reinforcement measured from outside edge to outside edge.
- $b_e$  : effective slab width for T and L beams
- $b_j$  : effective joint width
- $b_{j,wide}$  : effective joint width for wide beam-to-column connections
- $d$  : effective depth of the beam, measured from the center of tensile reinforcement to the outermost concrete fiber under compression
- $d_b$  : nominal diameter of bar
- $e$  : total eccentricity
- $e_{eff}$  : effective eccentricity
- $E$  : modulus of elasticity
- $G$  : modulus of rigidity (shear modulus)
- $G_{eff}$  : effective modulus of rigidity
- $I$  : modulus of inertia
- $f_c$  : specified concrete compressive strength
- $f_{cd}$  : design compressive strength of concrete
- $f_{ctd}$  : design tensile strength of concrete

$f_y$  : specified yield strength of reinforcement  
 $f_{yd}$  : design yield strength of reinforcement  
 $f_{yh}$  : specified yield strength of transverse reinforcement  
 $h_b$  : beam height  
 $h_c$  : column depth  
 $l_p$  : plastic hinge length  
 $M_r$  : ratio of the total column flexural strength to total beam strength, framing into the connection  
 $N$  : axial load on column  
 $s_h$  : transverse reinforcement spacing in the connection  
 $v_j$  : joint shear stress  
 $V_j$  : joint shear strength  
 $\rho_s$  : volumetric transverse reinforcement ratio, calculated considering the reinforcement aligned in the loading direction  
 $\rho_{total,gross}$  : ratio of total transverse reinforcement volume in the loading direction to total connection volume  
 $\rho_{total,core}$  : ratio of total transverse reinforcement volume in the loading direction to connection core volume  
 $\rho_{one,gross}$  : ratio of one layer of transverse reinforcement volume in the loading direction to total connection volume contained in one spacing of transverse reinforcement  
 $\rho_{one,core}$  : ratio of one layer of transverse reinforcement volume in the loading direction to core connection volume contained in one spacing of transverse reinforcement

# CHAPTER 1

## INTRODUCTION

### 1.1 BEAM-TO-COLUMN CONNECTIONS

Beam-to-column connections have vital importance on the performance of reinforced concrete moment resisting frame (RCMRF) structures, especially when subjected to earthquake loads. For a structure to perform satisfactorily under high seismic action, beam-to-column connections should preserve their integrity in order to be capable of transferring vertical and horizontal shear loads between beams and columns even for the most undesirable loading conditions.

In contrary to the general tendency to assume beam-to-column connections as rigid zones, inelastic response of connections is proven to significantly affect the overall structural behavior, especially for buildings which are subjected to high reversed cyclic loads. Even today, despite the increasing number of worldwide research projects on connection behavior, not enough attention is paid on the design of beam-to-column connections. However, when the joint shear deformations are not taken into consideration, overall structural deformations are underestimated and global structural performance cannot be realistically obtained. Both experimental studies and field observations after earthquakes clearly reveal that connections have an important role in lateral load resistance for reinforced concrete structures and if not properly designed, consequences may be irreversible, both in terms of life loss and property damage.

Until today, only simple guidelines are considered for beam-to-column connections in practical design applications. Main design principle of beam-to-column connections is the '*strong column-weak beam*' principle, without a detailed

understanding of interior mechanisms of connections. Philosophy behind the strong column-weak beam principle is the concentration of damage on the plastic hinge regions of beams and ensuring the columns do not fail even under high lateral loads. In other words, yielding of column reinforcement before beam bars is avoided and a bottom column plastic hinge mechanism which leads to the collapse of a structure is prevented. But it should not be forgotten that, in order to effectively apply the strong column-weak beam philosophy, beam-to-column connections should ensure satisfactory performance under high flexural and shear loads.

As stated previously, despite the importance that beam-to-column connections possess for structures, the behavior and performance of connections are probably the most important neglected characteristics in the design of RCMRF structures. Main reasons for that can be listed as the limited number of experimental and analytical research and a large variety of connection types, both in terms of material and geometric properties. Although the number of research projects on this topic increases from day to day, a common understanding on the connection behavior under earthquake loading could not be reached. The multitude of variables effective in the performance of connections also increases the complexity of the subject and makes it difficult to determine widely applicable and yet simple provisions. Although most of the contemporary structural codes impose some practical rules on design of beam-to-column connections, the equations in between codes differ significantly. Moreover, a large number of subjects ranging from wide beam-to-column connections to eccentric connections are specified as areas needing further research.

Analytical studies aim to represent several inelastic mechanisms responsible for the behavior of beam-to-column connections under cyclic loading. From modeling point of view, above mentioned difficulties in determination of connection response also complicate the simulation of inelastic behavior of connections analytically. Although several models have been generated, due to the complexity of parameters possibly effecting the joint shear response and wide range of parameters, a practically applicable analytical model that is capable of adequately representing the beam-to-column connection behavior has not been developed so far.

## 1.2 RESEARCH OBJECTIVE AND SCOPE

In this research project, first an extensive literature review of prior analytical and experimental research has been carried out. Then, an experimental database that contains information on a wide variety of connection properties is constructed and an analytical model defining the beam-to-column connection behavior under cyclic loading is developed. Finally, the analytical model is verified by the means of computer software, OpenSees.

Prior to the construction of the database to be used as the primary resource in modeling, an in depth research of the literature is conducted by examining analytical and experimental studies on beam-to-column connection behavior. Reports on analytical studies are utilized in order to create an in depth understanding on the general behavior of beam-to-column connections as well as constituting a basic reference on analytical models proposed up to this time. Besides giving important information on the effects of several geometric and material properties, experimental research projects have been taken as the main resource in the construction of the database by providing detailed information on specimens, loading conditions and responses. On the other hand, main problem encountered during the database construction is the inadequacy or deficiency of the data provided in experimental research reports. Detailed descriptions of literature review and database construction are presented in Chapters 2 and 3, respectively.

An analytical model addressing the performance of beam-to-column connections is developed considering two basic arguments: applicability for a wide range of specimens having different characteristics and simplicity in order for the model to be handy for practicing engineers. Throughout the research, a large variety of beam-to-column connections having different geometric and material properties have been evaluated in the light of prior research, seeking for the optimum analytical model to define the joint shear strength vs. strain response. From the large number of parameters possibly effective in the performance of connections, the key parameters with higher influence are revealed and presented in the final model. Description of

the variables utilized in defining the shear response of connections along with the final model is presented in Chapter 4.

Verification of the proposed shear force vs. shear strain model is explained in Chapter 5 of the thesis. The computer models of the experimental subassemblies are created and analyzed using '*OpenSees*' software framework, which is the abbreviation of the '*Open System for Earthquake Engineering Simulation*'. The developed analytical joint model is assigned to the connection region of the generated computer models, which are loaded using the time history presented in the respective experimental study. Obtained analytical results are compared with experimental data for verification purposes, a detailed description of which is also presented in Chapter 5.

The thesis is finalized with Chapter 6, in which a general summary of the investigation and recommendations for future research along with the conclusions inferred throughout the study are presented.

## **CHAPTER 2**

### **LITERATURE REVIEW**

#### **2.1 BACKGROUND INFORMATION**

Importance of the beam-to-column connections of earthquake resistant reinforced concrete structures started to arouse interest in 1960s. Hanson and Conner [1] are referred as the first researchers to experimentally analyze connection performance under seismic loading by many. Both experimental and analytical investigations on the seismic response of beam-to-column connections have been in progress since then, especially in seismically vulnerable countries such as the United States, Japan and New Zealand.

Briefly mentioning, experimental research is focused on the response of beam-to-column connections under different types of loadings. Variations in the geometric properties of connections, wide range of material properties and uncertainty in the response mechanisms for different combinations of connection characteristics provide an endless area of research for experimental investigations. On the other hand analytical research aims to mathematically represent the connection behavior. Creation of an easy to implement beam-to-column connection model, yet considering the diversity of connection characteristics and obtaining accurate results is the main objective of analytical studies.

Despite the increasing number of experimental and analytical studies carried on recently, many beam-to-column connection properties still remains the subject open for improvement from several aspects. In addition to the aforementioned diversities in the connection characteristics, connections involving eccentricity or wide beams

expand the research area and make it harder for researchers to come up with a global consensus.

Following parts of the literature review covers several subtopics. Primarily, definition and classification of beam-to-column connections are described with respect to effective joint width and joint strength definitions of contemporary structural codes and recommendations of several researchers. Sequential subtopics mention important parameters affecting joint behavior and are explained in the light of findings from prior experimental and analytical research. Next two topics are on special types of beam-to-column connections namely eccentric connections and wide beam-to-column connections.

Literature review is finalized with a brief statement of prior studies on analytical modeling of beam-to-column connections.

## **2.2 CLASSIFICATION OF BEAM-TO-COLUMN CONNECTIONS**

In this section of the report, classification of beam-to-column connections is addressed with respect to different characteristics, evaluated in accordance with the point of view of related researcher or institute. As presented in the following parts of this section, most contemporary provisions on structural engineering classify the connections with respect to the number of beams surrounding the connection, considering the ratio of the beam width to width of the column, which beams frame into.

Additionally, connections involving wide beams or eccentric beams in the direction of loading are also classified separately. Especially, the definitions of effective joint area and joint shear strength differ considerably.

In the following paragraphs, the beam-to-column connection definitions are presented with respective joint area and shear strength definitions in the contemporary structural codes.

### 2.2.1 ACI 318-R08

ACI 318R-08 [2], *Building Code Requirements for Structural Concrete and Commentary* is a comprehensive document covering the general requirements for design and construction of reinforced concrete structures involving additional commentary sections to further explain the provisions.

Though ACI 318R-08 constitutes a well detailed reference for construction of reinforced concrete structures, specifications on beam-to-column connections are described only briefly in '*Section 21, Earthquake Resistant Structures*'. In this section, along with the general requirements about earthquake resistant design, provisions for joint transverse reinforcement, design shear strength of joints and calculation of effective cross sectional area are described.

Confinement provided by the surrounding members is assumed as the main parameter in determination of the joint shear strength, on the condition that minimum joint shear transverse reinforcement is provided. In order to for the beam to provide sufficient confinement to the connection it frames into, at least 3/4 of the column width should be covered by the beam width. Accordingly, a beam-to-column connection is assumed to be fully confined if this condition is satisfied for all 4 faces of the column. Also, an effective joint area ( $A_j$ ) with respect to beam and column dimensions is defined and the joint shear strength to be taken into account in design is obtained considering effective joint area, square root of concrete compressive strength and a '*joint shear strength factor*' determined with respect to the confinement provided by the surrounding members.

Effective joint area ( $A_j$ ) has a width equal to effective joint width as defined below and a height equal to column height, with respect to ACI 318-R08 (**Figure 2.1**).

$$\text{Effective joint width, } b_{j,318} = \min\{b+h, b+2x\} \quad (2.1)$$

where,  $x$  = the minimum distance between the column edge and beam edges for eccentric connections.

$b$  = beam width,

$h$  = column depth,

In consideration of prior descriptions, joint shear strength is defined as,

For joints confined on all four faces:  $2.00\sqrt{f'_c}A_j$

For joints confined on three faces or on two opposite faces:  $1.67\sqrt{f'_c}A_j$

(2.2)

For other cases:  $1.00\sqrt{f'_c}A_j$

**Figure 2.1** covers the general definitions stated in ACI 318R-08.

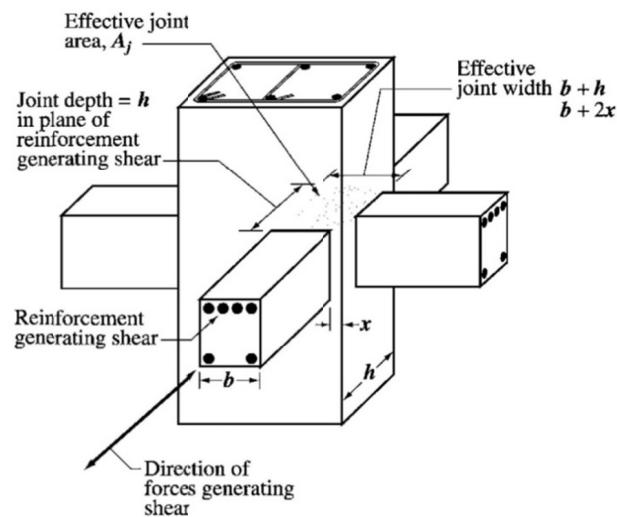


**Figure 2.1: Effective Joint Area ( $A_j$ ) in ACI 318R-08**

ACI318-08 provisions are applicable for structures with concrete compressive strengths higher than 17 MPa (2500 psi) with no definition of an upper limit.

### 2.2.2 ACI 352R-02

ACI 352R-02 [3], *Recommendations for Design of Beam-Column Connections in Monolithic Reinforced Concrete Structures* is a report developed by ACI-ASCE Committee 352 in 2002 as a document superseding ACI 352R-91. The report is

based on laboratory testing and field studies and constitutes a detailed summary of the current information. Scope of the recommendations is defined as '*proportions, design and details of monolithic beam-column connections in cast in place concrete frame construction*'. Main parameters considered are member proportions, confinement of the column core in the joint region, joint shear stress, ratio of column-to-beam flexural strength at the connection, development of reinforcing bars and details of columns and beams framing into the joint.

ACI 352R-02 recommendations define the beam-to-column connections as '*the portion of the column within the depth of the deepest beam that frames into the column*' and with six categories depending on the number of beams surrounding the connection (**Figure 2.2**). Although formulization of joint shear strength is very similar to ACI 318R-08 provisions, '*joint shear strength factor*' and joint shear area definitions constitute a remarkable difference between ACI 318R-08 and ACI 352R-02.

It should be noted that the recommendations do not apply to connections with beam widths exceeding the smaller of  $3b_c$  and  $(b_c+1.5h_c)$  and to structures built using concrete with compressive strength higher than 100 MPa (15000 psi).

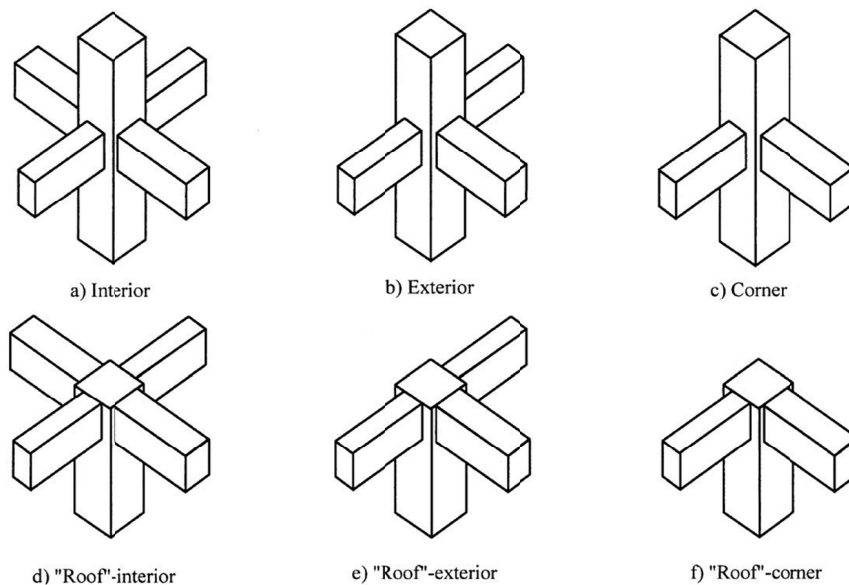


**Figure 2.2: Types of Connections (ACI 352R-02)**

Major classification of beam-to-column connections is performed based on the expected inelastic deformations in relation to the design load conditions of the connected frame members. *Type 1 connections* are designed on the basis of strength without considering significant inelastic deformation and expected to satisfy ACI 318R-08, excluding chapter 21, which includes seismic design provisions. *Type 2 connections* are designed to be effective under seismic loadings and be capable of dissipating energy through reversed deformations in the inelastic range.

The forces acting on the connection region that result from combination of several effects such as externally applied loads, creep, shrinkage, temperature, settlement and secondary effects are also identified in ACI 352-R02. In the document, forces are shown on two separate free body diagrams for gravity (*Type 1 connections*) and lateral (*Type 2 connections*) loading, which is illustrated on **Figure 2.3**.

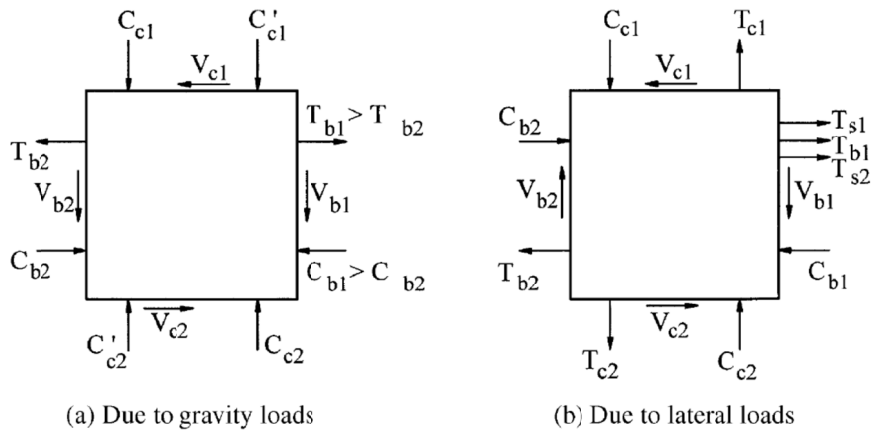


**Figure 2.3: Forces Acting on Connection Regions**

where, T = tension force,

C = compression force,

V = shear force,

b = subscript for beam,

c = subscript for column

s = subscript for slab.

As mentioned priory, the nominal shear strength of the joint ( $V_n$ ) is specified as a limiting value defining the capacity of the beam-to-column connection and determined in a similar manner with ACI 318R-08 provisions, excluding the different descriptions for effective joint area and confinement factors. Effective joint width in ACI352R-02 is defined basically according to beam and column dimensions in addition to a coefficient symbolized with ‘m’ which represents the strength reduction effect of eccentric connections as given below:

$$\text{Effective joint width, } b_{j,352} = \min \left\{ \frac{b_b + b_c}{2}, b_b + \sum m \frac{h_c}{2}, h_c \right\} \quad (2.3)$$

where,  $b_b$  = width of the beam in the loading direction,

$b_c$  = width of the column,

$h_c$  = height of the column,

$m = 0.3$  for connections with loading beam eccentricity exceeding  $b_c/8$ ,  $0.5$  for all other cases.

Effective joint area ( $A_j$ ) is specified as  $b_j h_c$  and nominal shear strength of the joint is determined as,

$$V_n = \gamma \sqrt{f'_c} A_j \quad (\text{psi}) \quad (2.4a)$$

$$V_n = 0.083 \gamma \sqrt{f'_c} A_j \quad (\text{MPa}) \quad (2.4b)$$

$\gamma$  is the *joint shear strength factor* and specified separately for Type 1 and Type 2 connections as illustrated in **Table 2.1**.

**Table 2.1: Joint Shear Strength Factors (ACI352R-02)**

Classification	Connection type	
	1	2
<b>A. Joints with a continuous column</b>		
A.1 Joints effectively confined on all four vertical faces	24	20
A.2 Joints effectively confined on three vertical faces or on two opposite vertical faces	20	15
A.3 Other cases	15	12
<b>B. Joints with a discontinuous column</b>		
B.1 Joints effectively confined on all four vertical faces	20	15
B.2 Joints effectively confined on three vertical faces or on two opposite vertical faces	15	12
B.3 Other cases	12	8

As the nominal joint shear strength ( $V_n$ ) stands for the maximum joint shear allowable for the connection, another parameter, the '*horizontal joint shear*' ( $V_u$ ) is defined in ACI 352R-02 different from ACI 318R-08.  $V_u$  is the '*design shear force*' and determined on a horizontal plane at the mid height of the joint. Calculation of  $V_u$  is addressed separately for Type1 and Type 2 connections and summarized on the sketches below (**Figure 2.4**).

In order to be evaluated as properly designed, horizontal joint shear ( $V_u$ ) of a beam-to-column connection should be less than 85% of nominal joint shear ( $V_n$ ) for both Type 1 and Type 2 connections.

$$0.85 V_n \geq V_u \quad (2.5)$$

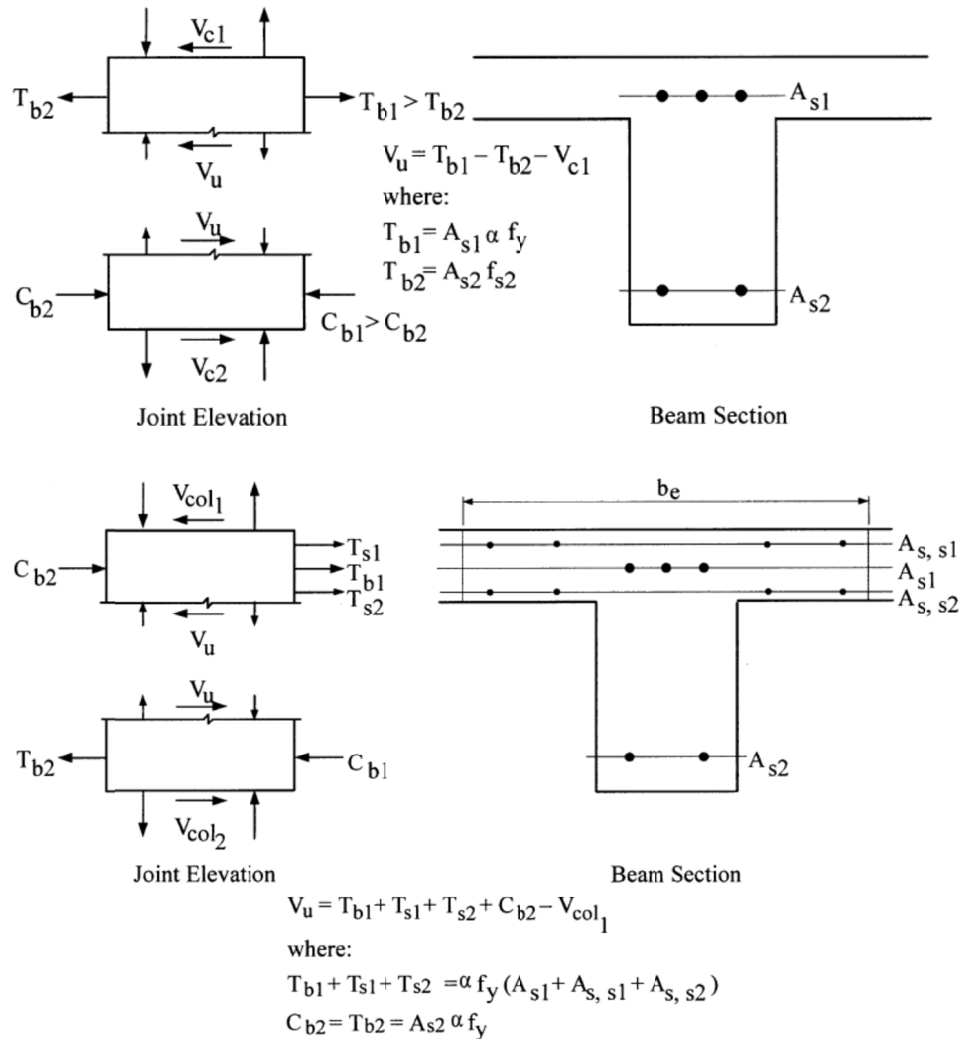


**Figure 2.4: Joint Shear Force Computation for Type 1 and Type 2 Connections**

where,

$A_{si}$  = area of beam longitudinal reinforcement layer  $i$ ,

$A_{ssi}$  = area of slab longitudinal reinforcement layer  $i$ ,

$T_{bi}$  = beam tension force created by  $A_{si}$ ,

$C_{bi}$  = beam compression force  $i$ ,

$\alpha$  = 1.25, the stress multiplier to account for the deviation of actual yield strength value from the nominal one and the strain hardening of reinforcement.

$V_{col1}$  = top column shear force,

$V_{col2}$  = bottom column shear force,

$b_e$  = effective slab width,

### 2.2.3 Eurocode 8

The Eurocode 8 [4], '*Design of Structures for Earthquake Resistance, Part 1: General rules, seismic actions and rules for buildings*' specifications are discussed in this section. The mentioned document is a member of set of building codes composed of 10 main documents involving 57 parts, each on specific subjects, prepared by European Committee for Standardization (CEN). The composition of the document involves a very large variety of design specifications applicable to reinforced concrete, steel, timber and masonry buildings along with comprehensive descriptions of performance requirements, ground conditions and seismic actions.

Design provisions for reinforced concrete structures under seismic action are classified in two classes according to the expected hysteretic energy dissipation capacities as DCM for medium ductility and DCH for high ductility demands. The structures designed following the code are aimed to *develop stable mechanisms associated with large dissipation of hysteretic energy under repeated reversed loading, without suffering brittle failures.*

#### Design of beam-to-column connections for DCM

For buildings designed according to achieve medium ductility, only simple provisions are stated in Eurocode 8, regarding transverse shear reinforcement in the connection region which will be stated in the transverse reinforcement section of this report. There are no provisions addressed for shear strength capacity of beam-to-column connections of buildings designed for DCM.

Design of beam-to-column connections for DCH

For structures expected to behave in a highly ductile manner under seismic loading, a more detailed approach is implemented in Eurocode 8.

Horizontal shear force acting on the beam-to-column connection core is defined similar to ACI 352R-02 recommendations and formulized as below, separately defined for interior and exterior beam-to-column connections.

$$\text{For interior joints,} \quad V_{jhd} = \gamma_{Rd} (A_{s1} + A_{s2}) f_{yd} - V_c \quad (2.6a)$$

$$\text{For exterior joints,} \quad V_{jhd} = \gamma_{Rd} A_{s1} f_{yd} - V_c \quad (2.6b)$$

where,  $A_{s1}$  = the area of the beam top reinforcement,

$A_{s2}$  = the area of the beam bottom reinforcement,

$V_c$  = the column shear force, from the analysis in the seismic design,

$\gamma_{Rd}$  = overstrength factor due to strain-hardening of reinforcement and the difference in the actual yield strength and the nominal value, which is specified to be a minimum of 1.2.

As it can be observed from the formulae, the design shear force on the joint is depends on the concrete compressive strength, axial force on the joint and effective shear area of the joint.

For interior beam-to-column connections, shear force is limited using the following equation, whereas for exterior joints, 80 % of the same expression is specified to be taken as maximum.

$$V_{jhd} \leq \eta f_{cd} \sqrt{\frac{1-v_d}{\eta}} (b_j h_c) \quad (2.7)$$

where,  $\eta = 0.6 \times (1 - f_{ck}/250)$ ,

$v_d$  = axial force on the column above the joint, normalized by column cross sectional area.

Effective joint width definition of connections in Eurocode 8 is more simple when compared to ACI 318R-08 and ACI 352R-02 definitions. Joint width effective for shear response is defined separately for wide beam-to-column connections and conventional beam-to-column connections:

$$\text{If } b_c > b_w, \quad b_j = \min \{b_c; (b_w + 0.5 h_c)\}, \quad (2.8a)$$

$$\text{If } b_c < b_w, \quad b_j = \min \{b_w; (b_c + 0.5 h_c)\}. \quad (2.8b)$$

#### 2.2.4 TEC 2007

TEC 2007 [5], ‘*Turkish Earthquake Code, Specifications for Structures to be Built in Disaster Areas*’ is a document published by the Ministry of Public Works and Settlement, in Turkey, addressing the general procedures and specifications to be considered for the design of structures built in areas under seismic risk.

Beam-to-column connections are classified depending on the beams surrounding the connection and proportion of the beam width covering the column face, similar to ACI 318R-08 provisions and ACI 325R-02 recommendations. A connection is accepted as ‘*confined*’ only when it is surrounded by beams on each face and none of the beams has a width narrower than 3/4 of the column width. For all other cases, the connection is defined as ‘*unconfined*’.

Also, horizontal joint shear (design joint shear,  $V_e$ ) and joint shear strength ( $V_n$ ) are identified in a similar manner to ACI 352R-02. Joint shear strength is designated as a limiting value for design joint shear  $V_e$ . A general summary of definitions related to beam-to-column connections in TEC 2007 is given in **Figure 2.5**.

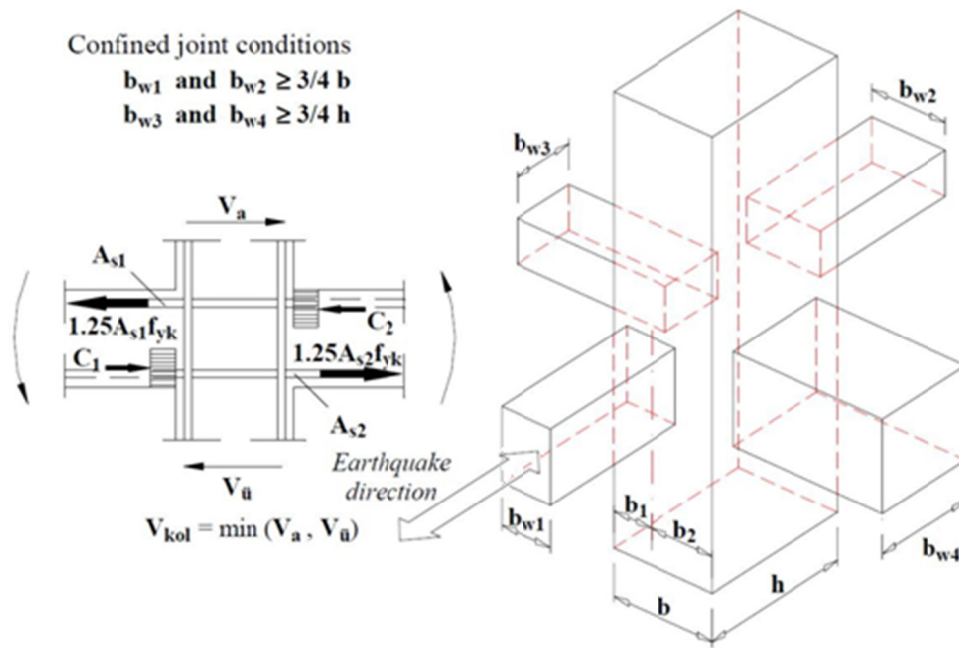


**Figure 2.5: Definitions about Beam-to-Column Connections (TEC 2007)**

$V_e$  is calculated in a similar manner to horizontal joint shear defined in ACI 352R-02, considering beam geometry and longitudinal reinforcement along with column shear force but without taking into account slab reinforcement.

$$V_e = 1.25 f_{yk} (A_{s1} + A_{s2}) - V_{kol} \quad (2.9)$$

where,  $f_{yk}$  = Characteristic yield strength of beam reinforcement,

$A_{si}$  = Area of beam longitudinal reinforcement layer  $i$ ,

$V_{kol}$  = Governing column shear force,

$V_a$  = Lower column shear force,

$V_u$  = Upper column shear force.

Design joint shear force ( $V_e$ ) is limited for confined and unconfined joints as given below:

For confined joints:  $V_e \leq 0.60 b_j h f_{cd} \quad (2.10a)$

For unconfined joints:  $V_e \leq 0.45 b_j h f_{cd}$  **(2.10b)**

Definition of the effective joint shear area is based on determination of the effective joint width ( $b_j$ ) since the height of joint shear area is assumed to be the column height. For wide beam-to-column connections,  $b_j$  is specified as column width whereas for other cases, following conditions are to be considered,

Effective joint width,  $b_{j,TEC} = \min\{2 \min(b_1, b_2), b_{w1} + h\}$  **(2.11)**

where,  $b_{1,2}$  = distances between beam axis and column edges,

$b_{w1}$  = width of the beam in the direction of loading.

### 2.2.5 AIJ Guideline (1999)

AIJ (Architecture Institute of Japan) Guideline [6] defines the shear strength of a beam-to-column connection ( $V_j$ ) based on effective joint area ( $A_j$ ), concrete compressive strength  $f'_c$  and shape factors, as stated in **Equation 2.12**.

$V_j = k \Phi 0.8 f'_c{}^{0.7} A_j$  (in MPa) **(2.12)**

where,  $k =$  1.00 for interior connections,

0.70 for exterior connections,

0.45 for knee connections,

$\Phi =$  1.00 for connections with two transverse beams,

0.85 for all other cases.

Effective joint area definition of AIJ guideline differs from priory mentioned provisions, because it includes both an effective depth definition in addition to the effective joint width.

Effective joint width of a connection is computed as follows,

$$b_{j,AIJ} = b_b + b_{a1} + b_{a2} \quad (2.13a)$$

$$b_{ai} = \min \left\{ \frac{x_i}{2}, \frac{h_c}{4} \right\} \quad (2.13b)$$

where,  $x$  is defined as the distance of beam edge to the column face for each side.

Effective joint depths of connections are determined based on the length at which the longitudinal beam bars are effective in transferring shear force. For interior joints, effective joint depth is the entire depth of the column whereas for exterior joints, joint depth ends at the point where the beam bars are hooked.

Effective width and depth definitions of AIJ guideline are given in **Figure 2.6**.

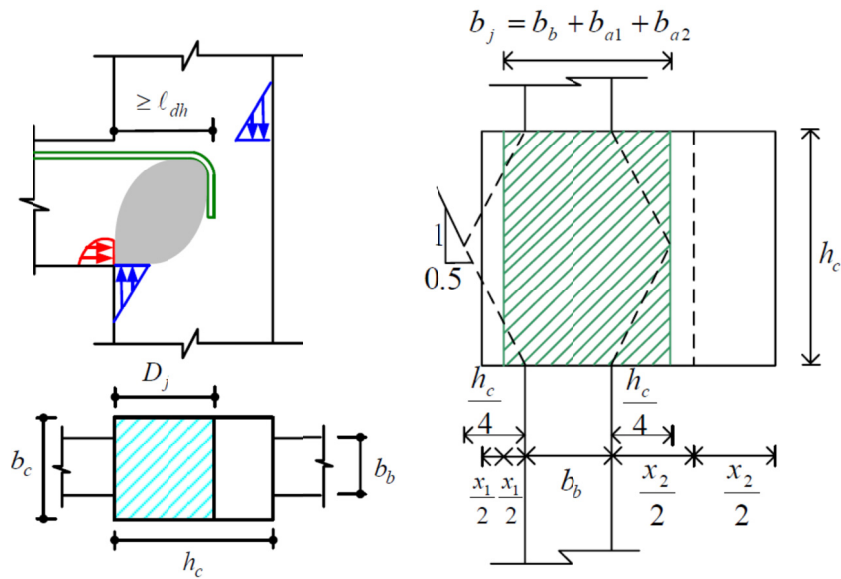


**Figure 2.6: Effective Joint Width and Depth Definitions (AIJ Guideline)**

## **2.3 PARAMETERS AFFECTING BEAM-TO-COLUMN CONNECTIONS**

Performance of beam-to-column connections under cyclic loading depends on several parameters. As mentioned priorly, geometric and material properties of the connections as well as loading conditions influence the response of beam-to-column connections considerably. In the following paragraphs of the report, effect of important parameters is explained by means of prior experimental and analytical investigations. Structural code provisions on the parameter discussed are also mentioned.

### **2.3.1 Joint Transverse Reinforcement**

Transverse shear reinforcement in the connection region is proven to be effective in the earthquake response of reinforced concrete structures from several aspects. Confinement of the joint core by transverse reinforcement helps the joint to transfer both axial and shear forces between beams and columns.

In a parametric research carried out by Bonacci and Pantazoupoulou [7] for the investigation of the effect of several design parameters on the behavior of beam-to-column connections, horizontal reinforcement in the joint region is determined to be effective in confining the concrete, increasing the compressive resistance and thereby preserving the integrity of the connection. It is also concluded that participation of joint hoops in the shear resisting mechanism of the joint is significant, particularly in the case where low amounts of confinement have been provided.

Alameddine and Ehsani [8] indicates the influence of transverse reinforcement on resisting the excess shear force in a joint after the concrete cracks, minimization of crack width prior to the yielding of transverse reinforcement and delaying joint deterioration by providing confinement of the concrete. In an experimental research conducted on 12 specimens with joint shear reinforcement ratios varying between 1.14% and 1.87%, it was concluded that transverse reinforcement leads to an increase in the energy dissipation capacity and delays the pullout of main beam bars and slippage of longitudinal column bars in the joint.

Ehsani & Wight [9] underlines the efficiency of joint transverse reinforcement in enhancing the overall behavior of specimens without transverse beams and slabs. It is noted that slippage of beam bars in the joint region is delayed, as well.

Confinement provided by transverse shear reinforcement in the beam-to-column connections is regarded as one of the most important subjects in contemporary structural codes. In the following paragraphs, provisions offered by ACI 352R-02, ACI 318R-08 and Eurocode 8 are discussed briefly.

ACI 352R-02 emphasizes the importance of lateral confinement of concrete in transmission of column axial load and shear forces from beams and columns to joint. Minimum transverse reinforcement ratio is defined separately for Type 1 and Type 2 connections and indicated as below.

If spiral reinforcement is used,

$$\text{for Type 1 connections, } \rho_s = (0.45 \frac{A_g}{A_c} - 1) \frac{f'_c}{f_{yh}} \quad (2.14)$$

$$\text{for Type 2 connections, } \rho_s = \min \left\{ (0.45 \frac{A_g}{A_c} - 1) \frac{f'_c}{f_{yh}} ; 0.12 \frac{f'_c}{f_{yh}} \right\} \quad (2.15a)$$

If rectangular hoop and crossties are used,

$$A_{sh} = \min \left\{ (0.3 \frac{s_h b_c f'_c}{f_{yh}} (\frac{A_g}{A_c} - 1)) ; 0.09 \frac{s_h b_c f'_c}{f_{yh}} \right\} \quad (2.15b)$$

In Eurocode 8, provisions regarding transverse shear reinforcement differ for DCM (ductility class medium) and DCH (ductility class high) structures.

For structures with DCM, transverse shear reinforcement applied in the critical regions of columns is obligated to continue also in the connection region, with the exception of beam-to-column connections surrounded by beams on all 4 sides. For

fully surrounded connections, spacing of the transverse shear reinforcement can be double of applied in the critical column region, without exceeding 150 mm.

For highly ductile structures, Eurocode 8 requires the use of horizontal hoops of 6 mm diameter bars in minimum, in order to provide adequate confinement in the joint region. The total area of the horizontal hoops should satisfy the condition specified below.

$$\frac{A_{sh} \cdot f_{ywd}}{b_j h_{jw}} \geq \frac{\left(\frac{v_{jhd}}{b_j h_{jc}}\right)^2}{f_{ctd} + v_d f_{cd}} - f_{ctd} \quad (2.16)$$

where,  $A_{sh}$  is the total area of the horizontal hoops,

$h_{jw}$  is distance between the outermost compression fiber of the beam and the reinforcement at the tension zone,

$h_{jc}$  is the distance between extreme layers of column reinforcement,

$f_{ywd}$  is the yield strength of transverse reinforcement,

$v_d$  is the normalized design axial force of the top column,  $N / (A_c f_{cd})$ .

An additional condition on horizontal joint hoop reinforcement is specified in Eurocode 8 in order to ensure integrity of joint after cracking. The condition is stated separately for interior and exterior connections and can be seen below.

$$\text{For interior joints,} \quad A_{sh} f_{ywd} \geq \gamma_{Rd} (A_{s1} + A_{s2}) f_{yd} (1 - 0.8 v_d) \quad (2.17)$$

$$\text{For exterior joints,} \quad A_{sh} f_{ywd} \geq \gamma_{Rd} A_{s2} f_{yd} (1 - 0.8 v_d)$$

The horizontal reinforcement provided in the joint region is required to be evenly spaced and placed between the top and bottom beam bars. It is also underlined that the longitudinal beam bars should be bent towards the joint in exterior beam-to-column connections in Eurocode 8.

### 2.3.2 Slab Participation

Experimental studies of beam-to-column connections including slabs reveal that, when properly designed, presence of slab increases the shear capacity of a connection. However, especially when the flexural strength ratio of a connection is considered, neglecting the effect of slabs may result in underestimation of flexural strength of beams and consequently having stronger beams than columns, which may lead to brittle failure of the structure. In that manner, determination of the slab effect have crucial importance in order to create a more realistic understanding of the connection and overall structure behavior when subjected to lateral loading.

Durrani and Zerbe [10] point out the effect of slab on the strength, stiffness and shear capacity of connections. It is noted that the lateral load resistance of a connection is increased by as much as 40% by the influence of slab participation. After underlining the likelihood of underestimation of lateral load resistance of connections ignoring slab contribution to the stiffness and strength of the beams, French and Boroojerdi [11] also state that all the experimentally tested models exhibited a ductile behavior with interstory drifts exceeding 8%. An increase between 22% and 49% has been observed on the flexural strengths of the models at 2% story drifts. Additionally, Cheung, Paulay and Park [12] also observed an increase in the negative moment flexural capacity and lateral loading capacity of the beam-column-slab systems tested.

In an experimental research on 4 exterior wide beam-to-column connections, LaFave and Wight [13] observed an increase in the connection shear strength resulting from the presence of slab. It was concluded that since the floor slab enhances the torsional capacity of the beams, the shear strength of the joint increased.

Burak and Wight [14] underlined the confinement effect provided by the slab in their experimental study on 3 eccentric beam-to-column connections. It was determined that the effect of eccentricity is minimized and the deterioration of shear strength and stiffness is delayed by including floor slabs and spandrel beams to the test setup. As a result, the specimens also preserved their energy dissipation capacities and the damage is significantly reduced.

Contribution of slab on the performance of a beam-to-column connection is directly related to the slab width effective under the loading as a part of the beam. It is hard to determine the effective slab width to be considered influential for different types of connections and loadings. Different regulations offered by ACI 318R-08 and Eurocode 8 are explained next.

Participation of slab is mentioned in Section 8.10, '*T-beam construction*' in ACI 318R-08. Maximum effective slab width is defined separately for beams having slab on both sides and on one side only, as defined below:

For beams having slab on both sides the equation that gives the minimum value of 'b' governs,

$$b \leq \frac{\text{span}}{4}$$

$$\frac{b - b_w}{2} \leq 8t_f \tag{2.18}$$

$$\frac{b - b_w}{2} \leq \frac{1}{2} * (\text{clear distance between beams})$$

Similarly, for beams having slab on one side only (edge beams), effective slab width is the minimum value of 'b' calculated from the equations below.

$$(b - b_w) \leq \frac{\text{span}}{12}$$

$$(b - b_w) \leq 6 t_f \tag{2.19}$$

$$(b - b_w) \leq \frac{1}{2} * (\text{clear distance between beams})$$

In Eurocode 8, effective flange widths of beams are considered to be effective in bending and shear resistance. Top reinforcement of the beam is required to be placed mainly in the web width and only a small portion of the top beam reinforcement is

allowed to be placed in the slab width. However, any ratio considering beam reinforcement to be placed in or outside the web width is not specified.

Effective flange widths for beams under seismic actions are specified as:

For exterior joints,

$b_w$  for connections without transverse beams,

$b_w + 2h_f$  (on each side) for connections with transverse beams.

(2.20)

For interior joints,

$b_w + 2h_f$  (on each side) connections without transverse beams,

$b_w + 4h_f$  (on each side) connections with transverse beams.

(2.21)

The effective slab width definition of Eurocode 8 is illustrated in **Figure 2.22**.

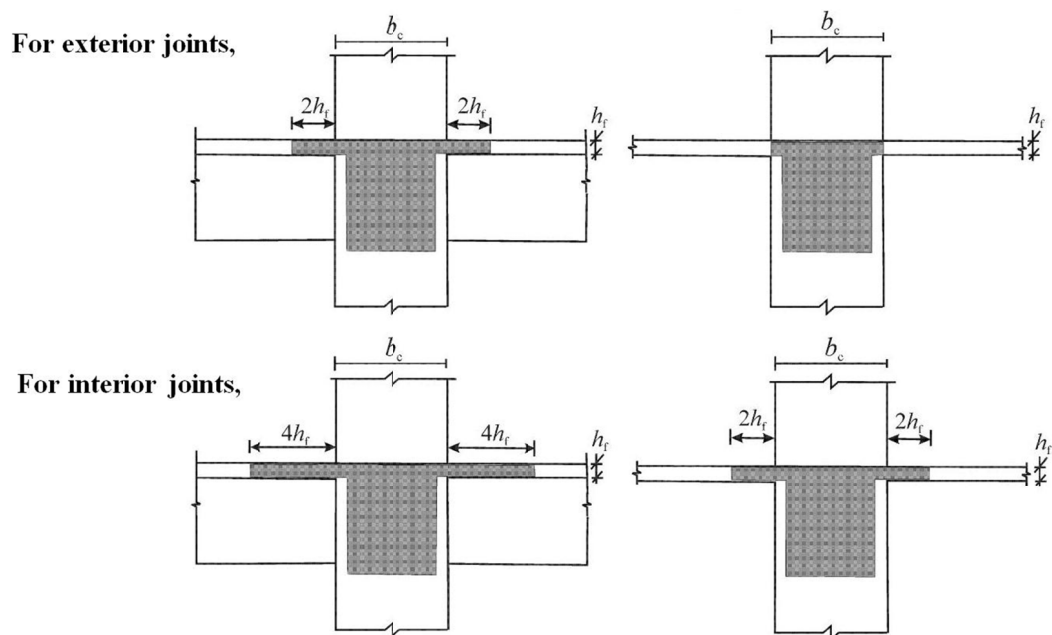


**Figure 2.7: Effective Flange Widths (Eurocode 8)**

Turkish Standards [15] also defines a detailed specification for the flange width determination of beams.

For beams with flanges on both sides (T beams) effective flange width (b) is the smallest of:

$$\begin{aligned} & b_w + 0.2 l_p, \\ & 6t_f, \\ & \frac{1}{2} * (\text{clear distance between beams}). \end{aligned} \tag{2.22}$$

For beams with unsymmetrical sections,

$$\begin{aligned} & b_1 + 0.2 l_p, \\ & 6t_f, \\ & \frac{1}{2} * (\text{clear distance between beams}). \end{aligned} \tag{2.23}$$

$l_p$  is defined as the distance between the two zero moment points of the beam. If detailed calculations are not carried out, for different loading conditions  $l_p$  can be taken as,

$$\begin{aligned} l_p &= 1.0 \times l \text{ (single span, simply supported beam)} \\ &= 0.8 \times l \text{ (end span of continuous beam)} \\ &= 0.6 \times l \text{ (internal span of continuous beam)} \\ &= 1.5 \times l \text{ (cantilever beam)} \end{aligned} \tag{2.24}$$

where,  $l$  is the span length of the beam.

The above mentioned definitions are illustrated in **Figure 2.8**.

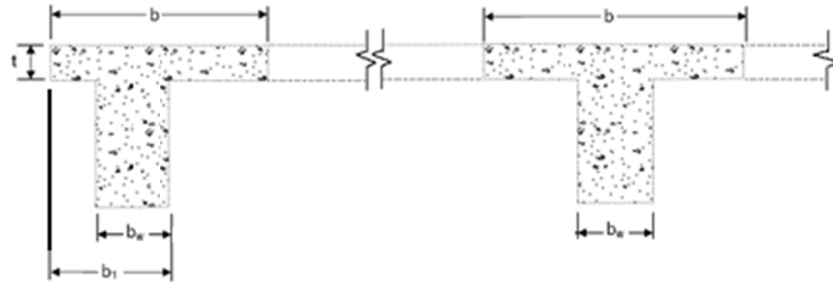


**Figure 2.8: Effective Flange Widths (TS-500)**

### 2.3.3 Bond

Another important property defining the beam-to-column connection performance is the bond between concrete and longitudinal reinforcement of framing members. Especially for structures in seismic regions, preservation of the bond resistance under high shear forces plays an important role in satisfactory lateral load response.

In addition to high shear forces introduced into the connection by earthquakes, continuous load reversals form hairline cracks around the longitudinal reinforcements, deteriorating the bond strength. If the imposed shear force exceeds the strength of the bond, bar slippage occur in the connection, resulting in the reduction of connection stiffness and increased deformations in the structure.

Burak and Wight [14] underline the loss of energy dissipation capacity of the structure in case of bar slippage and stress the reduction of beam end fixity and increased deflections of the structural frame as the expected results of decreased bond strength. Main parameters affecting bond resistance are specified as reinforcement anchorage length, level of shear stress and confinement of the joint core. Especially for exterior connections where adequate anchorage length for beam longitudinal reinforcement cannot be provided, the possibility of anchorage failure is highlighted. Basic precautions to prevent this situation are listed as increasing the column depth, reducing the beam bar diameter in order to reach a higher column depth to beam bar diameter ratio ( $h_c/d_b$ ).

Cheung, Paulay and Park [12] tested 3 beam-column-slab connections with different column depth to beam bar diameter ratios, varying between 21 and 25. It is concluded that the observed satisfactory performance of connections resulted from high joint shear reinforcement ratios and use of small diameter longitudinal beam bars to avoid slippage.

Also, in a research carried on interior wide beam-to-column connections, Quintero-Febres and Wight [16] observed that using larger column sections to increase the minimum value for column depth to beam bar diameter ratio improves the behavior of wide beam-to-column connections. It is also noted that, this improvement is valid for both wide and conventional beam-to-column connections.

Leon [17] examined the design provisions in the light of test data on bar slip and suggested 24 instead of 20 that is given in ACI 352R-02 recommendations (**Equation 2.25**) in order to improve joint performance especially for high joint shear stress levels.

In the following paragraphs, provisions on bond resistance by contemporary structural codes are discussed.

ACI 352R-02 does not include any recommendations for Type 1 connections however, for Type 2 connections, recommendations are classified considering the column width with respect to the beam width. ACI definition of idealized bond stress on a straight bar passing through the joint can be seen in **Figure 2.9**.

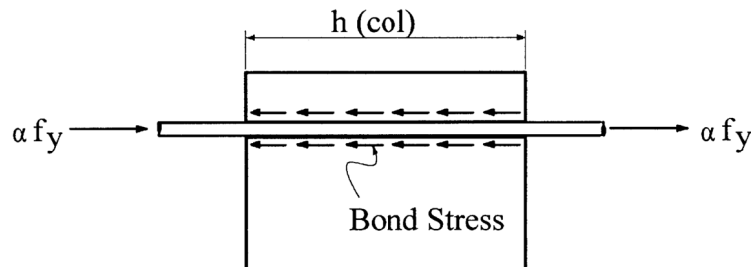


**Figure 2.9: Idealized Bond Stress (ACI 352R-02)**

In order to prevent bond related problems and provide smooth transfer of loads between concrete and longitudinal bars of beams and columns, provisions regarding bar diameters and beam and column dimensions are specified by ACI 352R-02 recommendations, which are listed below:

For connections where column width is larger than beam width,

$$\frac{h_{\text{(column)}}}{d_{\text{b (beam bars)}}} \geq 20 \frac{f_y}{60000} \geq 20 \quad (\text{psi})$$

$$\frac{h_{\text{(column)}}}{d_{\text{b (beam bars)}}} \geq 20 \frac{f_y}{420} \geq 20 \quad (\text{MPa}) \quad (2.25)$$

and

$$\frac{h_{\text{(beam)}}}{d_{\text{b (column bars)}}} \geq 20 \frac{f_y}{60000} \geq 20 \quad (\text{psi})$$

$$\frac{h_{\text{(beam)}}}{d_{\text{b (column bars)}}} \geq 20 \frac{f_y}{420} \geq 20 \quad (\text{MPa}) \quad (2.26)$$

For wide beam-to-column connections, in order to consider the absence of confinement effect provided by column axial load, limiting value for bars passing outside the column core is altered as:

$$\frac{h_{\text{(column)}}}{d_{\text{b (beam bars)}}} \geq 24 \frac{f_y}{60000} \geq 24 \quad (\text{psi})$$

$$\frac{h_{\text{(column)}}}{d_{\text{b (beam bars)}}} \geq 24 \frac{f_y}{420} \geq 24 \quad (\text{MPa}) \quad (2.27)$$

In Eurocode 8, bond resistance depends on several parameters such as longitudinal beam bar diameter, tensile strength of concrete and yield strength of beam bars. Limiting value for the beam bar diameter is given below for exterior and interior connections, respectively:

$$\text{For interior joints, } \frac{d_{bl}}{h_c} \geq \frac{7.5 f_{ctm}}{\gamma_{Rd} f_{yd}} \cdot \frac{1+0.8v_d}{1+0.75 k_D \cdot (\rho' - \rho_{max})} \quad (2.28)$$

$$\text{For exterior joints, } \frac{d_{bl}}{h_c} \geq \frac{7.5 f_{ctm}}{\gamma_{Rd} f_{yd}} \cdot (1+0.8v_d) \quad (2.29)$$

where ,

$v_d$  = normalized design axial force in the column for seismic design ( $v_d = N/f_{cd} \cdot A_c$ ),

$k_D$  = factor reflecting the ductility class equal to 1 for DCH (high ductility) and 2/3 for DCM (medium ductility),

$\rho'$  = compression reinforcement ratio of the beam bars passing through the joint,

$\rho_{max}$  = maximum allowed tension reinforcement ratio,

$\gamma_{Rd}$  = the model uncertainty factor on the design value of resistances, taken as 1,2 or 1,0 respectively for DCH or DCM (due to overstrengthening owing to strain-hardening of the longitudinal steel in the beam).

If these requirements cannot be satisfied in exterior joints, the beam or slab is allowed to be extended as exterior stubs. Headed bars or anchorage plates are also permitted for better anchorage, in Eurocode 8.

#### 2.3.4 Moment Strength Ratio

Moment strength ratio is defined as the ratio of sum of the nominal flexural strengths of columns to the sum of the nominal flexural strengths of beams framing into the joint, on a planar basis. It can be symbolized as:

$$M_r = \frac{\sum M_n (\text{columns})}{\sum M_n (\text{beams})} \quad (2.30)$$

In order to ensure beam hinging to occur before column hinging, moment strength ratio has to be higher than 1.0, in other words, total capacity of columns to bear flexural loads should be higher than total capacity of the beams. This approach is called the '*strong column weak beam philosophy*'.

Although any value higher than 1.0 is adequate to ensure strong column-weak beam behavior, several values has been proposed by different researchers and code provisions. ACI 352R-02 recommends a value higher than 1.2 for type 2 connections with the condition of considering the slab participation while calculating beam flexural ratios. TEC 2007 also requires  $M_r$  to be a minimum of 1.2.

Eurocode 8 also accentuates the importance of moment strength ratio in preventing soft story plastic mechanism. The moment strength ratio is required to be a minimum of 1.3.

Durrani and Wight [18] after evaluating 6 specimens (3 with and 3 without slab), suggested a minimum value of 1.5 for moment strength ratio. Also, in an experimental research carried out by Ehsani and Wight, 6 specimens with slabs (design  $M_r$  values varying from 1.1 to 2.0) are investigated and a minimum  $M_r$  value of 1.4 is recommended.

In his evaluation of ACI 318-83, Paulay [19] specifies the reasons for the possible deviation of  $M_r$  from the calculated values as follows:

- Additional strength enhancement occurs due to strain hardening of longitudinal beam bars.
- Slab bars are not considered when calculating the beam flexural ratio.
- Earthquake induced axial forces may decrease the flexural capacity of column, which is not considered in calculation.
- Bending-moment patterns along columns of multistory frames during instants of seismic excitation differ markedly from those derived by analyses of the elastic frames subjected to lateral static load.

- For earthquakes that hit the column in both principal directions, flexural capacity of column will be inadequate to stay in the elastic range before the beams bars yield.

Although current provisions restrict the calculation of beam flexural capacities neglecting slabs, other 4 reasons still exist. After representing the above mentioned reasons, Paulay suggests a minimum  $M_r$  value in the range of 2 and 2.5.

### **2.3.5 Presence of Transverse Beams**

Effect of transverse beams on beam-to-column connection performance is evaluated on two bases, resisting joint shear and providing confinement for the joint core.

Durrani and Wight [18] require a well confined joint core with transverse joint reinforcement for effective participation of transverse beams in resisting joint shear. Ehsani and Wight [9] underline the improvement of joint confinement and elimination of the beam bar pull out by the presence of transverse beams. Also Durrani and Zerbe [10] evaluated 6 specimens and found out that transverse beams are both effective in providing additional area for shear resistance and confining the joint core.

Another important aspect of the confinement provided by the transverse beams was observed in the experimental study carried out by Burak and Wight [9]. During the testing of the third specimen in the spandrel direction, a faster deterioration of strength and stiffness is experienced arising from the wide and shallow normal beam in the transverse direction. Since the total depth of the transverse beam was lower than 3/4 of the total depth of the spandrel beam, sufficient confinement was not provided, leading to increased damage of the beam-to-column connection.

Similarly, Bonacci and Pantazopoulou [7] in their parametric investigation of joint mechanics conclude that transverse beams confine the joint significantly in addition to increasing the volume of concrete to resist joint shear forces.

On the contrary, Cheung, Paulay and Park [12] concluded that confinement provided by the transverse beam did not affect beam-to-column connection behavior significantly.

### 2.3.6 Column Axial Load

Effect of column axial load on the behavior and strength of beam-to-column joints is one of the most debatable issues for researchers. Even if it has been investigated both experimentally and analytically; a consensus could not be reached.

Kaku and Asakusa [20] claim that axial loading on columns helps the joint to have less pinching, increased stiffness and anchorage of both hooked and straight beam bars passing through the joint. Bonacci and Pantazopoulou [7] indicated that the presence of column axial load influences the deformability of the members rather than the strength. Meinheit and Jirsa [21] also stated that ultimate shear capacity of the joint is not affected by axial loading on column but the shear at first cracking is highly increased. On the other hand, Fujii and Morita [22] report that an increase from  $f_c/12$  to  $f_c/4$  influences the shear strength of exterior joints by 11 %.

Also, Li and Kulkarni [23] obtained a shear strength increase around 6 to 8 % with an axial load level of  $0.25f_c A_g$  for the wide beam specimens tested.

## 2.4 ECCENTRIC BEAM-TO-COLUMN CONNECTIONS

Eccentric connections can be defined as the connections in which the column centroidal axis does not coincide with the beam centroidal axis (**Figure 2.10**). Due to architectural and aesthetical reasons, especially the centroidal axes of edge beams in the buildings do not coincide with the column centroidal axes in order not to produce an extension at the facade of the building.



eccentric joints is calculated as the same way with concentric joints except using  $m$  variable as 0.3 instead of 0.5, as mentioned in Section 2.1, ACI 352R-02 joint definition.

In 1992, Raffaele and Wight [24] carried out an experimental research on the performance of eccentric beam-to-column connections subjected to earthquake loading. Tested specimens had eccentricities varying from  $0.14 b_c$  to  $0.25 b_c$  and the specimens had neither transverse beams nor slabs. First observation was the excessive pinching of the lateral load – displacement hysteresis loops to reveal the reduced performance of the eccentric connections. It is also noted that cracking was concentrated on the flush side of the joint, the portion of the joint common to the column and the beam. In addition, an effective joint width for eccentric beam connections is proposed, as a consequence of observed reduction in lateral load capacities of the eccentric joints, as presented below:

$$b_{j, \text{eccentric}} = \frac{b_c}{1 + \frac{3e}{x_c}} \quad (\text{Raffaele and Wight, 1995}) \quad (2.31)$$

where  $e$  is eccentricity and  $x_c$  is the smaller of  $b_c$  and  $h_c$ .

Kusuhara et al. [25] tested 3 beam-to-column connections, 2 of which have 55 mm. ( $0.17 b_c$ ) of eccentricity, all specimens without a floor system. It is observed that the shear capacity of the eccentric joint was 94% of the one without eccentricity. Additionally, concrete damage on the joint flush side was more severe.

In a similar experimental investigation, Goto and Joh [26] tested 3 connections with varying eccentricities, 0,  $0.25 b_c$  and  $0.5 b_c$ . Comparison of the resultant shear strength of the connections revealed that, joint shear strength decreases with increasing eccentricity.

The experimental investigation carried out by Burak and Wight [14] was a more realistic research due to the inclusion of transverse beam and slab in the experimental setup. 3 specimens were tested under lateral loading in two principal directions. All 3 specimens were eccentric with eccentricities of  $0.21 b_c$ ,  $0.26 b_c$  and  $0.26 b_c$ . The

results of the experimental research revealed that the existence of slab and transverse beam added considerable torsional stiffness and consequently, specimens had high energy dissipation capacities. In other words, adverse effects of eccentricity on connections are reduced by transverse beam and slab. It is also stated that shear cracks formed at the core region of highly eccentric specimens and hence, column core dimensions should be taken as development length for spandrel beam bars, instead of full length. Similarly, Shin and LaFave [27] underlined the contribution of slab and transverse beam in the joint shear capacity of eccentric connections, as a conclusion of experimental research on 4 beam-column slab connections, 2 of which were eccentric.

## **2.5 WIDE BEAM-TO-COLUMN CONNECTIONS**

*'Wide beam-to-column connections'*, as the name implies, are connections where the beams framing into the joint is wider than the column. A wide beam structure is a category of structure that falls between the reinforced concrete frame and the flat plate and column system (Burak and Wight [14]). Use of wide beams in construction of structures is proven to be beneficial from several aspects such as economy, practicability and faster construction. Moreover, since the height of a wide beam is low, using wide beams is very effective in limiting the total height of a structure.

Wide beam-to-column connections are commonly used in construction of buildings in non-seismic areas, whereas its use in regions of high seismicity is very limited due to lack of experimental data regarding the performance of wide beam-to-column connections subjected to earthquake loading. Especially, the ability of a wide beam to form a plastic hinge, i.e. total yielding of longitudinal bars of the beam is questioned. This mainly stems from uncertainty in the response of beam bars passing outside the column core.

Another questionable property of a wide beam is its smaller moment of inertia when compared to a conventional beam with the same flexural capacity. Since the depth to width ratio of a wide beam is small, it has smaller lateral stiffness and this may cause excessive lateral drifts when subjected to strong earthquake loads.

ACI 352R-02 demands for type 2 connections, at least 1/3 of the wide-beam top longitudinal and slab reinforcement that is tributary to the effective width should pass through the confined column core. Additionally, effective joint width of a wide beam-to-column connection is limited to width of column.

Burak and Wight (2005), in their experimental study on beam-to-column connections considered the effective joint width definition of ACI 325R-02 to be highly conservative and recommended a larger effective joint width for wide beams:

$$b_{j,\text{wide}} = b_c + \frac{1}{4} (b_b - b_c) \quad (2.32)$$

Quintero-Febres and Wight [16] tested 3 interior wide beam-to-column connections with slab and transverse beams in an experimental research carried out at the University of Michigan. The specimens had varying widths between 660.4 mm to 889.0 mm (26 to 35 inches). It is concluded that, when properly designed, despite of the significant pinching of lateral load – deformation curves, the specimens possessed adequate strength and deformation capacities to withstand a severe deformation history. In addition, the use of larger column sections is encouraged to increase anchorage of beam longitudinal bars. Moreover, importance of confinement of the wide beam regions outside the column core is highlighted in order to develop a full width plastic hinge.

Experimental research on exterior wide beam-to-column connections revealed similar results. Gentry and Wight [28] analyzed 4 exterior wide beam-to-column connections and observed that satisfactory performance of wide beam-to-column connections can be ensured by limiting the amount of wide beam longitudinal reinforcement anchored in the transverse beam and beam width to column width ratio. Under these conditions, it is stated that wide beam-to-column connections could become preferable in seismic zones because of the reduced reinforcement congestion in the column core.

In the research program by LaFave and Wight [13] more encouraging results are obtained. From 3 exterior wide beam and 1 conventional beam-to-column

connections with slabs, it was observed that even with a beam width to column width ratio more than 3 and more than 2/3 of longitudinal reinforcement of beam anchored outside the column core, connections still performed satisfactorily.

## 2.6 ANALYTICAL MODELING OF CONNECTIONS

Performance of a connection is related to the combination of several inelastic response mechanisms. Lack of knowledge on some of the parameters possibly effective in the behavior of connections and insufficiency of experimental data regarding the effect of each and every parameter by itself makes it difficult to constitute an inclusive model on beam-to-column joints. Even today, despite of increasing number of experimental and analytical investigations, beam-to-column connections are generally assumed as rigid or elastic for modeling purposes, leading to invalid estimation of the response of the whole structure such as underestimation of story drifts and increased stiffness. Research on analytical modeling of beam-to-column connections aims to idealize the multivariate connection behavior in an accurate, simple and comprehensive model that is practically applicable.

Basic elements used to represent connection behavior in structural modeling can be named as plastic hinges, rotational springs and super models. Each element has its own advantage and disadvantage from the point of simplicity and accuracy. Also rigid end zones are commonly used in order to account for finite size of the connections. A number of beam-to-column connection models created up to date will be discussed in the following paragraphs.

One of the primary research on analytical modeling of beam-to-column connections is carried out by Anderson and Townsend [29] in 1977. From the two degrading trilinear models suggested, the one considering the effect of degrading concrete and connection stiffness is underlined to have a significant effect on the response of the reinforced concrete structures.

In 1988, El Metwally and Chen [30] studied the '*Moment-Rotation Modeling of Reinforced Concrete Beam-Column Connections*'. The proposed model is defined as a concentrated rotational spring the stiffness of which is determined based on the

linear elastic stiffness of the connection, ultimate moment capacity of the connection and an internal variable ‘a’, representing the dissipated energy for cyclic loading.

Later models of beam-to-column connections included combinations of rotational springs, plastic hinges, rigid end zones and plane stress elements. In addition, parallel to the increase in the number of experimental and analytical research, a more detailed understanding of the beam-to-column connection behavior is achieved, revealing itself as the increase in the degree of detailing of the connection models.

Model of Alath and Kunnath [31], the ‘*scissors model*’, includes a rotational spring located between beam centerline and column centerline. Finite size of the connection, i.e. the parts of the beams and columns included in the connection region, are modeled as rigid zones located at the end regions of beams and columns. The moment rotation behavior of the connection is represented using hysteretic material assigned to the rotational spring. A basic representation of scissors model can be seen in **Figure 2.12**.

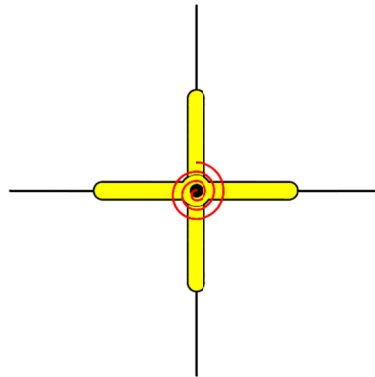


**Figure 2.12: Scissors Model Proposed by Alath and Kunnath (1995)**

Elmorsi et al. [32] developed a complex model composed of plane stress elements: a joint element with 12 nodes and 10 node transition elements. Also, concrete and steel reinforcement models are created to represent material non linearity and combined with the kinematic model in order to complete the analytical model characterizing the shear deformations in the joint panel as well as flexural and shear deformations in the plastic hinge zones. A simple sketch of the model is shown in **Figure 2.13**.

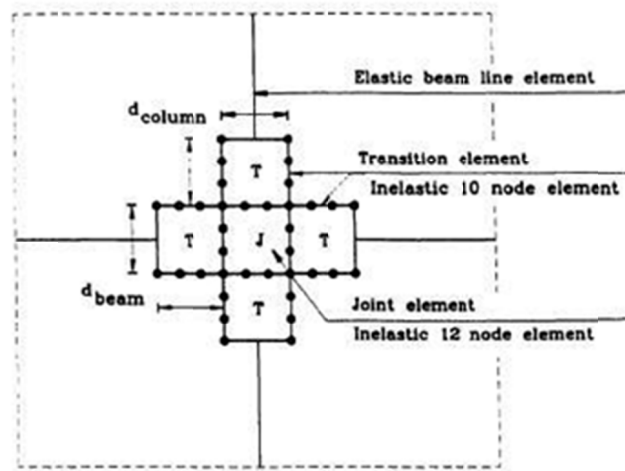


**Figure 2.13: Model of Elmors et al. (1998)**

Another connection model that considers response of concrete and steel and bond-slip performance under cyclic loading is proposed by Fleury et al. [33]. The model is a combination of two elements describing the core behavior, two elements representing the beam-to-column connection at the interface, two node bar elements for longitudinal bars of the column and a series of elements for bond behavior of steel bars through the connection. A simple representation of model can be seen in **Figure 2.14**.

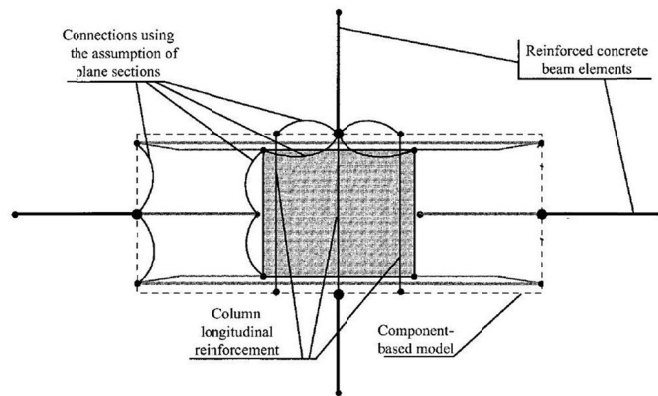


**Figure 2.14: Model of Fleury et al. (2000)**

The model proposed by Lowes and Altoontash [34] represents the beam-to-column connection characteristics using a shear panel and transition elements between the connection region and framing members. Transition elements are composed of two

zero length bar-slip spring and one interface zero length shear spring, connecting internal nodes to external nodes at each face of the connection, summing up a total of 12 springs surrounding the shear panel. Shear panel is modeled to represent the shear stress-strain behavior of the connection and free to deform by shifting angles between adjacent panel sides without any flexural or axial deformations. The model is implemented in Openses platform and graphical representation of the model can be seen in **Figure 2.15**.

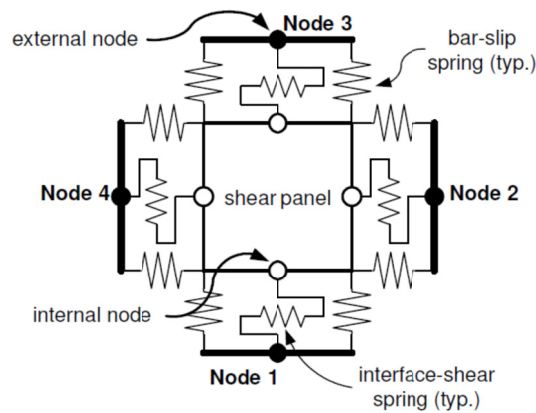


**Figure 2.15: Model of Lowes and Altoontash (2003)**

The model is re-evaluated and modified by Mitra and Lowes in 2004 [35]. First change was the reduction of distance between bar slip springs in order to calibrate the forces carried by the springs as revealed in the experimental results. Moreover, post peak response of bond slip springs and anchorage length of beam and column longitudinal reinforcements are calibrated. Calibration of the model aimed to widen the range of model applicability and provide an improved method for simulating anchorage response of beam and column reinforcement.

The joint model proposed by Shin and LaFave [36] is composed of seven rotational springs and a joint element. Joint element is made up of rigid links, the response of which is restricted by three rotational springs located at the corner of the element. Beams and columns are modeled as elasto-plastic elements and are connected to the joint region by two springs representing the bond slip and moment rotation

characteristics of the framing members. The joint is modeled in Drain-2DX nonlinear structural analysis program. The connection model can be seen in **Figure 2.16**.

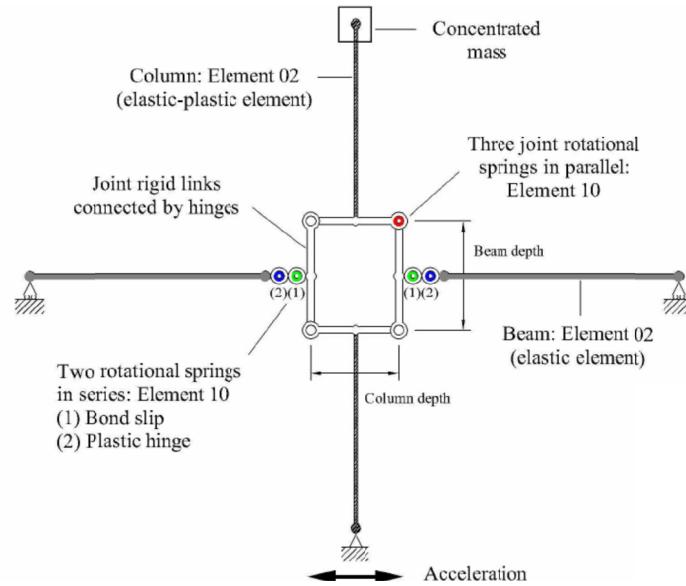


**Figure 2.16: Model of Shin and LaFave (2004)**

Burak and Wight [14] investigated modeling of both eccentric and concentric beam – column – slab connections. Considering the contribution of joint deformation on the total story drift, a model taking into account the joint shear distortion is developed and verified using experimental data. The beam and column elements are modeled as elastic elements with rigid end zones connected to columns with zero length moment hinges. Connection element is defined considering the effective joint width, the connection moment capacity, initial and strain hardening stiffness, and shear deformations at critical points. The joint model is applied to a 5 story, 5 bay frame structure in order to evaluate the performance of the model under dynamic time history analyses. The results of the comparisons between the cases with and without the joint model evidently showed that joint shear distortions contributed significantly to roof and interstory drifts. Including joint model in the analysis increased the roof drift from 1.6% to 2.1% and story drift between 3rd and 4th floors from 1.05% to 1.63%.

Kim et al. [37] conducted a statistical research on the influence of several parameters on the shear strength of beam-to-column connections in 2007. Whereas the basic parametric model contains eight variables; less significant ones are omitted in the later steps. The proposed basic joint shear strength prediction model can be seen below.

$$v_j = 1.04 \left( \frac{S_{pro}}{S_{req}} \right)^{-0.00513} \left( \frac{b_b}{b_c} \right)^{0.0151} \left( \frac{A_{sh,pro}}{A_{sh,req}} \right)^{0.0241} \left( \frac{h_b}{h_c} \right)^{-0.301} \times (JI)^{0.0886} (BI)^{0.236} (JP)^{1.28} (f'_c)^{0.765} \quad (2.33)$$

where,  $v_j$  = joint shear strength in MPa.

JP = 1.0 for interior connections, 0.75 for exterior connections, 0.50 for knee connections,

JI = joint transverse reinforcement index  $[(\rho \cdot f_y)_{jointrein} / f'_c]$ ,

BI = beam reinforcement index  $[(\rho \cdot f_y)_{beamrein} / f'_c]$ ,

$S_{pro}$  = proposed spacing of joint transverse reinforcement,

$S_{req}$  = recommended spacing of joint transverse reinforcement.

The basic model was evaluated later and after a step wise observation of less significant parameters of the model, the prediction equation was simplified as below, to make it more practical.

$$v_j (\text{MPa}) = \alpha \gamma (JI)^{0.07} (BI)^{0.25} (f'_c)^{0.75} \quad (2.34)$$

where, JP = 1.0 for interior connections,

0.7 for exterior connections,

0.4 for knee connections.

$\gamma = 1.02$ .

More recently, another beam to column connection model considering the inelastic response mechanisms of the members forming the assembly is created by Burak [38]. The beam and column members are modeled as elastic segments with rigid end zones intersecting at the connection. The joint model is composed of rigid links connected with hinges at the corners, one of which has a nonlinear rotational spring. Beam and column members also have rotational springs on the column and beam interfaces, respectively. Moment rotation relation of the beams, moment through connection versus shear strain of the joint panel and axial load-moment relationship of the columns are represented using Perform 3-D elements. The graphical representation of the connection model can be seen in **Figure 2.17**.

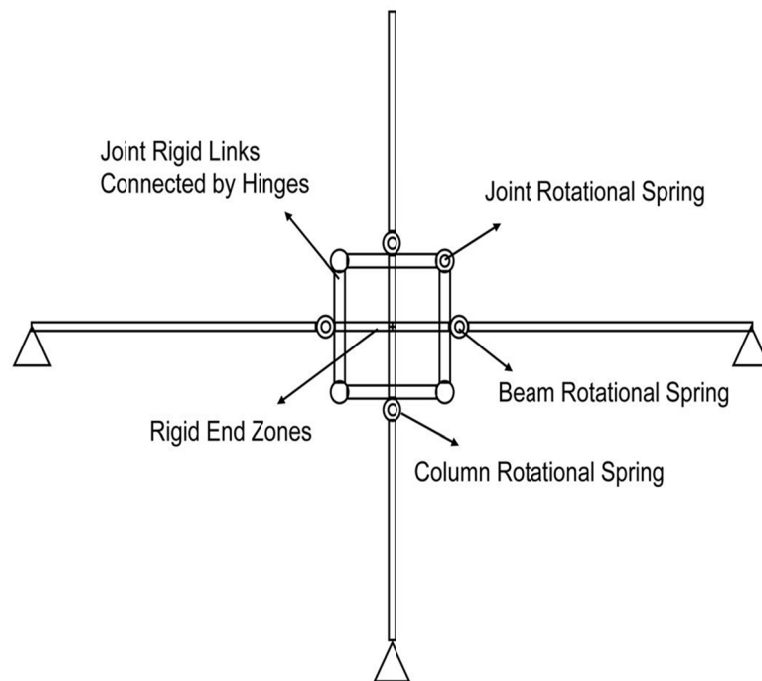


**Figure 2.17: Connection Model Proposed by Burak (2008)**

In 2010, an analytical study to predict the behavior of beam-to-column connections is carried out by Unal and Burak [39]. The researchers examined the effect of a number of parameters such as concrete strength, transverse reinforcement, beam eccentricity and axial load on a statistical basis, and come up with parametric equations defining

the shear strength vs. strain relationship of connections. The proposed model is later verified by PERFORM 3-D [40], using the panel zone element given in the software and beam and column elements with plastic hinges at member ends. An illustration of the panel zone element can be seen in **Figure 2.18**.

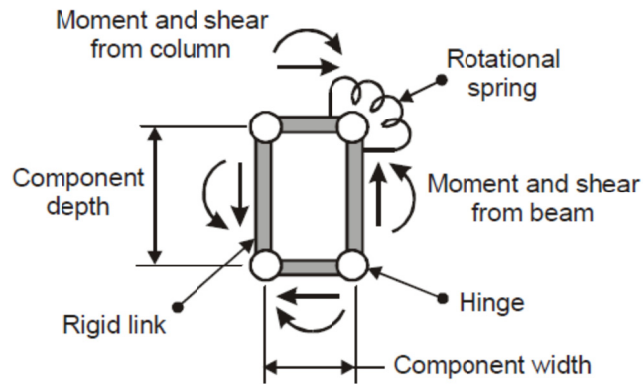


**Figure 2.18: Perform-3D Panel Zone Element**

## CHAPTER 3

### DATABASE CONSTRUCTION

#### 3.1 OVERVIEW

First step of the analytical study is the construction of a comprehensive and detailed database. A wide range of analytical and experimental studies have been investigated and a preliminary database composed of 160 beam-to-column connection subassemblies obtained from 29 different research projects is created. After a re-evaluation of adequacy of the data, the number of specimens included in the final database is reduced to 114.

Since the data collection for the beam-to-column connection tests is relatively more demanding than that of other structural members, extent and dependability of experimental results is strongly related to the instrumentation utilized during testing. Because of this reason, although the studies on connection subassemblies date back to 1960s, availability of detailed information is very limited. Therefore, main difficulty in constructing the database can be mentioned as the limited number of research projects with sufficient and dependable data, especially when the stress vs. strain relationships for the connection regions is considered.

A large variety of beam-to-column connection subassemblies having different geometric, material and loading characteristics are presented in the database, however, certain limitations are taken into consideration, especially for connections that have uncommon geometric and material properties, in order not to lose the accuracy and applicability of the analytical model to be created. A general summary on the characteristics considered in the selection process of specimens composing the database are presented below.

### 3.1.1 Range of Specimen Properties

#### Geometry

Specimens having a wide range of geometric properties are investigated. In addition to connection subassemblies with conventional beam and column members, wide beam-to-column connections, eccentric connections, specimens that have varying column aspect ratios, and subassemblies with floor systems including transverse beams and/or slabs are incorporated to the database. The only exclusions are corner connections where two perpendicular beams meet and roof connections where the specimen has only a bottom column.

#### Concrete Compressive Strength ( $f'_c$ )

All specimens selected for the database have concrete compressive strengths varying between 19.30 MPa and 94.60 MPa, considering actual concrete strengths. As ACI 352R-02 recommendations are followed as the main reference, specimens constructed using concrete compressive strengths exceeding 100 MPa (15000 psi) are excluded from the scope of this research.

#### Eccentricity

As being one of the main parameters investigated, 27 beam-to-column connections with eccentricity between beam and column centroidal axes are included in the study. Eccentricities vary from  $0.125 b_{\text{column}}$  to  $0.306 b_{\text{column}}$  for the selected specimens.

#### Beam Width to Column Width Ratio

The effect of the beam width to column width ratio on the behavior of connection regions is evaluated in terms of confinement provided by the beams. The beam width to column width ratio ranges from 0.40 to 3.10.

#### Transverse Shear Reinforcement Ratio

Effect of confinement provided by the transverse reinforcement is investigated using specimens with a wide range of shear reinforcement ratios. Some selected specimens

have no shear reinforcement, whereas others have up to 2.40 % volumetric ratio per one layer of transverse reinforcement, the definition of which is given in Section 4.2.2.4.

#### Moment Strength Ratio ( $M_r$ )

Flexural strength ratios of all the specimens are calculated considering the actual material properties. For specimens with slabs, effective flange width is defined based on ACI 318R-08 equations.

Although the  $M_r$  values of the vast majority of specimens (104) are more than 1.0, which represents strong column weak beam behavior, few specimens (10) with flexural ratios smaller than 1.0 are also included in the database in order to investigate the effect of other parameters such as high yield strength of longitudinal beam bars.

#### Axial Load on Column

Among the specimens considered, maximum axial load on the column framing into the beam-to-column connection is 1243.24 kN (corresponding to  $0.45 A_g \times f_c$ ), whereas no axial load is applied to some of the subassemblies.

### **3.2 SELECTED SPECIMENS**

In this part of the report, the experiments which take part in the database is summarized. General properties of the specimens and the main parameters investigated are listed.

Specimens of Durrani and Wight [18] are useful in monitoring the effect of presence of transverse beams and slab on the beam-to-column connection performance. From six interior specimens tested, three had transverse beams and slab, whereas other three had neither slab nor transverse beams. Joint transverse reinforcement was also one of the primary variables of the experimental investigation. The tests were conducted in 1982.

Tests carried out by Ehsani and Wight [9] in 1983 investigated the effect of transverse beams and slab on the performance of exterior beam-to-column connections. All six specimens were tested under cyclic lateral loading together with axial loading.

In 1988, three beam-column slab subassemblages were tested by Kurose et al. [41] one of which was exterior. Two specimens also had transverse beams. The specimens with transverse beams were tested in two principal directions, one at a time, summing up to 5 analyses in total. Axial load was not applied to the columns.

Specimens of Park et al. [12] were similar to the ones of Kurose et al., such that this group of specimens also included three subassemblies all with slabs and two of them with transverse beams. The specimens were loaded in both principal directions one at a time, one of which was exterior. The research was completed in 1989.

Twelve specimens were tested by Alameddine and Ehsani [8] in 1990 with varying concrete compressive strengths, joint shear reinforcement ratios, beam and column longitudinal reinforcement ratios. The connection subassemblies were two dimensional and did not include slabs or transverse beams. All specimens had axially loaded columns.

All four specimens of Raffaele and Wight [24] had spandrel beam eccentricities with varying beam dimensions and reinforcements. Specimens had neither slabs nor transverse beams. The investigation was conducted in 1992.

Gentry and Wight [28] investigated the behavior of exterior wide beam-to-column connections in 1992 by testing four specimens that had no slab or transverse beam. The column dimensions and reinforcement were the same for all specimens, whereas longitudinal reinforcement of the wide beams was altered. The columns were axially loaded.

Quintero-Febres and Wight [16] investigated the performance of interior wide beam-to-column connections in 1997. The specimens had neither a floor system nor axial load on the column.

In 1997, LaFave and Wight [13] conducted tests on exterior wide beam-to-column connections, similar to Gentry. In this test series, the subassemblies included slab and transverse beams. All four specimens were tested under cyclic loading in the wide beam direction, without any axial loading. One of the specimens had a conventional beam section in the loading direction for comparison of the behavior.

Chen and Chen [42] explored the effect of eccentricity on the performance of interior beam-to-column joints. From the six specimens tested, all were eccentric except one. Four of the eccentric specimens, called as JS series, were constructed using spread ended beams with varying longitudinal reinforcement. The joints did not include transverse beams or slabs. The experimental study was carried out in 1997.

Specimens of Teng and Zhou [43] were classified in two series composed of three specimens each. All specimens were interior and four of them were eccentric. Column height and transverse reinforcement ratio are the two altering parameters between series one and two. All specimens had axial load on columns in addition to lateral cyclic loading. The research project was completed in 2000.

Tests of Shin and LaFave [27] were conducted in 2004. Four exterior beam-column-slab connection specimens were tested, two of which had spandrel beam eccentricity. The lateral loading was applied in the spandrel beam direction without any axial load on the column.

The main scope of the research carried out by Goto and Joh [26] in 2004 was eccentricity. From four of the interior specimens tested, one was concentric, whereas the beam and column axes of others' did not coincide, with increasing eccentricities. While the first three specimens had similar joint shear reinforcement ratios, the last specimen was constructed with additional shear reinforcement in the joint region. All specimens had axial loads applied on the columns, but none had slab or transverse beams.

Interior beam-to-column connections tested by Hwang et al. [44] were aimed to explore the significance of joint transverse reinforcement. The research was carried out in 2004. None of the specimens had transverse beams and/or slabs.

In 2005, Burak and Wight [14] tested three 3/4 scale exterior specimens. All three specimens had slab and transverse beams in addition to eccentric spandrel beams. Moreover, one of the specimens had a wide beam in the normal beam direction. Axial load was applied on the column of each subassembly. This experimental study differs from other selected eccentric connection tests, because the specimens were loaded in two principal directions, one plane at a time.

Wong [45] tested seventeen beam-to-column connections in 2005 to observe the effect of several parameters such as the horizontal and vertical reinforcement ratios in the joint, the hooks of beam longitudinal bars, and anchorage. Four specimens in this test series are not included in the database, because beam longitudinal reinforcement that has no hooks extending inside the exterior joint creates an anchorage problem that is out of the scope of this report. All specimens had axial load but no floor system.

In their benchmark test series for the validation of mathematical models developed to define the behavior of connections, Shiohara and Kusuhara [46] tested six specimens, four of which were added to the database because of the lack of data on the maximum joint shear strength of two specimens. Different loading protocols and the confinement effect of surrounding beams were the primary parameters investigated in this study, which was completed in 2006. None of the specimens included transverse beams and slab, but the columns were axially loaded.

In 2006, Lee and Ko [47] tested five specimens, three of which were eccentric. The test setup included axial load on columns but no transverse beams and slab. Specimens were classified in two groups with respect to the orientation of column. In the first group, column was oriented such that the loading was applied in the strong direction (parallel to longer side) and the second group was loaded in the weak direction.

Li and Kulkarni [23] tested three wide beam-to-column connection subassemblies without slab, transverse beams, or axial load on the columns. The width of the column that the wide beam frames into was the main parameter of this experimental study completed in 2010.

One of the references mostly benefited from is the ACI SP-123, '*Design of Beam-Column Joints for Seismic Resistance*', which is published in 1991. The experiments and specimens which are discussed below are taken from the above mentioned document.

In their experimental investigation, Joh, Goto and Shibata [48] explored the effect of geometric properties of interior joints, especially the eccentricity. Of the five specimens tested, four, two eccentric and two concentric ones, which had the shear stress vs. shear strain data available, are added to the database. Slab and transverse beams did not exist in the test setup, but axial load was applied on the columns.

Main parameters investigated by Fujii and Morita [22] in 1991 were yield strength of beam bars, column axial load and amount of joint hoops. Half of the specimens were exterior and the other half were interior, all with axial loading of columns. Transverse beams and slab were not included in the test setup.

In 2004, Kusuha et al. [25] tested three interior specimens, two of which were eccentric. No axial load was applied on the columns and the specimens had neither slab nor transverse beams. The main parameters investigated were beam eccentricity and effect of transverse shear reinforcement in the joint.

### **3.3 LABELING OF SPECIMENS**

The specimens are classified with respect to the significant geometrical properties such as the number of beams framing into the connection and slab presence in the final database. The types of connections and respective labeling is presented below, in **Figure 3.1**.

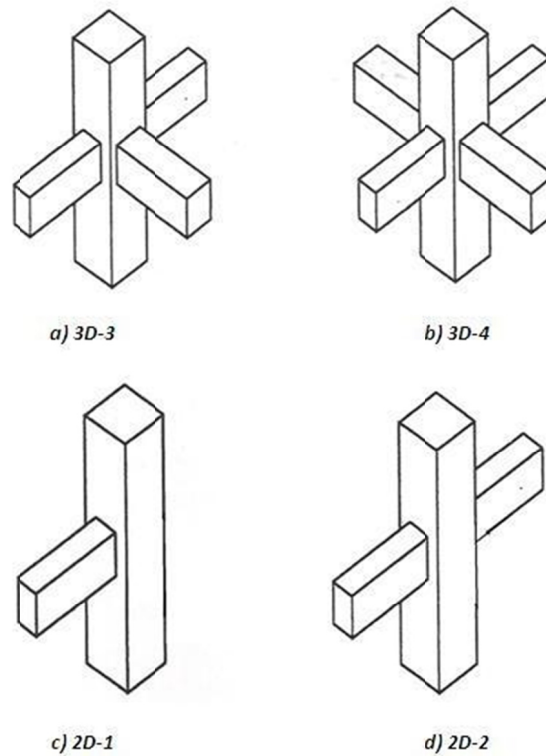


**Figure 3.1: Labeling of Connections in the Database**

### 3.4 FINAL DATABASE

The final database is composed of 114 specimens from 23 experimental studies. Selected specimens are presented in **Table 3.1**, classified with respect to the type of the connection, column to beam moment ratio, axial load ratio, eccentricity ratio, presence of wide beam, presence of slab and beam in the transverse direction. Moreover, the constructed database is summarized in **Table 3.2** based on the key properties of specimens.

Table 3.1: Selected Specimens

No.	Researcher	Specimen	Type	$M_r$	Ax. Load $N/(A_g f'_c)$	Ecc.Ratio $e/b_c$	Wide Beam	Trans. Beam	Slab
1	<i>B. Burak, J. K. Wight</i>	1-S	3D-3	1.51	0.053	0.21		+	+
2		2-S	3D-3	1.09	0.039	0.26		+	+
3		3-S	3D-3	1.04	0.042	0.26		+	+
4		1-N	3D-3	2.08	0.050			+	+
5		2-N	3D-3	1.89	0.031			+	+
6		3-N	3D-3	1.75	0.031		+	+	+
7	<i>G. S. Raffaello, J. K. Wight</i>	1	2D-2	1.18	0.025	0.14			
8		2	2D-2	1.76	0.026	0.25			
9		3	2D-2	1.72	0.019	0.23			
10		4	2D-2	1.00	0.036	0.23			
11	<i>M. Shin, J. LaFave</i>	SL 1	3D-3	1.14		0.19		+	+
12		SL 2	3D-3	1.25		0.31		+	+
13		SL3	3D-3	1.11				+	+
14		SL4	3D-3	1.07				+	+
15	<i>T. R. Gentry, J. K. Wight</i>	WB1	3D-3	1.32	0.025		+	+	+
16		WB2	3D-3	1.41	0.025		+	+	+
17		WB3	3D-3	1.31	0.019		+	+	+
18		WB4	3D-3	1.04	0.019		+	+	+
19	<i>J. La Fave, J. K. Wight</i>	EWB - 1	3D-3	1.29			+	+	+
20		EWB - 2	3D-3	1.24			+	+	+
21		EWB - 3	3D-3	1.46			+	+	+
22		ENB - 1	3D-3	1.65				+	+
23	<i>C. G. Quintero-Febre, J. K. Wight</i>	IWB - 1	3D-4	1.14			+	+	+
24		IWB - 2	3D-4	1.12			+	+	+
25		IWB - 3	3D-4	1.37			+	+	+
26	<i>A. J. Durrani J. K. Wight</i>	X1	2D-2	1.29	0.054				
27		X2	2D-2	1.29	0.056				
28		X3	2D-2	1.06	0.053				
29		S1	3D-3	1.26	0.057			+	+
30		S2	3D-3	1.26	0.077			+	+
31		S3	3D-3	1.08	0.065			+	+
32	<i>O. Joh, Y. Goto, T. Shibata</i>	JXO-B1	2D-2	1.45	0.161				
33		JXO-B2	2D-2	1.41	0.165				
34		JXO-B5	2D-2	1.48	0.149	0.25			
35		JXO-B6	2D-2	1.45	0.154	0.25			
36	<i>S.Fujii, S.Morita</i>	A1	2D-2	1.15	0.076				
37		A2	2D-2	1.15	0.076				
38		A3	2D-2	1.15	0.227				
39		A4	2D-2	1.15	0.227				
40		B1	2D-1	1.15	0.068				
41		B2	2D-1	1.15	0.068				
42		B3	2D-1	1.15	0.236				
43		B4	2D-1	1.15	0.236				
44	<i>Y. Kurose, G. N.Guimaraes, L. Zuhua, M. E. Kreger, J. O. Jirsa</i>	J1 (EW)	2D-2	1.19					
45		J2 (EW)	3D-4	1.50				+	+
46		J2 (NS)	3D-4	1.50				+	+
47		J3 (EW)	3D-3	1.85				+	+
48		J3 (NS)	3D-3	1.40				+	+

**Table 3.1: Selected Specimens (continued)**

No.	Researcher	Specimen	Type	$M_r$	Ax. Load	Ecc. Ratio	Wide Beam	Trans. Beam
					$N/(A_g f'_c)$	$e/b_c$		
49	<i>P.C.Cheung, T.Paulay, R.Park</i>	2D-E (EW)	3D-3	3.66				+
50	<i>S. Teng, H. Zhou</i>	S1	2D-2	1.82	0.111			
51		S2	2D-2	1.82	0.108	0.13		
52		S3	2D-2	1.82	0.105	0.25		
53		S5	2D-2	1.42	0.110	0.13		
54		S6	2D-2	1.41	0.113	0.25		
55	<i>F. Kusahara, K. Azukawa, H. Shiohara, S. Otani</i>	JE-0	2D-2	1.35				
56		JE-55	2D-2	1.35		0.17		
57		JE-55S	2D-2	1.35		0.17		
58	<i>H. Shioara, F. Kusahara</i>	A2	2D-2	2.01	0.085			
59		A3	2D-2	2.01	0.085			
60		B1	2D-2	1.12	0.085			
61		B2	2D-1	1.12	0.085			
62	<i>H. J. Lee, J. W. KO</i>	S0	2D-1	4.62	0.089			
63		S50	2D-1	4.65	0.085	0.13		
64		W0	2D-1	3.08	0.101			
65		W75	2D-1	3.09	0.096	0.13		
66		W150	2D-1	3.08	0.100	0.25		
67	<i>S. J. Hwang, H. J. Lee, K. C. Wang</i>	70 - 3T44	2D-1	2.77	0.014			
68		70 - 3T4	2D-1	2.86	0.013			
69		70 - 2T5	2D-1	2.84	0.013			
70		70 - 1T55	2D-1	2.81	0.014			
71		28- 3T4	2D-1	3.38	0.019			
72		28-0T0	2D-1	3.36	0.020			
73	<i>Y. Goto, O. Joh</i>	UM-0	2D-2	0.91	0.167			
74		UM-60	2D-2	0.92	0.167	0.13		
75		UM-125	2D-2	0.93	0.167	0.28		
76	<i>F. Alamedtine, M. R. Ehsani</i>	LL 8	2D-1	1.24	0.039			
77		LH 8	2D-1	1.24	0.039			
78		HL 8	2D-1	1.21	0.068			
79		HH 8	2D-1	1.21	0.068			
80		LL 11	2D-1	1.21	0.031			
81		LH 11	2D-1	1.22	0.029			
82		HL 11	2D-1	1.20	0.063			
83		HH 11	2D-1	1.23	0.065			
84		LL 14	2D-1	1.27	0.020			
85		LH 14	2D-1	1.28	0.019			
86	HH 14	2D-1	1.30	0.040				
87	<i>C. C. Chen, G. K. Chen</i>	JC	2D-1	1.85				
88		JE	2D-1	1.85		0.20		
89		JS1	2D-1	1.85		0.20		
90		JS2	2D-1	1.85		0.20		
91		JS3	2D-1	1.85		0.20		
92		JS4	2D-1	1.85		0.20		

**Table 3.1: Selected Specimens (continued)**

No.	Researcher	Specimen	Type	$M_r$	Ax. Load $N/(A_g f'_c)$	Ecc.Ratio $e/b_c$	Wide Beam	Trans. Beam	Slab
93	<i>H. F. Wong, J. S. Kuang</i>	JA-NN03	2D-1	2.29	0.030				
94		JA-NN15	2D-1	2.88	0.150				
95		JA-NY03	2D-1	2.29	0.030				
96		JA-NY15	2D-1	2.66	0.150				
97		JB-NN03	2D-1	3.46	0.030				
98		JB-NY03	2D-1	3.42	0.030				
99	<i>H. F. Wong, J. S. Kuang</i>	BS-L-300	2D-1	2.77	0.150				
100		BS-L-450	2D-1	1.48	0.150				
101		BS-L-600	2D-1	1.08	0.150				
102		BS-L-V2	2D-1	1.74	0.150				
103		BS-L-V4	2D-1	1.94	0.150				
104		BS-L-H1	2D-1	1.51	0.150				
105		BS-L-H2	2D-1	1.63	0.150				
106	<i>M.R.Ehsani, J.K.Wight</i>	1S	3D-3	1.39	0.358			+	+
107		2S	3D-3	1.35	0.358			+	+
108		3S	3D-3	1.82	0.358			+	+
109		4S	3D-3	1.81	0.358			+	+
110		5S	3D-3	2.34	0.446			+	+
111		6S	3D-3	1.82	0.380			+	+
112	<i>B. Li, S. A. Kulkarni</i>	EWB-1	2D-1	7.03			+		
113		EWB-2	2D-1	2.41					
114		EWB-3	2D-2	6.93			+		

**Table 3.2: Key Properties of Specimens Included in the Database**

DESCRIPTION	INTERIOR	EXTERIOR	TOTAL
Specimens with Axial Load on Column	24	61	85
Specimens without Axial Load on Column	10	20	30
Specimens with Concentric Beam in the Loading Direction	23	64	87
Specimens with Eccentric Beam in the Loading Direction	10	17	27
Specimens with Conventional Beam in the Loading Direction	30	71	101
Specimens with Wide Beam in the Loading Direction	3	10	13
Specimens with Transverse Beam	8	27	35
Specimens without Transverse Beam	25	54	79
Specimens with Slab	9	23	32
Specimens without Slab	24	58	82
<b>TOTAL</b>	<b>33</b>	<b>81</b>	<b>114</b>

## **CHAPTER 4**

### **ANALYTICAL MODEL**

#### **4.1 GENERAL DESCRIPTION**

Main purpose of this study is to develop an analytical model that accurately estimates the shear strength of beam-to-column connections and represents the key performance points of the shear stress vs. strain relationship. The model is kept simple enough so that it can be employed by practicing engineers while covering a variety of beam-to-column connections.

A wide range of parameters related to geometric and material properties of the connections have been investigated. The influence of a variable is initially determined based on the results of prior experimental and analytical studies. Each parameter is evaluated by several different approaches and variation of the joint shear strength estimate for each parameter is monitored, with an attempt to obtain the best fit for the variable. As the study proceed, the influence of the variables are re-evaluated with regard to their efficiencies in terms of reducing the total error and the number of effected specimens, leading to the omission of parameters with negligible effects.

While obtaining the key points for both shear strength and shear strain, utmost importance is given to define the prediction related to physical quantities without using fixed coefficients as much as possible. Moreover, basic predictions of both shear strength and shear strain capacities of the connections are determined based on the properties of beams in the loading direction, which is explained in detail in the following sections. Basic prediction is later improved by employing variables defined in accordance with the characteristics of the connection.

While defining the variables reflecting the effect of geometric and material properties of the connections, indices are created in order to be able to represent the relative influence of the parameter mentioned. After that, various combinations of the previously defined indices are evaluated to find out the rate of influence on the connection performance, while keeping the variable as simple as possible. ACI 352R-02 report has been used as the basic reference in definition of indices and determination of the adequacy of a parameter.

Since the experimental data on the shear strength of connections is easier to access, a more detailed investigation on the shear strength prediction is carried out when compared to the determination of the shear strain expected in the beam-to-column connections.

## **4.2 JOINT SHEAR STRENGTH PREDICTION**

### **4.2.1 Basic Joint Shear Strength Prediction ( $V_{j0}$ )**

The first step of joint shear strength prediction is the specification of a basic value related to the characteristics of the beam-to-column connections. Most of the prior research studies and current structural codes define certain shear capacity coefficients based on the location of the connection (interior or exterior) and the relative width of the beams framing into the connection (confined or unconfined).

In this analytical study, instead of defining fixed coefficients with respect to the surrounding beam properties, a basic shear prediction value is obtained as the first step, considering the longitudinal reinforcement properties of the beams framing into the connection in the loading direction. In other words, the shear demand imposed by the beams is considered to be the basic indicator of the shear loading of the connection region. Then, other geometric and material properties of the connection are examined to modify the basic prediction and determine the capacity of the connection to bear the shear strength demand imposed by the beams.

Basic shear strength prediction for joint shear strength is denoted by  $V_{j0}$  and defined as the total shear force imposed by the beams calculated as the multiplication of the

top longitudinal reinforcement area multiplied by the yield strength for exterior joints, whereas total reinforcement area is used instead of top reinforcement area in the calculation for interior connections. Formulation of basic shear strength prediction can be shown as below.

$$\text{For exterior joints: } V_{j0} = \sum (A_i \times f_{yi})_{\text{top}} \quad (4.1a)$$

$$\text{For interior joints: } V_{j0} = \sum (A_i \times f_{yi})_{\text{top}} + \sum (A_i \times f_{yi})_{\text{bottom}} \quad (4.1b)$$

In order not to overpredict the shear force imposed by the beam on the joint, any force arising from strain hardening is neglected.

The limitation applied on the basic shear prediction is on the maximum yield strength of longitudinal beam reinforcement. In order not to overestimate the shear capacity of the joint, 483.0 MPa limits the yield strength of longitudinal beam reinforcement, representing a 15% strain hardening of steel bars with 420.0 MPa yield strength.

#### 4.2.2 Adjustment Factors

As mentioned earlier, geometric and material properties along with the loading conditions are the basic parameters identifying the strength versus strain response of beam-to-column connections. Throughout this study, several parameters are examined and relatively significant ones are included in the final joint shear strength definition.

##### General methodology in determination of factors

First, all major characteristics of a connection are defined as normalized variables. For that purpose, simple indices representing the effect of the considered characteristic are generated. Main purpose of these indices is to have a basis for comparison of different connection subassemblies that have similar properties.

Then, the influence of each index on the behavior of the connection is investigated and an adjustment factor is obtained. This is accomplished by evaluation of priory

generated indices and optimizing the adjustment factor to adequately represent the effect of the considered characteristic on the behavior of the connection.

The final step is the determination of the limits for each factor, if necessary, in order to prevent unrealistic influence of a parameter on the behavior. ACI 352R-02 recommendations are taken as the benchmark for limitation purposes.

### 4.2.3 Axial Load Factor

Axial load applied on a column is proven to increase the joint shear strength because of the extra confinement it provides to the connection region. Effect of axial load is represented by defining an axial load index based on normalization of the axial load by the gross column area.

$$\text{Axial Load Index (Ax)} = N/A_g f'_c \quad (4.2)$$

where,

$N$  = Axial load on the column,

$A_g$  = Gross column area

From several trials to minimize the error, enhancing effect of axial load on the joint shear strength is best represented by half of the axial load index and the axial load factor is defined as:

$$\text{Axial Load Factor (AF)} = (1+Ax/2) \quad (4.3)$$

Although the confinement effect of axial load on the beam-to-column connections clearly enhances the shear strength capacity, in case of earthquake loading the axial load level on a column may fluctuate, which results in a decreased confinement effect than the proposed value. Since the experiments selected for the database were carried out under constant or no axial load, the proposed factor defines the effect of confinement provided under these circumstances. For design purposes, the possibility of fluctuating axial load level under seismic action should be considered and the axial load factor should be applied accordingly.

#### 4.2.4 Slab Factor

Experimental results of subassemblies that include slab reveal that beam-column-slab connections sustain higher shear stresses. Another important outcome that can be inferred is the additional confinement provided by slabs significantly diminishes the negative effect of eccentricity on shear capacity.

Slab efficiency in joint shear strength enhancement is investigated based on the amount of additional longitudinal reinforcement placed in the slab. Effective slab reinforcement is considered to be the longitudinal reinforcement placed in the effective slab width as defined by the ACI 318R-08 equations described in Section 2.3.2 of this report.

To obtain the slab reinforcement index, additional longitudinal reinforcement area aligned in the loading direction in the effective slab width is compared with the effective beam reinforcement area considered for the basic shear strength prediction ( $V_{j0}$ ). Since the area increase due to slab reinforcement is a direct indicator of shear strength enhancement of the connection, created index is directly used as the slab factor.

$$\text{Slab Factor (SF)} = (A_{\text{beam,eff}} + A_{\text{slab,eff}}) / A_{\text{beam,eff}} \quad (4.4)$$

where,  $A_{\text{beam,eff}} =$  top beam reinforcement area for exterior connections,

$A_{\text{beam,eff}} =$  total beam reinforcement area for interior connections,

$A_{\text{slab,eff}} =$  slab reinforcement area in the effective slab width.

As the study proceeds, it is noticed that excessive use of slab reinforcement, even in the effective slab width, does not enhance the shear strength as expected. In order to overcome this condition, a maximum effective slab reinforcement area derived from the minimum slab reinforcement ratio defined in ACI 318R-08 is computed. The maximum effective slab reinforcement area is limited to five times the minimum slab reinforcement area and slab reinforcement exceeding this limit is assumed to be

ineffective. This approach is preferred instead of specifying a fixed coefficient in order to make the limitation case-specific.

Upper Limit of  $A_{slab,eff} = 5 \times \text{min. Slab Reinf. Ratio}$

where,

min. Slab Reinf. Ratio is obtained as the minimum ratio given by the following three equations:

$$\begin{aligned}
 &= \frac{0.0018 \cdot 420}{f_y} && (f_y \text{ in MPa}) \\
 &= \frac{0.0018 \cdot 60000}{f_y} && (f_y \text{ in psi}) && \text{(4.5)} \\
 &\geq 0.0014
 \end{aligned}$$

The min. Slab Reinf. Ratio values for common reinforcement yield strengths are provided below:

min. Slab Reinf. Ratio = 0.0020 for slabs where deformed bars with yield strengths of 280 or 350 MPa (40 or 50 ksi) are used,  
 = 0.0018 for slabs where deformed bars with yield strengths of 420 MPa (60 ksi) or welded wire reinforcement are used

#### 4.2.5 Surrounding Beam Factor

Effect of surrounding beams in confining the joint region is one of the primary variables affecting the performance of beam-to-column connections. General tendency to account for the surrounding element conditions around beam-to-column connections is to assign certain coefficients in accordance with the number of beams framing into the connection. In this study, instead of establishing specific values based on number of beams, development of an index considering both the direction of the beam and the ratio of the width of the column face covered by the beam width

is preferred. The main reason to follow such an approach is to be able to represent the surrounding beam conditions accurately, not only depending on the number of beams but also considering the widths and directions of framing members. The resulting surrounding beam index is:

$$\text{Surrounding Beam Index (SBI): } \sum (b_{b,i}/b_{c,i} \times r_{\text{eff},i}) \quad (4.6)$$

where,  $b_{b,i}$  = beam width framing into the joint,

$b_{c,i}$  = column width where the beam frames into the joint,

$r_{\text{eff},i}$  = efficiency ratio of beam.

Determination of the relative efficiency of confinement provided by the beams in the loading direction compared to the transverse beams is based on the variation of coefficients specified in ACI 352R-02 recommendations and denoted by  $r_{\text{eff},i}$ .

*Determination of Efficiency Ratio ( $r_{\text{eff}}$ ):*

Relative efficiency of a beam in confining the joint region is addressed in terms of the direction of beam. ACI 352R-02 joint shear coefficients for connections under load reversals are used as a guide in determination of efficiency ratios for confinement provided by beams in the loading and transverse directions. In ACI 352R-02, confinement by two beams in the loading direction has the same coefficient with confinement by one beam in the loading direction and two in the transverse direction. In other words, confinement provided by two transverse beams is considered to be equal to the confinement provided by one beam in the loading direction. Referring to ACI 325R-02, any beam in the loading direction is accepted to be twice as efficient as a beam in the transverse direction. In this manner, efficiency ratio for a transverse beam is 1/6, whereas the ratio is 2/6 for a beam in the loading direction, summing up to 1 for a fully surrounded connection by four beams. Beam confinement is considered only when the beam width covers 3/4 of the column face, to be compatible with ACI 352R-02 Recommendations.

After determination of respective confinement indices for each beam-to-column subassembly, the factor for the enhancement of joint shear strength by surrounding beams is determined as:

$$\text{Surrounding Beam Factor (SBF)} = (1 + \text{SBI}/4) \quad (4.7)$$

#### 4.2.6 Shear Reinforcement Ratio Factor

The confinement provided by the joint shear reinforcement depends significantly on the selection of the transverse reinforcement ratio. Volumetric transverse reinforcement ratios are computed for the gross and core sections of the joint and for the effective volume that contains one layer of joint shear reinforcement in each section to observe which gives the best correlation with the confining effect. The definition of each volumetric ratio is given below:

$$\begin{aligned} \rho_{\text{gross,total}} &= \frac{A_{s,\text{one}} \times L_{s,\text{one}} \times n_{\text{total}}}{h_c \times b_c \times d_b} \\ \rho_{\text{core,total}} &= \frac{A_{s,\text{one}} \times L_{s,\text{one}} \times n_{\text{core}}}{h_{c,\text{core}} \times b_{c,\text{core}} \times d_{b,\text{core}}} \\ \rho_{\text{gross,one}} &= \frac{A_{s,\text{one}} \times L_{s,\text{one}}}{h_c \times b_c \times s} \\ \rho_{\text{core,one}} &= \frac{A_{s,\text{one}} \times L_{s,\text{one}}}{h_{c,\text{core}} \times b_{c,\text{core}} \times s} \end{aligned} \quad (4.8)$$

where,  $A_{s,\text{one}}$  = cross sectional area of transverse reinforcement,

$L_{s,\text{one}}$  = total length of transverse reinforcement for one layer, aligned in the direction of loading,

$n_{\text{gross}}$  = number of transverse reinforcement layers in total beam height,

$n_{\text{core}}$  = number of transverse reinforcement layers between top and bottom longitudinal beam reinforcement,

$s$  = transverse reinforcement spacing,

$h_c, b_c$  = depth and width of column, respectively,

$h_{c,core}, b_{c,core}$  = depth and width of confined column section,

$d_b, d_{b,core}$  = effective beam depth and distance between top and bottom longitudinal beam reinforcement, respectively.

After the selection of the joint shear reinforcement ratio that has the best correlation with the confinement effect, the joint shear reinforcement index is defined as the enhancement or deterioration of confinement by the use of transverse reinforcement over or under a limiting value, respectively. Experimental data in the constructed database is examined to determine an optimum value for this limit. Volumetric transverse reinforcement ratios ranging from 0.5 % to 2.5 % are evaluated and 0.75 % core shear reinforcement ratio for the effective volume that contains one layer of shear reinforcement ( $\rho_{core,one}$ ) is determined to be the best indicator of the transverse reinforcement confinement effect. However, a limiting value of 1.00 % is used in the definition of the index in order not to complicate the equation, since the error induced by changing the limit from 0.75% to 1.00% was negligible.

$$SRI = \rho_{core,one} - 0.01 \quad (4.9)$$

The shear reinforcement factor deteriorates the confinement effect for connections with core reinforcement ratios for the effective volume that contains one layer of shear reinforcement less than 1.0 % and enhances it for ratios higher than 1.0 %.

$$\text{Shear Reinforcement Factor (SRF)} = 1 + 10 \times SRI \quad (4.10)$$

#### 4.2.7 Shear Reinforcement $f_{yield}$ Factor

Another parameter that influences the efficiency of transverse shear reinforcement has been identified as the yield strength of the shear reinforcement. From the large spectrum of yield strength values tested, 483.0 MPa, which corresponds to a 15% strain hardening of 420 MPa reinforcement, is determined as a limiting value for the transverse shear reinforcement to be effective under high shear forces. It is observed

that as yielding of transverse shear reinforcement in the connection region is delayed, performance of the connection region improves.

The proximity of the yield strength to the limit is identified as the indicator of performance of the transverse reinforcement, after normalizing the difference by 483.0 MPa. The equations for the yield strength index (YSI) and yield strength factor (YS) are given below:

$$\text{Yield strength index, YSI} = \left( \frac{483.0 - f_y}{483.0} \right) \quad (4.11)$$

$$\text{Yield strength factor, YS} = (1 - \text{YSI}/4) \quad (4.12)$$

#### 4.2.8 Wide Beam Factor

For wide beam-to-column connection specimens, the longitudinal beam reinforcement outside the effective joint width does not function as effective as the reinforcement passing through the joint. Prior experimental research reveal that even at specimen failure, some of the exterior longitudinal beam bars do not reach their yield strength, although all the interior bars are yielded. Consequently, the basic shear strength prediction ( $V_{j0}$ ), which assumes all the longitudinal bars are yielded, is an over estimation for wide beam-to-column connections.

In order to overcome this problem, an index representing the longitudinal reinforcement layout of the wide beam framing into the connection region is defined. Main parameter that identifies the over estimation of shear strength capacity of wide beam-to-column connections is determined to be the longitudinal reinforcement area passing outside the joint width, in accordance with the wide beam effective joint width definition aforementioned in '*Section 2.6, Wide Beam-to-Column Connections*'.

Wide beam index (WBI) is specified as the ratio of the longitudinal reinforcement area passing inside the joint width to the total area of beam bars. For interior connections, area of both bottom and top bars passing through the effective joint width is divided by total reinforcement area, whereas for exterior connections, the

area of top beam bars inside the joint width is divided by the total area of top beam bars.

$$\text{Wide Beam Index (WBI)} = A_{bj,wide} / A_{wide} \quad (4.13)$$

where,  $A_{wide}$  : total area of wide beam bars,

$A_{bj,wide}$  : area of beam bars passing through the effective joint width.

Strain distributions observed in wide beam-to-column connections also reveal that, even if the beam bars away from the joint core do not reach their yield strength, they still experience considerable strains and cannot be seen as totally ineffective. In order to account for contribution of bars passing outside the core, square root of wide beam index is taken as the wide beam factor.

To limit the Wide Beam Factor in order not to create excessive strength reduction, in accordance with the geometrical properties of wide beam-to-column connections, minimum value of WBF is taken as *the ratio of effective joint width to wide beam width*:

$$\text{Wide Beam Factor (WBF)} = \sqrt{\text{WBI}} \leq b_{j,wide} / b_{w,wide} \quad (4.14)$$

#### 4.2.9 Bond Factor

The bond between longitudinal reinforcement of the beam in the loading direction and concrete is one of the vital parameters affecting the performance of beam-to-column connections, especially when subjected to cyclic loading. In the light of experimental data, it is obvious that both shear strength and shear strain response of a connection is strongly related to the bond characteristics.

The bond strength is evaluated in based on the column width to beam bar diameter ratio and the yield strength of longitudinal beam reinforcement. In determination of the bond adequacy, ACI 352R-02 recommendations (which are previously stated in section 2.3.3) are taken as reference. Bars passing through the column core and outside the column core are evaluated separately. Limiting values to define the

optimum bond conditions are restated below and defined as the bond limit in description of the bond index.

For bars passing through the column core:

$$\frac{h_{\text{(column)}}}{d_{\text{b(beam bars)}}} \geq 20 \frac{f_y}{60000} \geq 20 \quad (\text{psi}) \quad (2.25)$$

$$\frac{h_{\text{(column)}}}{d_{\text{b(beam bars)}}} \geq 20 \frac{f_y}{420} \geq 20 \quad (\text{MPa})$$

For bars passing outside the column core:

$$\frac{h_{\text{(column)}}}{d_{\text{b(beam bars)}}} \geq 24 \frac{f_y}{60000} \geq 24 \quad (\text{psi}) \quad (2.26)$$

$$\frac{h_{\text{(column)}}}{d_{\text{b(beam bars)}}} \geq 24 \frac{f_y}{420} \geq 24 \quad (\text{MPa})$$

Longitudinal beam bars evaluated as ‘bonded’ or ‘not bonded’ with respect to the aforementioned limits. If the bars are evaluated as ‘not bonded’, extent of bond deficiency is determined by comparing the ratio of beam bar diameter to column depth with the respective limit and termed as ‘bond index’ (*BI*) of the bar.

$$\text{Bond Index (BI)} = \frac{(h_{\text{column}}/d_{\text{b,beambars}})}{\text{Bond Limit}} \quad (4.15)$$

Weighted average of bond indices of all beam bars is taken as the indicator of bond resistance of the connection, forming bond factor.

$$\text{Bond Factor (BF)} = \frac{\sum (BI_i * A_i)}{\sum A_i} \quad (4.16)$$

where,  $A_i$  = Cross sectional area of longitudinal beam bar.

#### 4.2.10 Eccentricity Factor

Eccentric connections are observed on exterior faces of many reinforced concrete buildings. Prior research indicated that eccentricity decreases the shear strength capacity and increases deformations by means of additional shear forces created within the connection region. In this research project, the effect of eccentricity on the connection behavior is analyzed following ACI 352R-02 recommendations by checking the ratio of the distance between the beam and column centroidal axes to the column width.

For specimens that include a floor system, the deterioration of joint strength due to eccentricity is minimized, whereas for specimens without slab, eccentricity values exceeding one-eighth of column width is known to decrease shear strength. Accordingly, effective part of the eccentricity ( $e_{\text{eff}}$ ) is taken as the distance exceeding one eighth of the column width. Eccentricity index is the ratio of effective eccentricity to column width.

Eccentricity Index (EI) =  $e_{\text{eff}}$ /column width

where,  $e_{\text{eff}}$  = eccentricity –  $b_c/8$ . (4.17)

The deterioration of the shear strength capacity of an eccentric connection without slab is observed to be proportional to 25% of eccentricity index.

Eccentricity Factor (EF) =  $1 - EI/4$  (4.18)

For connections with slabs, effect of eccentricity is negligible based on prior experimental and analytical research, so if there is a floor system, the effect of eccentricity is neglected in the model.

#### 4.2.11 Summary of Joint Shear Strength Prediction

The joint shear strength prediction for selected experiments in the database is presented as a summary in **Table 4.1**. Basic shear strength prediction, adjustment

factors and resultant joint shear strength prediction are listed for each specimen. The resultant joint shear strength ( $V_{j,final}$ ) is:

$$V_{j,final} = V_{j0} (AF) (SF) (SBF) (SRF) (YS) (WBF) (BF) (EF) \quad (4.19)$$

**Table 4.1: Joint Shear Strength Prediction**

No.	Researcher	Specimen	Vj0	AF	SF	SBF	SRF	YS	WBF	BF	EF	Vj,final (kN)
			(kN)									
1	B. Burak, J. K. Wight	1-S	466.62	1.03	1.24	1.13	1.07	0.98	1.00	1.00	1.00	700.95
2		2-S	620.94	1.02	1.18	1.11	1.00	0.98	1.00	1.00	1.00	815.46
3		3-S	620.94	1.02	1.18	1.11	1.00	0.98	1.00	1.00	1.00	816.81
4		1-N	233.31	1.02	1.97	1.11	1.07	0.98	1.00	1.00	1.00	546.58
5		2-N	521.59	1.02	1.44	1.10	1.07	0.98	1.00	1.00	1.00	876.27
6		3-N	1,276.21	1.02	1.09	1.10	1.07	0.98	0.78	1.00	1.00	1,262.15
7	G. S. Raffaele, J. K. Wight	1	643.43	1.01	1.00	1.12	1.00	1.00	1.00	0.97	1.00	698.74
8		2	428.95	1.01	1.00	1.08	1.00	1.00	1.00	0.97	0.98	441.62
9		3	443.53	1.01	1.00	1.09	1.00	1.00	1.00	1.00	0.98	474.73
10		4	443.53	1.02	1.00	1.09	1.00	1.00	1.00	1.00	0.98	478.91
11	M. Shin, J. LaFave	SL 1	573.61	1.00	1.12	1.13	0.96	0.98	1.00	0.93	1.00	640.47
12		SL 2	573.61	1.00	1.12	1.10	0.96	0.98	1.00	0.93	1.00	619.53
13		SL3	573.61	1.00	1.12	1.13	0.96	0.98	1.00	0.93	1.00	636.45
14		SL4	573.61	1.00	1.24	1.16	1.01	0.98	1.00	0.98	1.00	797.17
15	T. R. Gentry, J. K. Wight	WB1	835.19	1.01	1.00	1.13	1.00	0.97	0.75	0.95	1.00	656.95
16		WB2	742.40	1.01	1.00	1.13	1.00	0.97	0.77	0.95	1.00	607.89
17		WB3	783.01	1.01	1.00	1.13	1.00	0.97	0.84	0.99	1.00	719.93
18		WB4	1,043.28	1.01	1.00	1.13	1.00	0.97	0.75	0.95	1.00	822.23
19	J. LaFave, J. K. Wight	EWB - 1	727.98	1.00	1.09	1.13	1.00	1.00	0.82	0.99	1.00	728.24
20		EWB - 2	800.26	1.00	1.08	1.12	1.00	1.00	0.84	0.96	1.00	784.61
21		EWB - 3	1,059.22	1.00	1.05	1.11	1.01	1.00	0.72	1.00	1.00	890.98
22		ENB - 1	295.76	1.00	1.58	1.11	1.01	1.00	1.00	1.00	1.00	523.27
23	C. G. Quintero-Febres, J. K. Wight	IWB - 1	1,048.20	1.00	1.00	1.19	1.02	1.00	0.74	0.98	1.00	915.04
24		IWB - 2	1,048.20	1.00	1.06	1.19	1.02	1.00	0.81	0.98	1.00	1,059.83
25		IWB - 3	1,285.22	1.00	1.00	1.19	1.00	1.00	0.80	1.00	1.00	1,226.83
26	A. J. Durrani J. K. Wight	X1	906.60	1.03	1.00	1.13	0.98	0.93	1.00	0.94	1.00	899.30
27		X2	906.60	1.03	1.00	1.13	1.03	0.93	1.00	0.94	1.00	938.24
28		X3	679.95	1.03	1.00	1.13	0.98	0.93	1.00	0.94	1.00	673.94
29		S1	738.90	1.03	1.15	1.19	0.98	0.93	1.00	0.95	1.00	904.37
30		S2	738.90	1.04	1.15	1.19	1.03	0.93	1.00	0.95	1.00	952.25
31		S3	551.56	1.03	1.19	1.19	0.98	0.93	1.00	0.94	1.00	697.93
32	O. Joh, Y. Goto, T. Shibata	JXO-B1	295.22	1.08	1.00	1.08	0.92	0.91	1.00	1.00	1.00	290.04
33		JXO-B2	295.22	1.08	1.00	1.13	0.92	0.91	1.00	1.00	1.00	301.73
34		JXO-B5	295.22	1.07	1.00	1.08	0.92	0.91	1.00	1.00	0.98	281.17
35		JXO-B6	295.22	1.08	1.00	1.08	0.92	0.91	1.00	1.00	0.98	281.77
36	S.Fujii, S.Morita	A1	606.96	1.04	1.00	1.12	0.96	0.90	1.00	0.72	1.00	436.07
37		A2	513.89	1.04	1.00	1.12	0.96	0.90	1.00	1.00	1.00	515.57
38		A3	606.96	1.11	1.00	1.12	0.96	0.90	1.00	0.72	1.00	467.84
39		A4	606.96	1.11	1.00	1.12	1.06	0.90	1.00	0.72	1.00	519.74
40		B1	303.48	1.03	1.00	1.06	0.96	0.90	1.00	0.72	1.00	205.45
41		B2	256.94	1.03	1.00	1.06	0.96	0.90	1.00	1.00	1.00	242.90
42		B3	303.48	1.12	1.00	1.06	0.96	0.90	1.00	0.72	1.00	222.23
43		B4	303.48	1.12	1.00	1.06	1.06	0.90	1.00	0.72	1.00	246.88
44	Y. Kurose, G. N.Guimaraes, L. Zuhua, M. E. Krieger, J. O. Jirsa	J1 (EW)	1,640.96	1.00	1.12	1.13	0.98	1.00	1.00	0.97	1.00	1,978.53
45		J2 (EW)	2,234.63	1.00	1.09	1.19	0.98	1.00	1.00	0.97	1.00	2,754.06
46		J2 (NS)	2,234.63	1.00	1.11	1.19	0.98	1.00	1.00	0.97	1.00	2,791.96
47		J3 (EW)	1,480.26	1.00	1.13	1.13	0.98	1.00	1.00	0.92	1.00	1,705.62
48		J3 (NS)	1,640.96	1.00	1.10	1.16	0.98	1.00	1.00	0.97	1.00	1,996.74
49	P.C. Cheung et al.	2D-E (EW)	700.60	1.00	1.13	1.11	1.07	0.92	1.00	1.00	1.00	861.02

**Table 4.1: Joint Shear Strength Prediction (continued)**

No.	Researcher	Specimen	$V_{jo}$	AF	SF	SBF	SRF	YS	WBF	BF	EF	$V_{j,final}$
			(kN)									(kN)
50	S. Teng, H. Zhou	S1	776.90	1.06	1.00	1.08	0.98	0.98	1.00	0.89	1.00	756.31
51		S2	776.90	1.05	1.00	1.08	0.98	0.98	1.00	0.89	1.00	755.14
52		S3	776.90	1.05	1.00	1.08	0.98	0.98	1.00	0.89	0.98	735.18
53		S5	451.29	1.05	1.00	1.08	1.02	0.98	1.00	0.88	1.00	451.23
54		S6	451.29	1.06	1.00	1.08	1.02	0.98	1.00	0.88	0.98	440.55
55		F. Kusuvara, K. Azukawa, H. Shiohara, S. Otani	JE-0	585.91	1.00	1.00	1.09	0.93	0.94	1.00	1.00	1.00
56	JE-55		585.91	1.00	1.00	1.09	0.93	0.94	1.00	1.00	0.99	551.39
57	JE-55S		585.91	1.00	1.00	1.09	0.95	0.94	1.00	1.00	0.99	568.33
58	H. Shioara, F. Kusuvara	A2	484.21	1.04	1.00	1.06	0.95	0.92	1.00	1.00	1.00	466.90
59		A3	484.21	1.04	1.00	1.06	0.95	0.92	1.00	1.00	1.00	466.90
60		B1	605.26	1.04	1.00	1.06	0.95	0.92	1.00	1.00	1.00	583.62
61		B2	605.26	1.04	1.00	1.06	0.95	0.92	1.00	1.00	1.00	583.62
62	H. J. Lee, J. W. KO	S0	691.08	1.04	1.00	1.06	0.97	0.99	1.00	1.00	1.00	737.11
63		S50	691.08	1.04	1.00	1.06	0.97	0.99	1.00	1.00	1.00	735.63
64		W0	691.08	1.05	1.00	1.04	0.97	0.99	1.00	0.92	1.00	669.70
65		W75	691.08	1.05	1.00	1.04	0.97	0.99	1.00	0.92	1.00	668.12
66		W150	691.08	1.05	1.00	1.04	0.97	0.99	1.00	0.92	0.98	652.74
67	S. J. Hwang, H. J. Lee, K. C. Wang	70-3T44	871.54	1.01	1.00	1.06	1.11	1.00	1.00	0.90	1.00	938.41
68		70-3T4	978.96	1.01	1.00	1.06	1.00	0.98	1.00	0.88	1.00	893.67
69		70-2T5	978.96	1.01	1.00	1.06	0.97	0.99	1.00	0.88	1.00	880.42
70		70-1T55	978.96	1.01	1.00	1.06	0.97	0.99	1.00	0.88	1.00	880.76
71		28-3T4	978.96	1.01	1.00	1.06	0.94	0.98	1.00	0.96	1.00	924.68
72		28-0T0	978.96	1.01	1.00	1.06	0.90	1.00	1.00	0.96	1.00	906.18
73	Y. Goto, O. Joh	UM-0	1,101.62	1.08	1.00	1.07	0.93	0.93	1.00	0.71	1.00	782.11
74		UM-60	1,101.62	1.08	1.00	1.07	0.93	0.93	1.00	0.71	1.00	780.81
75		UM-125	1,101.62	1.08	1.00	1.07	0.93	0.93	1.00	0.71	0.97	758.21
76	F. Alameddine, M. R. Ehsani	LL 8	926.23	1.02	1.00	1.06	1.03	0.98	1.00	0.82	1.00	833.02
77		LH 8	926.23	1.02	1.00	1.06	1.09	0.98	1.00	0.82	1.00	885.52
78		HL 8	1,142.07	1.03	1.00	1.06	1.03	0.98	1.00	0.79	1.00	1,006.79
79		HH 8	1,142.07	1.03	1.00	1.06	1.09	0.98	1.00	0.79	1.00	1,070.25
80		LL 11	926.23	1.02	1.00	1.06	1.03	0.98	1.00	0.82	1.00	829.47
81		LH 11	926.23	1.01	1.00	1.06	1.10	0.98	1.00	0.82	1.00	884.52
82		HL 11	1,142.07	1.03	1.00	1.06	1.03	0.98	1.00	0.79	1.00	1,007.11
83		HH 11	1,142.07	1.03	1.00	1.06	1.10	0.98	1.00	0.79	1.00	1,072.74
84		LL 14	926.23	1.01	1.00	1.06	1.04	0.98	1.00	0.82	1.00	829.46
85		LH 14	926.23	1.01	1.00	1.06	1.09	0.98	1.00	0.82	1.00	876.54
86		HH 14	1,142.07	1.02	1.00	1.06	1.09	0.98	1.00	0.79	1.00	1,055.73
87	C. C. Chen, G. K. Chen	JC	910.52	1.00	1.00	1.05	1.00	0.96	1.00	1.00	1.00	917.57
88		JE	910.52	1.00	1.00	1.05	1.00	0.96	1.00	1.00	0.99	903.80
89		JS1	910.52	1.00	1.00	1.05	1.00	0.96	1.00	1.00	0.99	903.80
90		JS2	910.52	1.00	1.00	1.05	1.00	0.96	1.00	1.00	0.99	903.80
91		JS3	910.52	1.00	1.00	1.05	1.00	0.96	1.00	1.00	0.99	903.80
92		JS4	910.52	1.00	1.00	1.05	1.00	0.96	1.00	1.00	0.99	903.80

**Table 4.1: Joint Shear Strength Prediction (continued)**

No.	Researcher	Specimen	$V_{jo}$	AF	SF	SBF	SRF	YS	WBF	BF	EF	$V_{j,final}$
			(kN)									(kN)
93	<i>H. F. Wong, J. S. Kuang</i>	JA-NN03	303.48	1.02	1.00	1.06	0.90	1.00	1.00	0.92	1.00	271.67
94		JA-NN15	303.48	1.08	1.00	1.06	0.90	1.00	1.00	0.92	1.00	287.73
95		JA-NY03	303.48	1.02	1.00	1.06	0.95	1.00	1.00	0.92	1.00	287.93
96		JA-NY15	303.48	1.08	1.00	1.06	0.95	1.00	1.00	0.92	1.00	304.95
97		JB-NN03	303.48	1.02	1.00	1.06	0.90	1.00	1.00	0.92	1.00	271.67
98		JB-NY03	303.48	1.02	1.00	1.06	0.95	1.00	1.00	0.92	1.00	287.93
99	<i>H. F. Wong, J. S. Kuang</i>	BS-L-300	455.22	1.08	1.00	1.06	0.90	1.00	1.00	0.80	1.00	375.71
100		BS-L-450	455.22	1.08	1.00	1.06	0.90	1.00	1.00	0.80	1.00	375.71
101		BS-L-600	455.22	1.08	1.00	1.06	0.90	1.00	1.00	0.80	1.00	375.71
102		BS-L-V2	455.22	1.08	1.00	1.06	0.90	1.00	1.00	0.80	1.00	375.71
103		BS-L-V4	455.22	1.08	1.00	1.06	0.90	1.00	1.00	0.80	1.00	375.71
104		BS-L-H1	455.22	1.08	1.00	1.06	0.91	1.00	1.00	0.80	1.00	381.47
105		BS-L-H2	455.22	1.08	1.00	1.06	0.94	1.00	1.00	0.80	1.00	394.45
106	<i>M.R.Ehsani, J.K.Wight</i>	1S	294.77	1.18	1.41	1.13	1.02	0.98	1.00	0.89	1.00	490.63
107		2S	294.77	1.18	1.41	1.13	1.06	0.98	1.00	0.89	1.00	509.42
108		3S	294.77	1.18	1.41	1.13	1.03	0.98	1.00	0.89	1.00	495.84
109		4S	294.77	1.18	1.41	1.13	1.07	0.98	1.00	0.89	1.00	516.38
110		5S	385.17	1.22	1.38	1.13	1.00	0.98	1.00	0.95	1.00	676.48
111		6S	385.17	1.19	1.25	1.13	1.00	0.98	1.00	0.95	1.00	595.77
112	<i>B. Li, S. A. Kulkarni</i>	EWB-1	1,391.66	1.00	1.00	1.06	1.06	0.88	0.76	1.00	1.00	1,051.42
113		EWB-2	1,391.66	1.00	1.00	1.06	0.97	0.88	1.00	0.89	1.00	1,116.42
114		EWB-3	1,391.66	1.00	1.00	1.06	1.06	0.88	0.76	1.00	1.00	1,051.42

#### 4.2.12 Evaluation of Joint Shear Strength Prediction

The proposed joint shear strength ( $V_{j,proposed}$ ) is evaluated by comparing the prediction with the experimental values. The joint shear capacities are also obtained by following the procedures in TEC 2007 and ACI 352-02 and the accuracy of the proposed joint shear strength is compared with the accuracy of each code formulation in **Tables 4.2** and **4.3**, respectively. The tables also include the error and absolute error percentages for the proposed strength and the code values and the average error of each for the constructed database.

The error, absolute error and average error values are computed as:

$$\text{Error} = \frac{V_{j,\text{experimental}} - V_{j,\text{proposed}}}{V_{j,\text{experimental}}} \quad (4.20)$$

$$\text{Absolute Error} = |\text{Error}| \quad (4.21)$$

$$\text{Average Error} = \frac{\sum \text{Error}}{n} \quad (4.22)$$

where,  $V_{j,\text{experimental}}$  = The experimental value of joint shear strength,

$V_{j,\text{proposed}}$  = The analytical prediction of joint shear strength,

$n$  = number of specimens.

**Table 4.2: Comparison of Joint Shear Strength Accuracy,  $V_{j,proposed}$  vs.  $V_{j,TEC}$**

No.	Researcher	Specimen	$V_{j,experimental}$ (kN)	$V_{j,proposed}$ (kN)	% Error	% Abs. Error	$V_{j,TEC}$	% Error	% Abs. Error
1	<i>B. Burak, J. K. Wight</i>	1-S	778.44	700.95	9.955	9.955	839.84	7.888	7.888
2		2-S	862.95	815.46	5.503	5.503	1,405.70	62.894	62.894
3		3-S	827.37	816.81	1.276	1.276	1,045.26	26.336	26.336
4		1-N	569.37	546.58	4.002	4.002	1,466.84	157.623	157.623
5		2-N	809.58	876.27	-8.238	8.238	2,958.96	265.495	265.495
6		3-N	1,156.54	1,262.15	-9.132	9.132	2,200.25	90.245	90.245
7	<i>G. S. Raffaele, J. K. Wight</i>	1	650.77	698.74	-7.370	7.370	1,033.77	58.852	58.852
8		2	420.58	441.62	-5.003	5.003	678.30	61.278	61.278
9		3	469.73	474.73	-1.064	1.064	1,021.93	117.557	117.557
10		4	412.35	478.91	-16.143	16.143	523.11	26.861	26.861
11	<i>M. Shin, J. LaFave</i>	SL 1	644.99	640.47	0.701	0.701	1,104.26	71.206	71.206
12		SL 2	649.44	619.53	4.605	4.605	848.44	30.641	30.641
13		SL3	644.99	636.45	1.325	1.325	2,864.51	344.116	344.116
14		SL4	791.78	797.17	-0.680	0.680	1,282.76	62.009	62.009
15	<i>T. R. Gentry, J. K. Wight</i>	WB1	616.13	656.95	-6.626	6.626	1,405.42	128.106	128.106
16		WB2	643.07	607.89	5.471	5.471	1,405.42	118.548	118.548
17		WB3	725.59	719.93	0.780	0.780	1,911.10	163.384	163.384
18		WB4	813.72	822.23	-1.046	1.046	1,911.10	134.860	134.860
19	<i>J. LaFave, J. K. Wight</i>	EWB - 1	752.73	728.24	3.254	3.254	1,464.71	94.586	94.586
20		EWB - 2	819.96	784.61	4.312	4.312	1,534.46	87.138	87.138
21		EWB - 3	1,094.69	890.98	18.609	18.609	2,135.15	95.045	95.045
22		ENB - 1	540.37	523.27	3.165	3.165	1,537.31	184.491	184.491
23	<i>C. G. Quintero- Febres, J. K. Wight</i>	IWB - 1	903.18	915.04	-1.313	1.313	2,706.05	199.612	199.612
24		IWB - 2	991.37	1,059.83	-6.906	6.906	2,085.12	110.327	110.327
25		IWB - 3	1,128.75	1,226.83	-8.689	8.689	2,557.10	126.543	126.543
26	<i>A. J. Durrani J. K. Wight</i>	X1	840.04	899.30	-7.054	7.054	1,799.31	114.194	114.194
27		X2	853.59	938.24	-9.917	9.917	1,763.18	106.561	106.561
28		X3	628.67	673.94	-7.200	7.200	1,625.88	158.621	158.621
29		S1	924.04	904.37	2.128	2.128	3,268.02	253.666	253.666
30		S2	924.95	952.25	-2.952	2.952	2,417.14	161.328	161.328
31		S3	720.81	697.93	3.173	3.173	2,222.04	208.271	208.271
32	<i>O. Joh, Y. Goto, T. Shibata</i>	JXO-B1	293.38	290.04	1.136	1.136	766.10	161.131	161.131
33		JXO-B2	311.24	301.73	3.056	3.056	748.44	140.472	140.472
34		JXO-B5	298.14	281.17	5.691	5.691	414.82	39.136	39.136
35		JXO-B6	310.85	281.77	9.354	9.354	402.46	29.472	29.472

**Table 4.2: Comparison of Joint Shear Strength Accuracy,  $V_{j,proposed}$  vs.  $V_{j,TEC}$  (continued)**

Researcher	Specimen	$V_{j,experimental}$ (kN)	$V_{j,proposed}$ (kN)	% Error	% Abs. Error	$V_{j,TEC}$	% Error	% Abs. Error
<i>S. Fujii, S. Morita</i>	A1	412.02	436.07	-5.838	5.838	778.41	88.926	88.926
	A2	379.65	515.57	-35.803	35.803	778.41	105.036	105.036
	A3	412.02	467.84	-13.549	13.549	778.41	88.926	88.926
	A4	420.85	519.74	-23.497	23.497	778.41	84.962	84.962
	B1	246.23	205.45	16.563	16.563	580.96	135.942	135.942
	B2	213.86	242.90	-13.582	13.582	580.96	171.658	171.658
	B3	272.72	222.23	18.514	18.514	580.96	113.027	113.027
	B4	287.43	246.88	14.110	14.110	580.96	102.121	102.121
<i>Y. Kurose, G. N. Guimaraes, L. Zuhua, M. E. Kreger, J. O. Jirsa</i>	J1 (EW)	2,001.70	1,978.53	1.157	1.157	2,491.00	24.444	24.444
	J2 (EW)	2,962.52	2,754.06	7.036	7.036	4,280.97	44.505	44.505
	J2 (NS)	2,562.18	2,791.96	-8.968	8.968	4,280.97	67.083	67.083
	J3 (EW)	1,825.55	1,705.62	6.570	6.570	3,345.06	83.236	83.236
	J3 (NS)	1,921.63	1,996.74	-3.909	3.909	3,345.06	74.074	74.074
<i>P.C. Cheung et al.</i>	2D-E (EW)	925.09	861.02	6.926	6.926	4,180.00	351.847	351.847
<i>S. Teng, H. Zhou</i>	S1	775.80	756.31	2.512	2.512	1,584.00	104.176	104.176
	S2	772.20	755.14	2.209	2.209	1,224.00	58.508	58.508
	S3	742.50	735.18	0.985	0.985	840.00	13.131	13.131
	S5	452.40	451.23	0.259	0.259	936.00	106.897	106.897
	S6	439.20	440.55	-0.308	0.308	608.00	38.434	38.434
<i>F. Kusuhara, K. Azukawa, H. Shiohara, S. Otani</i>	JE-0	609.28	556.61	8.644	8.644	967.68	58.824	58.824
	JE-55	504.56	551.39	-9.282	9.282	635.04	25.860	25.860
	JE-55S	497.14	568.33	-14.319	14.319	635.04	27.739	27.739
<i>H. Shioara, F. Kusuhara</i>	A2	444.10	466.90	-5.134	5.134	1,018.80	129.410	129.410
	A3	414.62	466.90	-12.610	12.610	1,018.80	145.722	145.722
	B1	559.25	583.62	-4.357	4.357	1,018.80	82.171	82.171
	B2	525.62	583.62	-11.035	11.035	1,018.80	93.829	93.829
<i>H. J. Lee, J. W. KO</i>	S0	828.00	737.11	10.977	10.977	3,129.60	277.971	277.971
	S50	789.00	735.63	6.764	6.764	2,462.40	212.091	212.091
	W0	775.00	669.70	13.587	13.587	2,774.40	257.987	257.987
	W75	780.00	668.12	14.344	14.344	2,188.80	180.615	180.615
	W150	710.00	652.74	8.064	8.064	1,396.80	96.732	96.732
<i>S. J. Hwang, H. J. Lee, K. C. Wang</i>	70-3T44	1,065.00	938.41	11.886	11.886	5,419.01	408.827	408.827
	70-3T4	1,110.00	893.67	19.489	19.489	6,091.20	448.757	448.757
	70-2T5	1,162.00	880.42	24.232	24.232	6,204.60	433.959	433.959
	70-1T55	1,126.00	880.76	21.780	21.780	5,645.70	401.394	401.394
	28-3T4	1,290.00	924.68	28.319	28.319	4,235.00	228.295	228.295
	28-0T0	1,138.00	906.18	20.371	20.371	3,993.00	250.879	250.879
<i>Y. Goto, O. Joh</i>	UM-0	810.00	782.11	3.443	3.443	1,296.00	60.000	60.000
	UM-60	780.00	780.81	-0.103	0.103	974.16	24.892	24.892
	UM-125	670.00	758.21	-13.166	13.166	604.80	-9.731	9.731

**Table 4.2: Comparison of Joint Shear Strength Accuracy,  $V_{j,proposed}$  vs.  $V_{j,TEC}$   
(continued)**

No.	Researcher	Specimen	$V_{j,experimental}$ (kN)	$V_{j,proposed}$ (kN)	% Error	% Abs. Error	$V_{j,TEC}$	% Error	% Abs. Error	
76	<i>F. Alameddine, M. R. Ehsani</i>	LL 8	860.29	833.02	3.170	3.170	2,990.45	247.611	247.611	
77		LH 8	838.04	885.52	-5.665	5.665	2,990.45	256.837	256.837	
78		HL 8	986.62	1,006.79	-2.045	2.045	2,990.45	203.102	203.102	
79		HH 8	985.73	1,070.25	-8.574	8.574	2,990.45	203.375	203.375	
80		LL 11	769.10	829.47	-7.849	7.849	3,724.55	384.275	384.275	
81		LH 11	934.13	884.52	5.310	5.310	3,724.55	298.720	298.720	
82		HL 11	967.49	1,007.11	-4.095	4.095	3,724.55	284.971	284.971	
83		HH 11	1,020.87	1,072.74	-5.081	5.081	3,724.55	264.842	264.842	
84		LL 14	877.63	829.46	5.489	5.489	4,784.72	445.184	445.184	
85		LH 14	890.53	876.54	1.571	1.571	4,784.72	437.287	437.287	
86		HH 14	1,032.43	1,055.73	-2.257	2.257	4,784.72	363.442	363.442	
87		<i>C. C. Chen, G. K. Chen</i>	JC	904.42	917.57	-1.453	1.453	1,999.20	121.048	121.048
88			JE	864.22	903.80	-4.581	4.581	1,193.64	38.118	38.118
89			JS1	954.98	903.80	5.359	5.359	1,193.64	24.991	24.991
90	JS2		966.21	903.80	6.459	6.459	1,270.08	31.449	31.449	
91	JS3		971.83	903.80	7.000	7.000	1,217.16	25.244	25.244	
92	JS4		977.45	903.80	7.535	7.535	1,205.40	23.321	23.321	
93	<i>H. F. Wong, J. S. Kuang</i>	JA-NN03	249.00	271.67	-9.104	9.104	1,612.80	547.711	547.711	
94		JA-NN15	311.00	287.73	7.483	7.483	1,656.00	432.476	432.476	
95		JA-NY03	235.60	287.93	-22.211	22.211	1,255.68	432.971	432.971	
96		JA-NY15	308.50	304.95	1.151	1.151	1,385.28	349.037	349.037	
97		JB-NN03	313.00	271.67	13.205	13.205	1,707.84	445.636	445.636	
98		JB-NY03	307.30	287.93	6.303	6.303	1,229.76	300.182	300.182	
99	<i>H. F. Wong, J. S. Kuang</i>	BS-L-300	505.00	375.71	25.602	25.602	1,227.60	143.089	143.089	
100		BS-L-450	315.50	375.71	-19.084	19.084	1,112.40	252.583	252.583	
101		BS-L-600	283.90	375.71	-32.338	32.338	1,310.40	361.571	361.571	
102		BS-L-V2	398.80	375.71	5.790	5.790	1,173.60	194.283	194.283	
103		BS-L-V4	402.90	375.71	6.749	6.749	1,018.80	152.867	152.867	
104		BS-L-H1	389.30	381.47	2.010	2.010	1,198.80	207.937	207.937	
105		BS-L-H2	479.30	394.45	17.703	17.703	1,515.60	216.211	216.211	
106	<i>M.R.Ehsani, J.K.Wight</i>	1S	566.26	490.63	13.356	13.356	1,531.08	170.387	170.387	
107		2S	599.24	509.42	14.989	14.989	1,419.60	136.899	136.899	
108		3S	552.35	495.84	10.230	10.230	1,040.54	88.385	88.385	
109		4S	605.10	516.38	14.663	14.663	1,055.41	74.419	74.419	
110		5S	646.25	676.48	-4.679	4.679	1,108.63	71.548	71.548	
111		6S	744.08	595.77	19.932	19.932	1,626.20	118.551	118.551	
112	<i>B. Li, S. A. Kulkarni</i>	EWB-1	1,125.80	1,051.42	6.607	6.607	6,922.80	514.924	514.924	
113		EWB-2	1,726.02	1,116.42	35.318	35.318	7,117.20	312.348	312.348	
114		EWB-3	1,227.12	1,051.42	14.318	14.318	5,162.40	320.692	320.692	
<b>Average Error, %</b>						<b>8.92</b>			<b>170.26</b>	

**Table 4.3: Comparison of Joint Shear Strength Accuracy,  $V_{j,proposed}$  vs.  $V_{j,ACI,352}$**

No.	Researcher	Specimen	$V_{j,experimental}$ (kN)	$V_{j,proposed}$ (kN)	% Error	% Abs. Error	$V_{j,ACI}$	% Error	% Abs. Error
1	<i>B. Burak, J. K. Wight</i>	1-S	778.44	700.95	9.955	9.955	489.30	37.143	37.143
2		2-S	862.95	815.46	5.503	5.503	679.79	21.226	21.226
3		3-S	827.37	816.81	1.276	1.276	586.19	29.150	29.150
4		1-N	569.37	546.58	4.002	4.002	629.79	-10.612	10.612
5		2-N	809.58	876.27	-8.238	8.238	1,095.52	-35.321	35.321
6		3-N	1,156.54	1,262.15	-9.132	9.132	1,017.36	12.034	12.034
7	<i>G. S. Raffaele, J. K. Wight</i>	1	650.77	698.74	-7.370	7.370	577.46	11.266	11.266
8		2	420.58	441.62	-5.003	5.003	423.97	-0.805	0.805
9		3	469.73	474.73	-1.064	1.064	530.37	-12.909	12.909
10		4	412.35	478.91	-16.143	16.143	379.46	7.977	7.977
11	<i>M. Shin, J. LaFave</i>	SL 1	644.99	640.47	0.701	0.701	591.76	8.253	8.253
12		SL 2	649.44	619.53	4.605	4.605	449.38	30.804	30.804
13		SL3	644.99	636.45	1.325	1.325	819.86	-27.111	27.111
14		SL4	791.78	797.17	-0.680	0.680	715.20	9.673	9.673
15	<i>T. R. Gentry, J. K. Wight</i>	WB1	616.13	656.95	-6.626	6.626	829.86	-34.690	34.690
16		WB2	643.07	607.89	5.471	5.471	829.86	-29.046	29.046
17		WB3	725.59	719.93	0.780	0.780	967.70	-33.367	33.367
18		WB4	813.72	822.23	-1.046	1.046	967.70	-18.924	18.924
19	<i>J. LaFave, J. K. Wight</i>	EWB - 1	752.73	728.24	3.254	3.254	847.18	-12.548	12.548
20		EWB - 2	819.96	784.61	4.312	4.312	693.70	15.399	15.399
21		EWB - 3	1,094.69	890.98	18.609	18.609	905.49	17.284	17.284
22		ENB - 1	540.37	523.27	3.165	3.165	768.33	-42.186	42.186
23	<i>C. G. Quintero- Febres, J. K. Wight</i>	IWB - 1	903.18	915.04	-1.313	1.313	1,253.61	-38.799	38.799
24		IWB - 2	991.37	1,059.83	-6.906	6.906	1,100.42	-11.000	11.000
25		IWB - 3	1,128.75	1,226.83	-8.689	8.689	1,403.55	-24.345	24.345
26	<i>A. J. Durrani J. K. Wight</i>	X1	840.04	899.30	-7.054	7.054	846.75	-0.799	0.799
27		X2	853.59	938.24	-9.917	9.917	838.21	1.802	1.802
28		X3	628.67	673.94	-7.200	7.200	804.91	-28.033	28.033
29		S1	924.04	904.37	2.128	2.128	1,242.34	-34.446	34.446
30		S2	924.95	952.25	-2.952	2.952	1,068.44	-15.513	15.513
31		S3	720.81	697.93	3.173	3.173	1,024.41	-42.120	42.120
32	<i>O. Joh, Y. Goto, T. Shibata</i>	JXO-B1	293.38	290.04	1.136	1.136	310.14	-5.713	5.713
33		JXO-B2	311.24	301.73	3.056	3.056	493.87	-58.680	58.680
34		JXO-B5	298.14	281.17	5.691	5.691	279.71	6.182	6.182
35		JXO-B6	310.85	281.77	9.354	9.354	275.51	11.368	11.368
36	<i>S.Fujii, S.Morita</i>	A1	412.02	436.07	-5.838	5.838	263.99	35.928	35.928
37		A2	379.65	515.57	-35.803	35.803	263.99	30.464	30.464
38		A3	412.02	467.84	-13.549	13.549	263.99	35.928	35.928
39		A4	420.85	519.74	-23.497	23.497	263.99	37.272	37.272
40		B1	246.23	205.45	16.563	16.563	228.06	7.378	7.378
41		B2	213.86	242.90	-13.582	13.582	228.06	-6.643	6.643
42		B3	272.72	222.23	18.514	18.514	228.06	16.374	16.374
43		B4	287.43	246.88	14.110	14.110	228.06	20.655	20.655

**Table 4.3: Comparison of Joint Shear Strength Accuracy,  $V_{j,proposed}$  VS.  $V_{j,ACI,352}$   
(continued)**

No.	Researcher	Specimen	$V_{j,experimental}$ (kN)	$V_{j,proposed}$ (kN)	% Error	% Abs. Error	$V_{j,ACI}$	% Error	% Abs. Error
44	Y. Kurose, G. N. Guimaraes, L. Zuhua, M. E. Kreger, J. O. Jirsa	J1 (EW)	2,001.70	1,978.53	1.157	1.157	1,420.47	29.037	29.037
45		J2 (EW)	2,962.52	2,754.06	7.036	7.036	2,027.26	31.570	31.570
46		J2 (NS)	2,562.18	2,791.96	-8.968	8.968	2,027.26	20.877	20.877
47		J3 (EW)	1,825.55	1,705.62	6.570	6.570	1,646.07	9.832	9.832
48		J3 (NS)	1,921.63	1,996.74	-3.909	3.909	1,646.07	14.340	14.340
49	P.C. Cheung et al.	2D-E (EW)	925.09	861.02	6.926	6.926	1,519.59	-64.264	64.264
50	S. Teng, H. Zhou	S1	775.80	756.31	2.512	2.512	472.03	39.156	39.156
51		S2	772.20	755.14	2.209	2.209	479.13	37.953	37.953
52		S3	742.50	735.18	0.985	0.985	433.09	41.671	41.671
53		S5	452.40	451.23	0.259	0.259	311.00	31.255	31.255
54		S6	439.20	440.55	-0.308	0.308	282.43	35.695	35.695
55		F. Kusuhara, K. Azukawa, H. Shiohara, S. Otani	JE-0	609.28	556.61	8.644	8.644	362.28	40.540
56		JE-55	504.56	551.39	-9.282	9.282	321.70	36.241	36.241
57		JE-55S	497.14	568.33	-14.319	14.319	321.70	35.290	35.290
58	H. Shioara, F. Kusuhara	A2	444.10	466.90	-5.134	5.134	596.08	-34.223	34.223
59		A3	414.62	466.90	-12.610	12.610	596.08	-43.767	43.767
60		B1	559.25	583.62	-4.357	4.357	596.08	-6.585	6.585
61		B2	525.62	583.62	-11.035	11.035	476.86	9.276	9.276
62	H. J. Lee, J. W. KO	S0	828.00	737.11	10.977	10.977	1,194.23	-44.230	44.230
63		S50	789.00	735.63	6.764	6.764	1,223.18	-55.030	55.030
64		W0	775.00	669.70	13.587	13.587	856.70	-10.542	10.542
65		W75	780.00	668.12	14.344	14.344	878.65	-12.647	12.647
66		W150	710.00	652.74	8.064	8.064	773.69	-8.971	8.971
67		S. J. Hwang, H. J. Lee, K. C. Wang	70-3T44	1,065.00	938.41	11.886	11.886	1,356.41	-27.362
68	70-3T4		1,110.00	893.67	19.489	19.489	1,496.38	-34.809	34.809
69	70-2T5		1,162.00	880.42	24.232	24.232	1,510.24	-29.969	29.969
70	70-1T55		1,126.00	880.76	21.780	21.780	1,440.62	-27.941	27.941
71	28-3T4		1,290.00	924.68	28.319	28.319	1,506.99	-16.821	16.821
72	28-0T0		1,138.00	906.18	20.371	20.371	1,463.30	-28.585	28.585
73	Y. Goto, O. Joh	UM-0	810.00	782.11	3.443	3.443	402.55	50.303	50.303
74		UM-60	780.00	780.81	-0.103	0.103	363.09	53.450	53.450
75		UM-125	670.00	758.21	-13.166	13.166	367.49	45.151	45.151
76	F. Alameddine, M. R. Ehsani	LL 8	860.29	833.02	3.170	3.170	916.53	-6.538	6.538
77		LH 8	838.04	885.52	-5.665	5.665	916.53	-9.365	9.365
78		HL 8	986.62	1,006.79	-2.045	2.045	916.53	7.104	7.104
79		HH 8	985.73	1,070.25	-8.574	8.574	916.53	7.020	7.020
80		LL 11	769.10	829.47	-7.849	7.849	1,022.86	-32.995	32.995
81		LH 11	934.13	884.52	5.310	5.310	1,022.86	-9.499	9.499
82		HL 11	967.49	1,007.11	-4.095	4.095	1,022.86	-5.723	5.723
83		HH 11	1,020.87	1,072.74	-5.081	5.081	1,022.86	-0.195	0.195
84		LL 14	877.63	829.46	5.489	5.489	1,159.33	-32.097	32.097
85		LH 14	890.53	876.54	1.571	1.571	1,159.33	-30.184	30.184
86		HL 14	1,032.43	1,055.73	-2.257	2.257	1,159.33	-12.291	12.291

**Table 4.3: Comparison of Joint Shear Strength Accuracy,  $V_{j,proposed}$  VS.  $V_{j,ACI,352}$  (continued)**

No.	Researcher	Specimen	$V_{j,experimental}$ (kN)	$V_{j,proposed}$ (kN)	% Error	% Abs. Error	$V_{j,ACI}$	% Error	% Abs. Error
87	<i>C. C. Chen, G. K. Chen</i>	JC	904.42	917.57	-1.453	1.453	890.67	1.520	1.520
88		JE	864.22	903.80	-4.581	4.581	832.96	3.617	3.617
89		JS1	954.98	903.80	5.359	5.359	832.96	12.778	12.778
90		JS2	966.21	903.80	6.459	6.459	859.21	11.074	11.074
91		JS3	971.83	903.80	7.000	7.000	841.12	13.450	13.450
92		JS4	977.45	903.80	7.535	7.535	837.05	14.364	14.364
93	<i>H. F. Wong, J. S. Kuang</i>	JA-NN03	249.00	271.67	-9.104	9.104	559.99	-124.894	124.894
94		JA-NN15	311.00	287.73	7.483	7.483	567.44	-82.456	82.456
95		JA-NY03	235.60	287.93	-22.211	22.211	494.11	-109.726	109.726
96		JA-NY15	308.50	304.95	1.151	1.151	518.99	-68.229	68.229
97		JB-NN03	313.00	271.67	13.205	13.205	576.25	-84.105	84.105
98		JB-NY03	307.30	287.93	6.303	6.303	488.99	-59.124	59.124
99	<i>H. F. Wong, J. S. Kuang</i>	BS-L-300	505.00	375.71	25.602	25.602	488.56	3.256	3.256
100		BS-L-450	315.50	375.71	-19.084	19.084	465.07	-47.407	47.407
101		BS-L-600	283.90	375.71	-32.338	32.338	504.77	-77.797	77.797
102		BS-L-V2	398.80	375.71	5.790	5.790	477.69	-19.782	19.782
103		BS-L-V4	402.90	375.71	6.749	6.749	445.07	-10.468	10.468
104		BS-L-H1	389.30	381.47	2.010	2.010	482.79	-24.016	24.016
105		BS-L-H2	479.30	394.45	17.703	17.703	542.85	-13.259	13.259
106		<i>M.R.Ehsani, J.K.Wight</i>	1S	566.26	490.63	13.356	13.356	680.56	-20.185
107	2S		599.24	509.42	14.989	14.989	655.31	-9.357	9.357
108	3S		552.35	495.84	10.230	10.230	561.04	-1.574	1.574
109	4S		605.10	516.38	14.663	14.663	565.04	6.621	6.621
110	5S		646.25	676.48	-4.679	4.679	663.34	-2.645	2.645
111	6S		744.08	595.77	19.932	19.932	803.40	-7.971	7.971
112	<i>B. Li, S. A. Kulkarni</i>	EWB-1	1,125.80	1,051.42	6.607	6.607	2,153.04	-91.246	91.246
113		EWB-2	1,726.02	1,116.42	35.318	35.318	2,061.78	-19.453	19.453
114		EWB-3	1,227.12	1,051.42	14.318	14.318	1,859.25	-51.513	51.513
Average Error, %						8.92			27.01

**Table 4.2** indicates that TEC 2007 significantly overpredicts the capacity of beam-to-column connections. Since in TEC 2007 the shear strength of a connection is linearly related to the concrete compressive strength ( $f_{cd}$ ), as specified in equations **2.10a** and **2.10b**, the capacity exceeds the experimental value, considerably.

As the square root of compressive shear strength ( $\sqrt{f'_c}$ ) is considered in ACI 352R-02 [2], the shear strength capacity values specified using ACI 352R-02 are more conservative and accurate than TEC 2007 values. However, the equations still have an error of 27.01% in the determination of the joint shear strength for the selected

database. Since the proposed shear strength,  $V_{j,pro}$ , considers the effect of several parameters, the shear strength values determined using  $V_{j,pro}$  are more accurate than both ACI 352R-02 and TEC 2007 capacity values. Although the predicted shear strength values are not always on the conservative side, the average error for  $V_{j,pro}$  is only **8.92%**.

#### 4.2.13 Efficiency of Shear Strength Adjustment Factors

In **Table 4.4**, the effect of each variable on the accuracy of the joint shear strength prediction is evaluated. The variation of the average error with the application of each parameter is examined both for only the specimens effected by that parameter and for the total database. Efficiency of each parameter, which indicates the enhancement of prediction accuracy, is also investigated by comparing the error of the shear strength prediction when the parameter is considered (error with parameter) with the error when the parameter is not considered (error without parameter). The error for the cases when the parameter is considered or not and the efficiency are computed by the equations given below:

$$\text{Error for each specimen} = \frac{|V_{j,proposed} - V_{j,exp}|}{V_{j,exp}} \quad (4.23)$$

$$\text{Error} = \frac{\sum \text{Error for each specimen}}{n} \quad (4.24)$$

where, n = If the parameter is considered, n is equal to the number of specimens effected by the parameter, if not, n is the total number of specimens.

$V_{j,proposed}$  = Joint shear strength that includes the effect of parameter for error with parameter and the corresponding parameter is neglected for error without parameter

$$\text{Efficiency} = \frac{\text{Error without Parameter} - \text{Error with Parameter}}{\text{Error with Parameter}} \quad (4.25)$$

**Table 4.4: Efficiency of Shear Strength Adjustment Factors**

Parameter	Number of Effected Specimens	For Specimens Effected from Parameter			For All Specimens		
		Error with Parameter, %	Error without Parameter, %	Efficiency	Error with Parameter, %	Error without Parameter, %	Efficiency
Axial Load (AF)	85	9.51	11.08	14.2%	8.92	10.09	11.6%
Presence of Slab (SF)	30	6.74	20.31	66.8%	8.92	12.49	28.5%
Conf. by Beams (SBF)	114	8.92	12.30	27.4%	8.92	12.30	27.4%
Trans. Reinf. Ratio (SRF)	114	8.92	9.60	7.0%	8.92	9.60	7.0%
Eccentricity (EF)	18	6.77	7.08	4.4%	8.92	8.97	0.5%
Bond Strength (BF)	79	9.11	16.12	43.5%	8.92	13.78	35.2%
Wide Beam (WBF)	13	6.70	26.32	74.6%	8.92	11.16	20.0%
Trans. Reinf. $f_{y,eq}$ (YS)	91	8.48	9.53	11.0%	8.92	9.76	8.6%
Exterior Specimens	81				9.73		
Interior Specimens	33				6.94		

From **Table 4.4**, it can be observed that taking into account the parameters SF, SBF, BF, and WBF are essential in the accurate prediction of the shear strength, whereas the effect of EF is relatively low.

### 4.3 DETERMINATION OF CONNECTION PERFORMANCE POINTS

#### 4.3.1 Definition of Performance Points

The response of beam-to-column connections when subjected to lateral loads resulting in high drift ratios can be represented by four different regions, the boundaries of which are defined with 4 performance points.

First region of the connection response stands for the uncracked behavior and typically possesses a stiff load vs. deformation relationship. The point where the cracking of the connection region results in loss of stiffness is identified as the cracking point and denoted as ' $P_{cr}$ '.

After the primary cracks are formed in the connection region, although the stiffness does not reduce considerably, the connection starts to deviate from elastic behavior and continues to carry the applied lateral load with increasing strength. This region ends at the point where the inelastic activity increases and crack maturation occurs and the stiffness loss of the connection becomes significant. Second performance

point, which is the boundary of the second region is defined as point of inelasticity and denoted as ' $P_{inel}$ '.

The third region represents the inelastic activity region where the stiffness of the connection is considerably reduced, although the strength of the connection is still increasing, or at least preserved. The point where the beam-to-column connection starts to lose strength denotes the end of the third region and called the maximum point, ' $P_{max}$ '.

The last performance point is specified as the end of descending region of the connection response and defined to be the final point, denoted by ' $P_{final}$ '. An illustration of performance points can be seen in **Figure 4.1**, demonstrated on the experimental joint shear force vs. joint shear deformation relationship of specimen SL4, tested by Shin and LaFave [27].

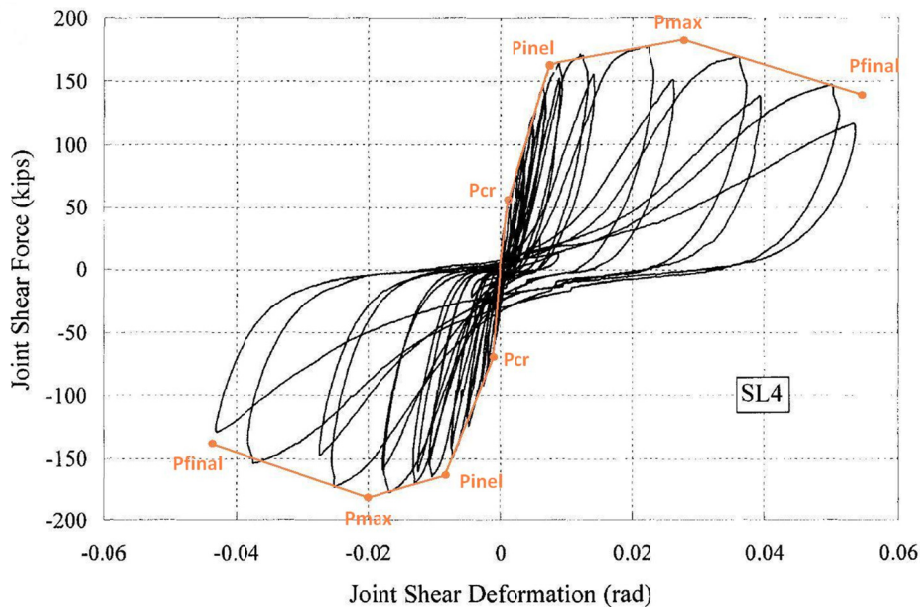


**Figure 4.1: Definition of Performance Points**

### 4.3.2 Prediction of Performance Point $P_{inel}$

The target point in generation of the analytical model for the shear force vs. shear deformation response of beam-to-column connections is determined as the point where inelastic activity of the connection is concentrated,  $P_{inel}$ . This point is selected as the target, because the strain can be determined with high accuracy due to the significant stiffness decrease at this point. Additionally, as many of the experimental joint shear force vs. shear strain response envelopes do not provide data on  $P_{max}$  and  $P_{final}$  due to the limitations of either the test setup or the instrumentation,  $P_{inel}$  constitutes the most reliable point for shear strength prediction of connections.

#### Basic Joint Shear Strain Prediction for $P_{inel}$

For the first prediction of the joint shear strain at point of inelasticity, a procedure similar to the joint shear strength prediction is followed. First, all shear force vs. shear strain data are digitized using a simple graph digitizing software called 'Engauge Digitizer'. The digitized shear force vs. shear strain curves are linearized for four performance points as illustrated in **Figure 4.2**. From the data acquired, the ratio of the shear force of a joint at  $P_{inel}$  to the maximum joint shear strength is determined as 0.804. The basic joint shear force at point of inelasticity is determined as 80.4% of basic joint shear strength.

$$V_{j0,inel} = 0.804 V_{j0} \quad (4.26)$$

Accordingly, basic joint shear stress at point of inelasticity,  $v_{j0,inel}$  is determined as below.

$$v_{j0,inel} = \frac{V_{j0,inel}}{A_{ACI,352}} \quad (4.27)$$

In order to predict the shear strain at point of inelasticity, an effective shear modulus, ' $G_{eff}$ ', based on elastic shear modulus is defined. Elastic shear modulus is determined as:

$$G_{\text{elastic}} = \frac{E}{2(1+\nu)} \quad (4.28)$$

where, E = modulus of elasticity,

$\nu$  = poisson's ratio, 0.2.

Determination of the effective shear modulus is carried out using prior experimental data on the shear force vs. shear strain performance curves. The modulus of elasticity values for both the elastic and cracked regions of these curves are calculated and the average ratio of these two values is obtained to be 0.35, when all the specimens are considered. Since the shear modulus and modulus of elasticity values are linearly correlated, effective shear modulus of the connection to be used in the prediction of second performance point is determined to be 35% of elastic shear modulus.

$$G_{\text{eff}} = G_{\text{elastic}} \times 0.35 \quad (4.29)$$

Consequently, basic prediction of the shear strain at  $P_{\text{inel}}$  is given in **Equation 4.30**.

$$\gamma_{\text{inel,basic}} = \frac{V_{j0,\text{inel}}}{G_{35}} \quad (4.30)$$

Determination of Final Prediction for  $P_{\text{inel}}$ :

Prior experimental research proved confinement significantly affects the shear force vs. shear strain response of a beam-to-column connection. In order to reflect the effect of confinement by surrounding members and transverse shear reinforcement, the basic shear strain prediction is improved using priory computed surrounding beam index (SBI) and transverse shear reinforcement confinement factor (SRF). Since confinement is inversely proportional to the shear strain magnitude, basic prediction is divided to the above mentioned parameters to generate the final shear strain prediction for performance point  $P_{\text{inel}}$ ,  $\gamma_{\text{inel}}$ .

$$\gamma_{\text{inel}} = \frac{\gamma_{\text{inel,basic}}}{\text{SBI} \times \text{SRF}} \quad (4.31)$$

**Equation 4.30** decreases the average error to 33% for predicted shear strains with an average prediction of  $1.15 \gamma_{exp}$ .

### 4.3.3 Construction of Joint Shear Stress vs. Strain Curve

After the determination of the shear force and strain values for performance point  $P_{inel}$ , shear strain and shear force values for  $P_{cr}$  and  $P_{final}$  and shear strain value for  $P_{max}$  are specified according to the ratios obtained by examining the experimental data. Average ratios for shear force and shear strain values of performance points are presented below, in **Tables 4.5** and **4.6**. The proportions are determined with respect to the shear force and shear strain values for performance point  $P_{max}$ .

**Table 4.5: Summary Table for Joint Shear Force Proportions**

<i>Shear Force Proportions</i>	$V_{j,cr}/V_{j,inel}$	$V_{j,max}/V_{j,inel}$	$V_{j,final}/V_{j,inel}$
<b>For Exterior Connections</b>	0.27	2.49	6.61
<b>For Interior Connections</b>	0.23	2.77	7.82

**Table 4.6: Summary Table for Joint Shear Strain Proportions**

<i>Shear Strain Proportions</i>	$\gamma_{cr}/\gamma_{inel}$	$\gamma_{max}/\gamma_{inel}$	$\gamma_{final}/\gamma_{inel}$
<b>For Exterior Connections</b>	0.11	0.40	2.65
<b>For Interior Connections</b>	0.09	0.36	2.83

Accuracy of the predicted shear force and shear strain are determined by computing average error and average prediction values, the magnitudes of which are given in **Tables 4.7** and **4.8**, respectively:

$$\text{Error for each specimen} = \frac{|\gamma_{prop} - \gamma_{exp}|}{\gamma_{exp}} \quad (4.32)$$

$$\text{Average Error} = \frac{\sum \text{Error for each specimen}}{\text{Number of specimens}} \quad (4.33)$$

$$\text{Average Prediction} = \frac{\sum(\gamma_{prop}/\gamma_{exp})}{\text{Number of specimens}} \quad (4.34)$$

( $V_j$  values are used, instead of  $\gamma$ , in case of joint shear force prediction)

**Table 4.7: Summary Table for Joint Shear Force Prediction Accuracy**

	$V_{j,cr}$	$V_{j,inel}$	$V_{j,max}$	$V_{j,final}$
Average Error, %	21.23	11.42	9.54	11.94
Average Prediction	1.08	1.04	1.04	1.03

**Table 4.8: Summary Table for Joint Shear Strain Prediction Accuracy**

	$\gamma_{cr}$	$\gamma_{inel}$	$\gamma_{max}$	$\gamma_{final}$
Average Error, %	47.26	32.95	30.13	31.78
Average Prediction	1.26	1.15	1.11	1.17

#### 4.3.4 Accuracy of Joint Shear Strain Prediction

The accuracy of joint shear strain prediction for each performance point is determined by comparing each point with prior experimental studies which collected joint strain data. In **Table 4.9**, predicted performance points are presented along with the experimental values. The error for each prediction is defined as previously stated in Equation 4.32:

$$\text{Error} = \frac{|\gamma_{prop} - \gamma_{exp}|}{\gamma_{exp}} \quad (4.32)$$

where,  $\gamma_{prop}$  = proposed joint shear strain value,

$\gamma_{exp}$  = experimental joint shear strain value,

**Table 4.9: Accuracy of Joint Shear Strain Values**

No.	Researchers	Specimen	$\gamma_{cr}$			$\gamma_{inel}$			$\gamma_{max}$			$\gamma_{final}$		
			Prop.	Exp.	% Error	Prop.	Exp.	% Error	Prop.	Exp.	% Error	Prop.	Exp.	% Error
1	B. Burak, J. K. Wight	1-S	0.0005	0.0004	29.83	0.0024	0.0021	12.35	0.1235	0.0066	1.15	0.0184	0.0000	0.00
2		2-S	0.0007	0.0004	67.69	0.0029	0.0024	21.95	0.2195	0.0120	33.68	0.0224	0.0217	3.42
3		3-S	0.0008	0.0002	246.78	0.0033	0.0023	47.71	0.4771	0.0081	13.46	0.0260	0.0250	3.96
4		2-N	0.0004	0.0012	67.79	0.0014	0.0044	67.60	0.6760	0.0087	58.91	0.0094	0.0000	0.00
5		3-N	0.0008	0.0009	11.98	0.0029	0.0025	19.25	0.1925	0.0059	24.51	0.0193	0.0000	0.00
6	G. S. Raffaele, J. K. Wight	1	0.0007	0.0009	17.99	0.0032	0.0032	0.20	0.0020	0.0100	11.25	0.0250	0.0220	13.45
7		2	0.0010	0.0017	43.68	0.0041	0.0052	19.56	0.1956	0.0121	4.94	0.0324	0.0197	64.35
8		3	0.0007	0.0006	23.10	0.0032	0.0033	3.16	0.0316	0.0125	29.31	0.0250	0.0296	15.62
9		4	0.0010	0.0012	13.61	0.0045	0.0056	20.02	0.2002	0.0165	24.92	0.0349	0.0355	1.66
10	M. Shin, J. LaFave	SL1	0.0006	0.0010	41.69	0.0026	0.0050	47.07	0.4707	0.0115	37.00	0.0205	0.0289	29.23
11		SL2	0.0011	0.0007	57.83	0.0048	0.0060	19.66	0.1966	0.0158	16.07	0.0374	0.0399	6.30
12		SL3	0.0004	0.0006	20.53	0.0019	0.0021	7.75	0.0775	0.0041	29.12	0.0146	0.0086	72.87
13		SL4	0.0005	0.0008	33.45	0.0022	0.0053	58.86	0.5886	0.0145	58.81	0.0169	0.0487	65.34
14	S. Fujii, S. Moita	A1	0.0016	0.0015	4.31	0.0069	0.0052	32.36	0.3236	0.0124	54.10	0.0538	0.0426	26.42
15		A2	0.0013	0.0010	34.68	0.0058	0.0048	21.40	0.2140	0.0134	20.70	0.0455	0.0000	0.00
16		A3	0.0016	0.0015	7.48	0.0069	0.0066	4.44	0.0444	0.0191	0.36	0.0538	0.0566	4.96
17		A4	0.0014	0.0010	37.68	0.0062	0.0052	19.14	0.1914	0.0133	28.81	0.0484	0.0497	2.63
18		B1	0.0022	0.0011	104.74	0.0080	0.0066	20.71	0.2071	0.0143	39.38	0.0527	0.0308	71.19
19		B2	0.0018	0.0019	1.41	0.0067	0.0045	51.07	0.5107	0.0133	26.92	0.0446	0.0303	47.48
20		B3	0.0022	0.0008	171.69	0.0080	0.0034	137.81	1.3781	0.0117	69.76	0.0527	0.0326	61.62
21		B4	0.0019	0.0010	94.43	0.0072	0.0040	79.28	0.7928	0.0136	31.46	0.0474	0.0395	20.08
22	Y. Kurose, G.N. Guimaraes, L. Zuhua, M.E. Kreger, J.O. Jisa	J1 (EW)	0.0009	0.0016	41.59	0.0040	0.0047	13.96	0.1396	0.0101	10.72	0.0316	0.0000	0.00
23		J2 (EW)	0.0008	0.0009	11.92	0.0034	0.0031	10.64	0.1064	0.0071	34.53	0.0268	0.0000	0.00
24		J2 (NS)	0.0008	0.0008	0.34	0.0034	0.0026	31.16	0.3116	0.0081	17.82	0.0268	0.0000	0.00
25		J3 (EW)	0.0009	0.0008	0.00	0.0031	0.0045	0.00	0.0000	0.0000	0.00	0.0208	0.0000	0.00
26	J3 (NS)	0.0006	0.0006	0.82	0.0028	0.0020	39.59	0.3959	0.0066	16.97	0.0218	0.0372	41.34	
27	C. C. Chen, G. K. Chen	JC	0.0018	0.0011	66.82	0.0066	0.0045	49.33	0.4933	0.0103	60.23	0.0440	0.0379	15.94
28		JE	0.0019	0.0013	44.31	0.0071	0.0076	6.99	0.0699	0.0188	5.77	0.0470	0.0395	19.01
29		JS1	0.0019	0.0016	24.29	0.0071	0.0045	57.90	0.5790	0.0117	51.41	0.0470	0.0312	50.42
30		JS4	0.0019	0.0013	48.04	0.0071	0.0053	34.68	0.3468	0.0109	61.73	0.0468	0.0289	61.78
<b>Average Error, %</b>					<b>47.26</b>			<b>32.95</b>			<b>30.13</b>			<b>31.78</b>

#### 4.4 SUMMARY OF THE ANALYTICAL MODEL

The analytical study is finalized by the generation of an analytical model that predicts the shear force vs. shear strain response of beam-to-column connections under cyclic loading. As mentioned earlier, a wide variety of geometrical and material characteristics are taken into consideration in the development of the final model. A brief summary of the proposed equations are presented below along with the graphical illustration of the shear force vs. shear strain response with performance points. The coefficients are obtained from the average values in the constructed database of experimental studies.

Joint Shear Strength Prediction Equations

$$V_{j,max} = V_{j3} = V_{j0} \text{ (AF) (SF) (SBF) (SRF) (YS) (WBF) (BF) (EF)} \quad (4.35)$$

$$\begin{aligned} \text{For exterior connections, } V_{j,cr} &= V_{j,max} \times 0.44, \\ V_{j,incl} &= V_{j,max} \times 0.81, \\ V_{j,final} &= V_{j,max} \times 0.72. \end{aligned} \quad (4.36)$$

$$\begin{aligned} \text{For interior connections, } V_{j,cr} &= V_{j,max} \times 0.40, \\ V_{j,incl} &= V_{j,max} \times 0.80, \\ V_{j,final} &= V_{j,max} \times 0.87. \end{aligned} \quad (4.37)$$

Joint Shear Strain Prediction Equation:

$$\gamma_{inel} = \frac{\gamma_{inel,basic}}{SBI \times SRF}. \quad (4.38)$$

Although the basic shear strain prediction is obtained for performance point  $P_{inel}$ , the equations given below are given with respect to the shear strain at maximum shear force, in order to be compatible with the shear strength prediction.

$$\begin{aligned} \text{For exterior connections, } \gamma_{max} &= \gamma_{inel} \times 2.49, \\ \gamma_{inel} &= \gamma_{max} \times 0.40, \\ \gamma_{cr} &= \gamma_{max} \times 0.11, \\ \gamma_{final} &= \gamma_{max} \times 2.65. \end{aligned} \quad (4.39)$$

$$\begin{aligned} \text{For interior connections, } \gamma_{max} &= \gamma_{inel} \times 2.77, \\ \gamma_{inel} &= \gamma_{max} \times 0.36, \\ \gamma_{cr} &= \gamma_{max} \times 0.09, \end{aligned} \quad (4.40)$$

$$\gamma_{\text{final}} = \gamma_{\text{max}} \times 2.83.$$

The final models for exterior and interior connections are illustrated on the representative curves given below.

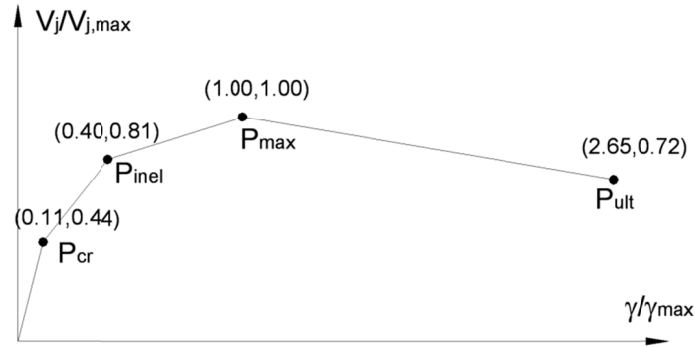


**Figure 4.2:: Joint Shear Force vs. Strain Curve for Exterior Connections**

*Summary of Performance Points for Exterior Connections*

$$\begin{aligned}
 P_{\text{cr}}; \quad \gamma_{\text{cr}} &= \gamma_{\text{max}} \times 0.11, & V_{\text{j,cr}} &= V_{\text{j,max}} \times 0.44. \\
 P_{\text{inel}}; \quad \gamma_{\text{inel}} &= \gamma_{\text{max}} \times 0.40, & V_{\text{j,inel}} &= V_{\text{j,max}} \times 0.81. \\
 P_{\text{final}}; \quad \gamma_{\text{final}} &= \gamma_{\text{max}} \times 2.65, & V_{\text{j,final}} &= V_{\text{j,max}} \times 0.72.
 \end{aligned}
 \tag{4.41}$$

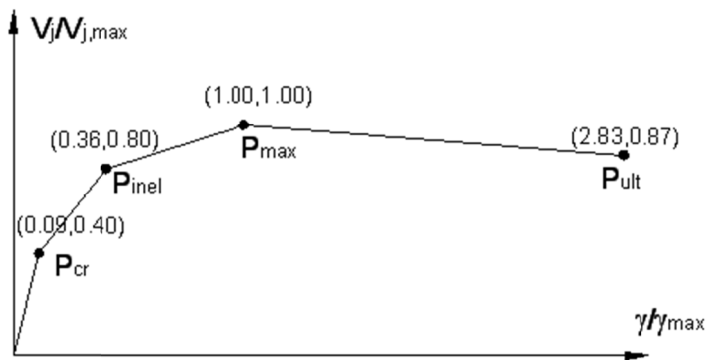


**Figure 4.3: Joint Shear Force vs. Strain Curve for Interior Connections**

Summary of Performance Points for Interior Connections

$$\begin{aligned} P_{\text{cr}}; \quad \gamma_{\text{cr}} &= \gamma_{\text{max}} \times 0.09, & V_{\text{j,cr}} &= V_{\text{j,max}} \times 0.40. \\ P_{\text{inel}}; \quad \gamma_{\text{inel}} &= \gamma_{\text{max}} \times 0.36, & V_{\text{j,inel}} &= V_{\text{j,max}} \times 0.80. \\ P_{\text{final}}; \quad \gamma_{\text{final}} &= \gamma_{\text{max}} \times 2.83, & V_{\text{j,final}} &= V_{\text{j,max}} \times 0.87. \end{aligned} \tag{4.42}$$

## CHAPTER 5

### VERIFICATION OF THE JOINT MODEL

#### 5.1 OVERVIEW

Developed analytical model to predict the beam-to-column connection behavior in terms of shear strength and shear strain response is implemented in the computer environment for the purpose of verification. Verification process is carried out using the experimental data acquired from prior research. Computer models of beam-to-column connection subassemblies previously tested under cyclic loading are generated and the compatibility of analytical results with experimental results are monitored.

The software ‘*OpenSees*’ [49], the ‘*Open System for Earthquake Engineering Simulation*’, is selected for analytical verification of the model. Main properties of OpenSees, which are influential in the selection process of the software, are the variety of structural elements, the consequent freedom provided to the user while modeling and a number of unique material properties, such as the availability of identifying the pinching characteristics of hysteretic materials, which is not currently possible with most of the available software. Also, since OpenSees is an open source computing framework, a transparent approach is maintained throughout the computing process, leading to a more research oriented analytical modeling. On the other hand, main disadvantages of the software may be specified as the lack of user interface and requirement of full text input, modeling and output files, leading to complicated post processing procedures. Brief description of OpenSees is presented in the following paragraphs.

### OpenSees Software Framework

OpenSees is described as ‘*a software framework for developing applications to simulate the performance of structural and geotechnical systems subjected to earthquakes*’ [49]. Goals of the software framework are indicated as,

- new open-source code development,
- education,
- community discussion.

Fundamental advantages of OpenSees software framework can be listed as,

- availability of large variety of materials, elements and analysis alternatives,
- open source modeling rather than a black box approach,
- goal oriented improvement of computational and modeling properties by means of continual discussion and direct contact with developers.

## **5.2 DESCRIPTION OF ELEMENTS**

Two different models are generated representing interior and exterior beam-to-column connections for analytical verification process. Beam and column elements are linked through the connection element. Cyclic loading histories of tested subassemblies are applied from the beam or column end depending on the experimental loading scheme.

Detailed descriptions of elements composing the connection model are listed in the following sections.

### **5.2.1 Beam and Column Elements**

Modeling of beams and columns framing into the joint is carried out using *elastic beam column element* of OpenSees with zero length rotational springs placed at their end sections. The reason for using such a combination of elements rather than the *beam with hinges element* already implemented in OpenSees is to be able to control the moment rotation response of beams and columns, specify the length of the

longitudinal elements where the inelastic activity is concentrated (plastic hinge length) and also define the cracked section properties of beams and columns in the elastic parts.

Definition of Elastic Regions of Beams and Columns

Required input parameters for the elastic beam column element of OpenSees are the cross sectional area, modulus of elasticity and moment of inertia of the element. Modulus of elasticity is defined in accordance with the ACI 318R-08 provisions, using the compressive strength of concrete for the elements:

$$E_c = 4700 \sqrt{f'_c} \quad (f'_c \text{ in MPa}) \quad (5.1)$$

Additionally, effective stiffness determination of beams and columns are carried out in accordance to the ‘*Update to ASCE/SEI 41 Concrete Provisions*’ published in 2007, with the exception of beams with slabs. The proposed cracked stiffness definition relates the stiffness of an element to the level of axial load. Calculation of stiffness properties of beams without slabs and columns are given in **Equation 5.2**.

$$\begin{aligned} EI_{\text{eff}}/EI_g &= 0.3 && \text{for } P/A_g f'_c < 0.1 \\ EI_{\text{eff}}/EI_g &= 0.3 + (P/A_g f'_c - 0.1) && \text{for } 0.1 \leq P/A_g f'_c < 0.5 \\ EI_{\text{eff}}/EI_g &= 0.7 && \text{for } 0.5 \leq P/A_g f'_c \end{aligned} \quad (5.2)$$

In this document for beams with effective slab widths, the cracked moment of inertia is taken as the stiffness of the web of the beam, assuming the flange parts are ineffective. However, in this research project, a better match is obtained with the experimental data, when the effective stiffness values computed from **Equation 5.2** is utilized for specimens with slabs, rather than the stiffness values for the web of the beam.

**Figure 5.1** illustrates the comparison of *ASCE/SEI 41* updated stiffness definition with experimental data.

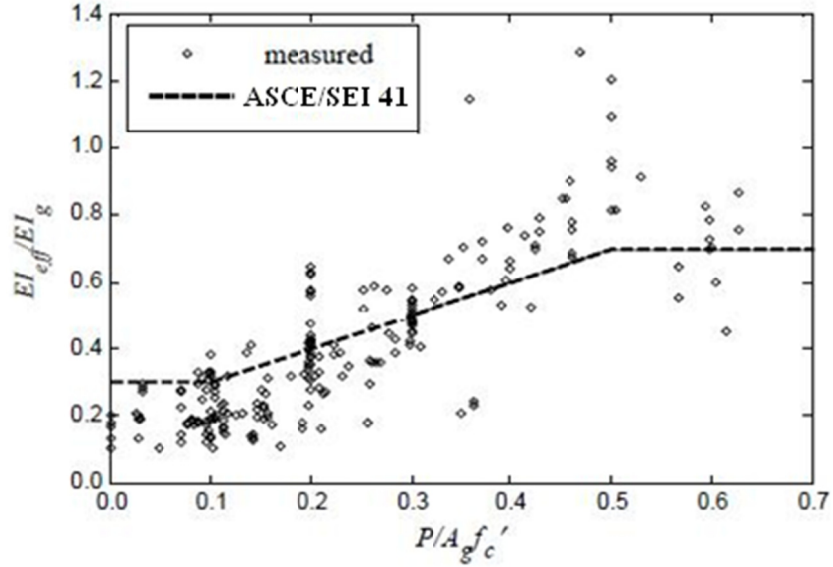


**Figure 5.1: Comparison of Stiffness Model with Experimental Data  
(Update to ASCE/SEI 41 Concrete Provisions, 2007)**

Definition of Moment vs. Rotation Behavior of Beams and Columns

As mentioned previously, beam and column elements are linked to the connection element via zero length rotational springs, the moment vs. rotation behavior of which is defined using hysteretic material.

The moment vs. curvature relationship of beams and columns are obtained by utilizing ‘*Response2000, Reinforced Concrete Sectional Analysis*’ [50] software. Then, the curvature values are multiplied with the plastic hinge length of the elements to attain the moment vs. rotation relationship of the member. In the computation of the member length, where inelastic activity is concentrated, the equation proposed by Mattock [51] is used. Shear span of the member and effective depth of the beam are the main parameters affecting the plastic hinge length.

$$l_p = d/2 + 0.05z \quad (5.3)$$

where,  $l_p$  : plastic hinge length,

$d$  : effective depth of the beam,

$z$  : shear span, distance of critical section to point of inflection

### 5.2.2 Beam-to-Column Connection Element

The connection model proposed by Alath and Kunnath in 1995 is taken as the basis for defining the properties of beam-to-column connection elements used in OpenSees models of this analytical study. This model is preferred due to several features such as the control the user have on defining the load vs. deformation relationship, when compared to the models available in commercial software, such as Perform 3D [40], and simplicity of application of this model when compared to more detailed models that contains numerous springs, the properties of which cannot be accurately defined. This OpenSees connection model does not include bar slip response, however, since the influence of beam bar slip on connection behavior is already introduced explicitly in the analytical equations defined in Chapter 4, the above mentioned more detailed connection models are not required to be employed in the analysis.

The connection model is composed of 2 parts, rigid end zones of beams and columns representing the finite length of these members enclosed in the connection region and a rotational spring representing connection shear force and shear strain characteristics. The spring is used to connect two nodes defined at the same location, each of which is utilized to connect the longitudinal members oriented in one principal direction, either the columns or the beams. Since the working mechanism of this model resembles that of scissors, the connection model is named as '*the scissors model*'. (Figure 5.2)

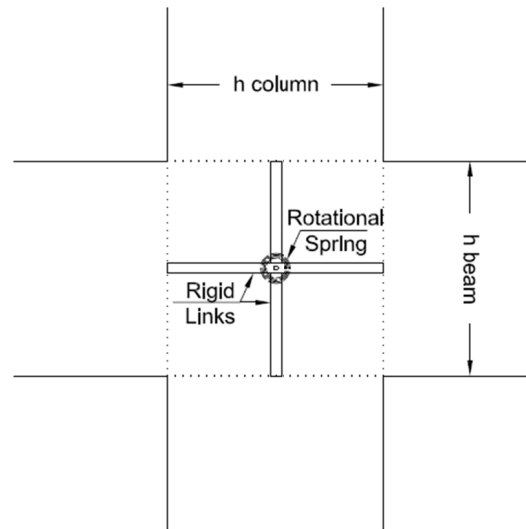


**Figure 5.2: Scissors Connection Model (Alath and Kunnath, 1995).**

Definition of the Hysteretic Spring Material:

The moment vs rotation relationship of the joint spring is represented by using the ‘Pinching4’ uniaxial material. As the name implies, the most remarkable function of this material is its capability of representing the pinching characteristic of the connection response. Moreover, since the material allows defining four performance points, it is possible to represent the strength loss of the connection after reaching its maximum shear capacity.

Response of Pinching4 uniaxial material depends on a considerable amount of input values. The parameters needed to define the Pinching4 material response include the load vs. deformation data for 8 points (4 for the positive envelope and 4 for the negative envelope), 6 parameters to shape the hysteretic behavior of the curve and 15 parameters to define the cyclic degradation of material in terms of force and stiffness, as listed below with corresponding explanations. The constitutive model for this material was proposed by Lowes and Altoontash in 2003.

Definition of the material in the model and related explanations are as follows:

*'uniaxialMaterial Pinching4 \$matTag \$ePf1 \$ePd1 \$ePf2 \$ePd2 \$ePf3 \$ePd3 \$ePf4 \$ePd4 \$eNf1 \$eNd1 \$eNf2 \$eNd2 \$eNf3 \$eNd3 \$eNf4 \$eNd4 \$rDispP \$rForceP \$uForceP \$rDispN \$rForceN \$uForceN \$gK1 \$gK2 \$gK3 \$gK4 \$gKLim \$gD1 \$gD2 \$gD3 \$gD4 \$gDLim \$gF1 \$gF2 \$gF3 \$gF4 \$gFLim \$gE \$dmgType'.*[40]

where,

- \$matTag : Material tag.
- \$ePf1 - \$ePf4 :Force values assigned to the positive performance points.
- \$ePd1 - \$ePd4 :Deformation values assigned to the positive performance points.
- \$eNf1 - \$eNf4 :Force values assigned to the negative performance points.
- \$eNd1 - \$eNd4 :Deformation values assigned to the negative performance points.
- \$rDispP :Ratio of the deformation at which reloading occurs to the maximum deformation
- \$rForceP :The ratio of the force at which reloading occurs to the force at maximum deformation,
- \$uForceP :The ratio of strength developed upon unloading from negative load to the maximum strength developed under monotonic loading.
- \$rDispN :The ratio of the deformation at which reloading occurs to the minimum historic deformation demand,
- \$rForceN :The ratio of the force at which reloading begins to the force corresponding to the minimum historic deformation demand,

$S_{uForceN}$  : The ratio of the strength developed upon unloading from a positive load to the minimum strength developed under monotonic loading.

$S_{gK1}$ - $S_{gK4}$ ,  $S_{gKLim}$  : Cyclic degradation values for unloading stiffness degradation.

$S_{gD1}$ - $S_{gD4}$ ,  $S_{gDLim}$  : Cyclic degradation model for reloading stiffness degradation.

$S_{gF1}$ - $S_{gF4}$ ,  $S_{gFLim}$  : Cyclic degradation model for strength degradation.

$S_{gE}$  : Value used to define maximum energy dissipation under cyclic loading. Total energy dissipation capacity is defined as this factor multiplied by the energy dissipated under monotonic loading.

$S_{dmgType}$  : Type of damage (option: "cycle", "energy")

The above mentioned parameters are illustrated in **Figure 5.3**.

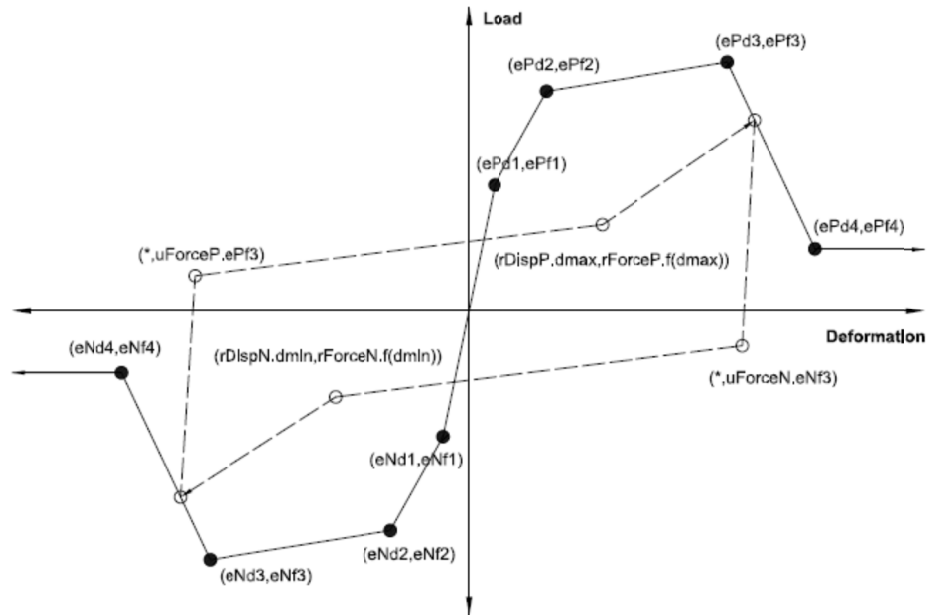


**Figure 5.3: Pinching4 Material Definition (Lowes and Altoontash, 2003)**

Lowes and Altoontash [34] also developed a calibration procedure for the hysteretic behavior and cyclic degradation parameters of the Pinching4 material. The presented parameters were generated using the experimental data by Stevens et al. [52], which had an extremely pinched behavior that resulted in a deviation from the assigned load deformation points for the material.

In another study performed using pinching4 material, Çelik and Ellingwood [53] presented a simple definition of pinching parameters, which led to satisfactory results. Moreover, since the degradation parameters for deformation and force were assumed to be zero, the hysteretic material responded following exactly the load deformation points defined by the user.

In this analytical study, since the basic goal in using the Pinching4 material is to be able to address the previously generated performance points for connection response defined in Chapter 4, damage parameters for reloading stiffness and force degradation are also assumed to be zero and pinching parameters are taken as the ones presented in the study by Çelik and Ellingwood.

$$uForceP = uForceN = 0.10 \quad (5.4a)$$

$$rForceP = rDispP = dForceN = dDispN = 0.15 \quad (5.4b)$$

The unloading stiffness degradation parameters are taken as defined in the ‘Pinching4 Uniaxial Material Model Discussion’ [49]:

$$[gK1 \ gK2 \ gK3 \ gK4] = [1.0 \ 0.2 \ 0.3 \ 0.2 \ 0.9] \quad (5.5)$$

where,

$gK1 \ gK2 \ gK3 \ gK4$  = Cyclic degradation values for unloading stiffness degradation

It is observed that the analytical results have a satisfactory match with the experimental data when the above mentioned parameters are used in the cyclic loading of specimens.

### 5.2.3 Loading Procedure and Generated Models

Reversed cyclic loading for each specimen, the displacement history of which is extracted from the related experimental study, is modeled using a simple procedure based on the peak points of the loading and the step size. Load increments are applied to the beam or column end, as specified in the related experiment. The maximum step size is taken as 0.5 mm, in order to keep the number of computation steps high enough to prevent inconvergence problems and low enough not to increase the computation time.

The displacement controlled integrator object [49] is used with the implementation of several solution algorithms. The procedure starts with 'Newton' algorithm and tries 'Modified Newton' and 'Newton with Line Search' solution algorithms, respectively, in case of a convergence problem. Generated OpenSees models are illustrated in **Figures 5.4** and **5.5**.

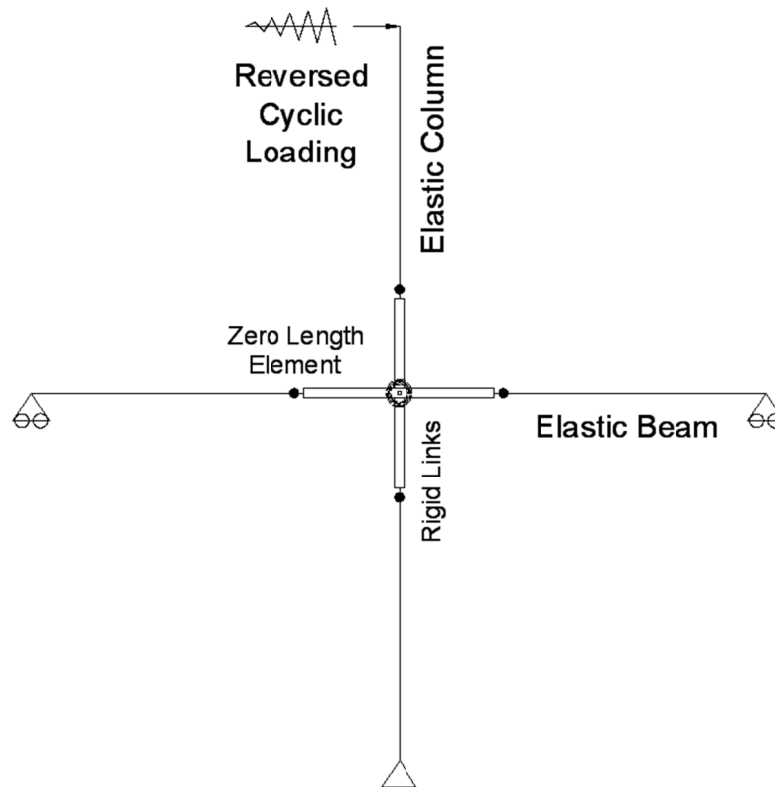


**Figure 5.4: OpenSees Model for Interior Beam-to-Column Connections**

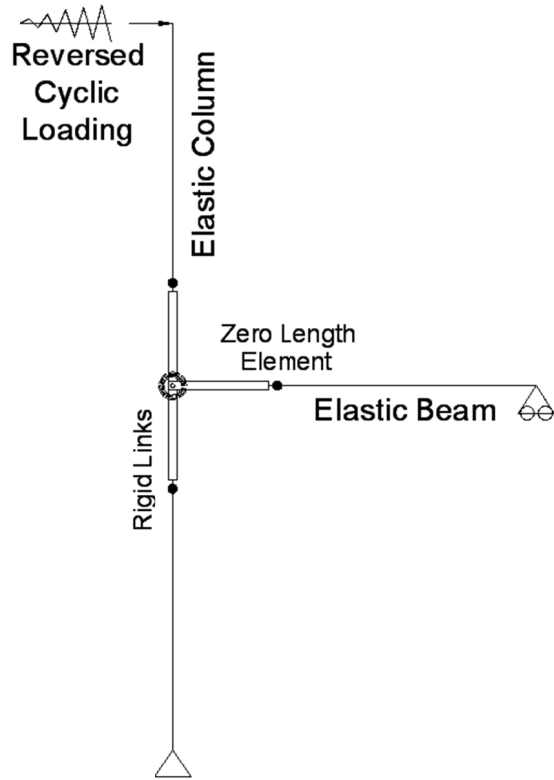


**Figure 5.5: OpenSees Model for Exterior Beam-to-Column Connections**

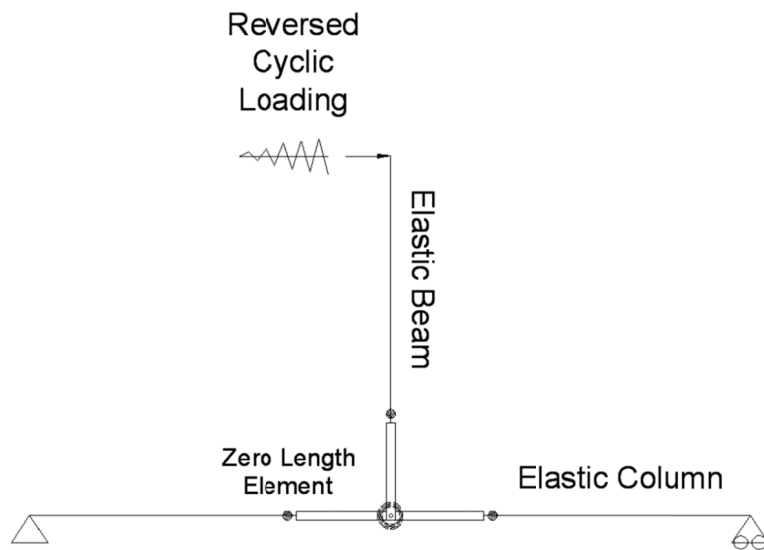


**Figure 5.6: OpenSees Model for Connections Loaded on Beam**

### 5.3 DETERMINATION OF JOINT MOMENT ARM

In order to define the moment vs. rotation relationship of the rotational spring that represents the connection, the joint moment arm is required to obtain the flexural capacity. The previously determined joint shear forces at each performance point are multiplied with the joint moment arm to establish the joint moment values.

Determination of the joint moment arm is carried out considering the geometric properties of the members using basic force equilibrium equations. Length of the beams and columns, width and depth of the connection region and distance between the tension and compression force couple for the beams are the main parameters affecting the joint moment arm.

Moment arm calculation procedures for exterior and interior connections are presented below, following the derivation presented by Çelik and Ellingwood [53].

#### Determination of Joint Moment Arm for Exterior Connections:

The free body diagram and a close up view of the forces acting on the joint region for a laterally loaded exterior connection specimen are presented in **Figure 5.7**.

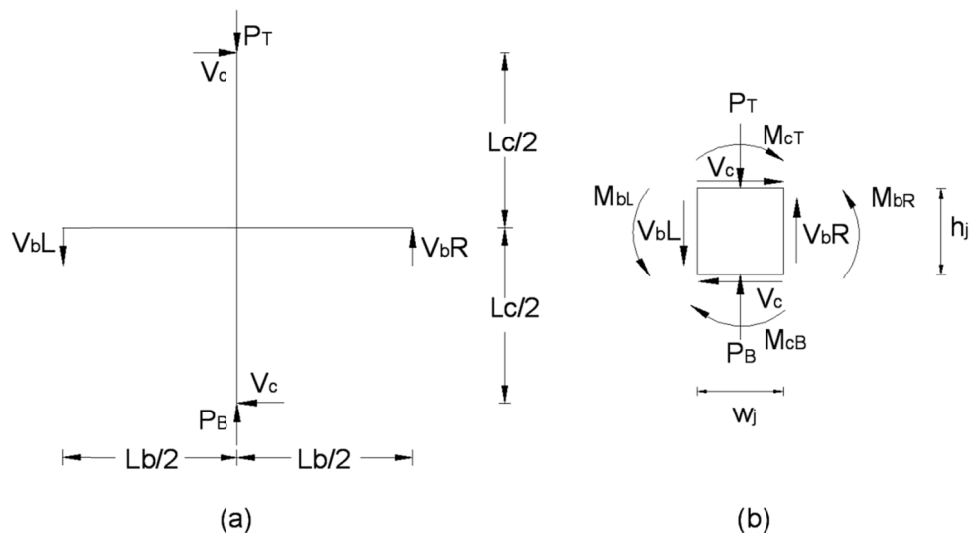


**Figure 5.7: (a) Free Body Diagram of an Exterior Joint Subassembly and (b) Forces Acting on the Joint Region**

If the moments transferred from the right and the left beams are resolved into compression and tension force couples acting on the joint face, forces acting on the joint and the force equilibrium on joint mid-height can be represented as in **Figure 5.8**.

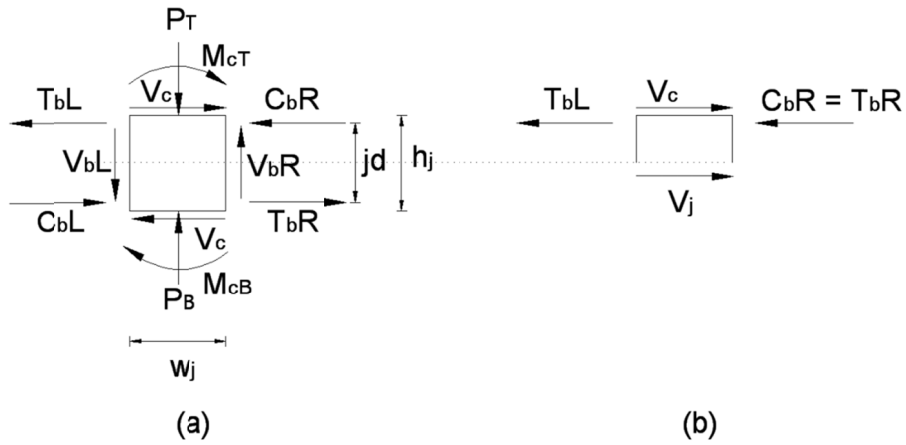


**Figure 5.8: (a) Forces Acting on the Joint Region and (b) Horizontal Force Equilibrium at the Mid-Height of the Joint**

As can be inferred from **Figure 5.8 (b)**,

$$V_j = T_{bL} + T_{bR} - V_c \quad (5.6)$$

If the tension forces imposed by the beams are represented in terms of beam moments and the distance between tension and compression couples,

$$V_j = \frac{M_{bL}}{jd} + \frac{M_{bR}}{jd} - V_c \quad (5.7a)$$

$$V_j = \frac{V_{bL} * (L_b/2 - w_j/2)}{jd} + \frac{V_{bR}(L_b/2 - w_j/2)}{jd} - V_c \quad (5.7b)$$

$$V_j = (V_{bL} + V_{bR}) * \frac{(L_b - w_j)}{2 * jd} - V_c \quad (5.7c)$$

From the free body diagram presented in **Figure 5.7**, the lateral load applied on the column can be defined as,

$$V_c = (V_bL * \frac{L_b}{2} + V_bR * \frac{L_b}{2}) / L_c \quad (5.8a)$$

$$V_c = (V_bL + V_bR) * (\frac{L_b}{2 * L_c}) \quad (5.8b)$$

Finally, from **Equations (5.7c) and (5.8b)**, joint shear force can be defined as,

$$V_j = (V_bL + V_bR) * \frac{(L_b - w_j)}{2 * j d} - (V_bL + V_bR) * (\frac{L_b}{2 * L_c}) \quad (5.9a)$$

$$V_j = (V_bL + V_bR) * (\frac{L_b - w_j}{2 * j d} - \frac{L_b}{2 * L_c}) \quad (5.9b)$$

Defining beam shear forces in terms of joint shear,

$$(V_bL + V_bR) = \frac{V_j}{(\frac{L_b - w_j}{2 * j d} - \frac{L_b}{2 * L_c})} \quad (5.10)$$

Considering the scissors model representing the beam-to-column connection, the free body diagram of the generated model is as presented in **Figure 5.8**.

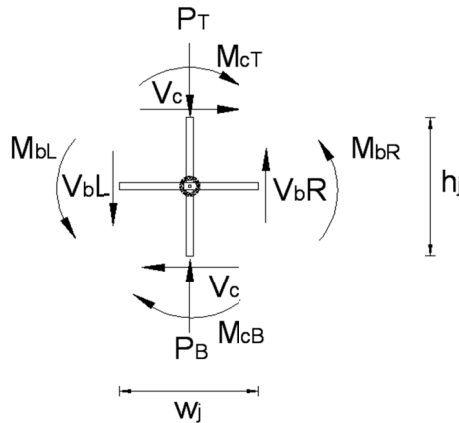


**Figure 5.9: The Free Body Diagram of the Scissors Model**

Rotational spring moment is expressed in terms of shear forces on the beams as:

$$M_j = (V_bL + V_bR) * \frac{L_b}{2} \quad (5.11)$$

Replacing beam shear forces in **Equation (5.11)** with **Equation (5.10)**,

$$M_j = V_j * \frac{L_b}{2 * \left( \frac{L_b - w_j}{2 * jd} - \frac{L_b}{2 * L_c} \right)} \quad (5.12)$$

Simplifying the **Equation (5.12)**, the joint moment arm can be finally expressed as,

$$J_{ma} = \frac{1}{\left( \frac{1 - (w_j / L_b)}{jd} - \frac{1}{L_c} \right)} \quad (5.13)$$

The symbols used in the derivation process are explained below:

$P_T$  = axial load on the top column,

$P_B$  = axial load on the bottom column,

$V_C$  = lateral load applied to the top column,

$V_bL$  = shear force imposed by the left beam,

$V_bR$  = shear force imposed by the right beam,

$M_{CT}$  = moment imposed by the top column,

$M_{CB}$  = moment imposed by the bottom column,

$M_{BL}$  = moment imposed by the left beam,

$M_{BR}$  = moment imposed by the right beam,

$T_{BL}$  = tension force on the top reinforcement of the left beam,

$T_{BR}$  = tension force on the top reinforcement of the right beam,

$C_{BL}$  = compression force on concrete for the left beam,

$C_{BR}$  = compression force on concrete for the right beam,

$w_j$  = width of the beam and column intersection region, equal to the depth of the column,

$h_j$  = depth of the beam and column intersection region, equal to the depth of the beam.

## **5.4 COMPARISON OF ANALYTICAL AND EXPERIMENTAL RESULTS**

In this section of the document, results obtained from the analyses performed using OpenSees are compared with experimental data in order to verify the accuracy of the developed model. Primarily, the joint shear force vs. shear strain responses of the connections are used to verify the analytical model, if available, since this curve directly represents the connection behavior. Moreover, in order to consider the global response of the subassemblies, the lateral loads vs. displacement relationships are presented for each specimen.

Specimens of Burak and Wight [14] are used as the primary source of the verification, due to the availability of detailed data. Then, specimens of Raffaele and Wight [24], Kurose et al. [41] and Chen and Chen [42] are examined for both lateral load vs. lateral drift and joint shear stress vs. strain response evaluation.

### **5.4.1 Specimens of Burak and Wight**

Specimens tested by Burak and Wight [14] constitute an important source for verification of the model, because most of the parameters studied for model development are present in this experimental series, such as floor slab, eccentricity in the loading beam direction, transverse beams and wide beam-to-column connections.

#### Specimen 1, Spandrel Beam Direction (1-S)

The first specimen of the test series is loaded eccentrically in the direction of the spandrel beam. The beam in the loading direction frames into a square column and

the beam to column connection subassembly involves a transverse beam and floor slab.

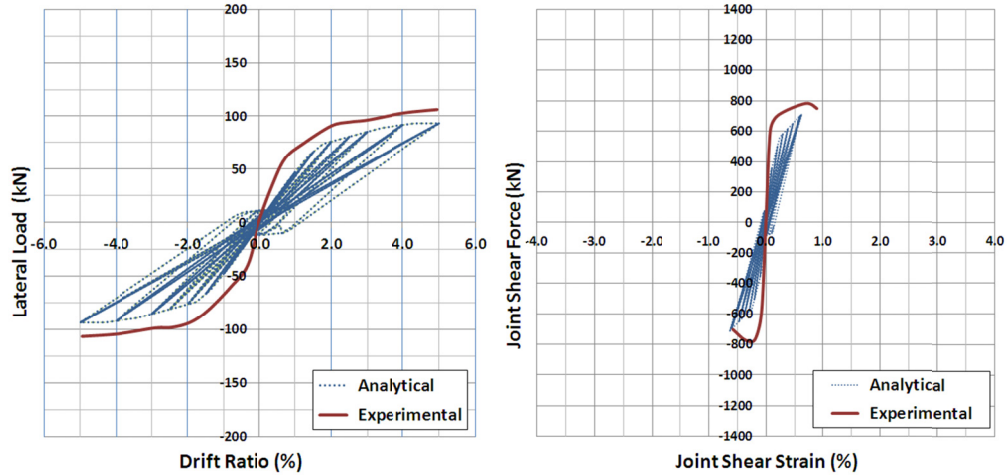


**Figure 5.10: Burak and Wight, Specimen 1-S**

As can be seen in **Figure 5.10**, the analytical model is successful in representation of the general behavior of Sp1, loaded in the spandrel beam direction. Although the joint force is estimated to be lower than the experimental value, the analytical response is satisfactory in representing the limited strain in the connection region.

The prediction of a low joint shear strength and initial stiffness manifests itself in the comparison of lateral load vs. drift ratio relationship as slightly reduced and conservative lateral load estimation.

#### Specimen 2, Spandrel Beam Direction (2-S)

The second specimen has a rectangular column as a major difference from the first specimen. Also the geometric and reinforcement properties of the members are altered.

A comparison of lateral load vs. story drift and joint shear force vs. shear strain responses of analytical model and experimental results is given in **Figure 5.11**.

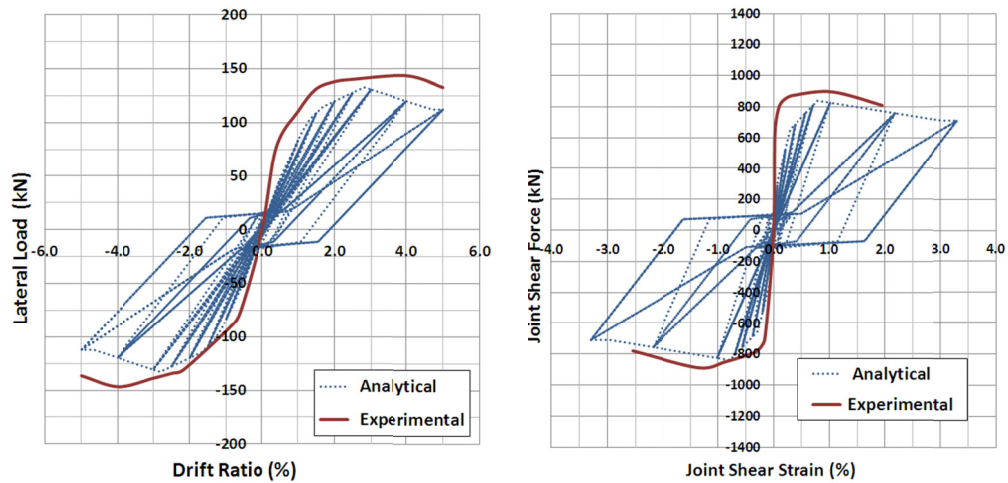


**Figure 5.11: Burak and Wight, Specimen 2-S**

The analytical response of Sp2, eccentrically loaded in the direction of the spandrel beam matches with the experimental results with a considerable accuracy from the point of primary stiffness, general response and the stiffness after peak value of joint shear.

Although a displacement controlled integrator with different solution algorithms is utilized in the reversed cyclic loading scheme of the analysis, the use of the hysteretic material Pinching4 led to deviation of the analytical results from the experimental ones in the descending region of the joint shear force vs. strain response, which resulted in a sudden increase in the joint shear strain.

### Specimen 3, Spandrel Beam Direction (3-S)

The third specimen of this test series is similar to the second specimen, except the wide-beam framing into the connection in the normal direction. In **Figure 5.12**, response of the OpenSees model is compared with the experimental results.

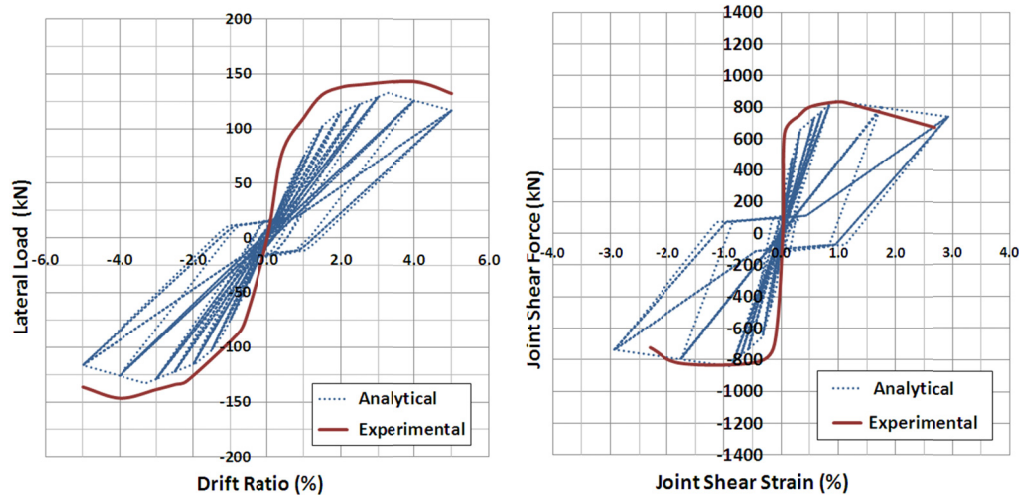


**Figure 5.12: Burak and Wight, Specimen 3-S**

The experimental joint shear force vs. shear strain response of Sp3 is accurately represented by the analytical model from the point of stiffness and strength. Also, the lateral load vs. story drift response of the connection is adequately predicted, being slightly on the conservative side.

#### Specimen 1, Normal Beam Direction (1-N)

In the normal beam direction, the test setup represents a concentric exterior beam-to-column connection, since there are no beams framing into the joint in the opposite direction. For the analyses performed in the normal beam direction, it should be noted that the specimens were initially tested in the spandrel beam direction which caused a decrease in the stiffness of the connections. Since the effect of prior loading is not reflected in the analytical model, a stiffer joint shear force vs. shear strain response of the connection region is observed in the analyses.

The comparison of analytical and experimental results of Sp1 loaded in the normal beam direction can be seen in **Figure 5.13**. Since experimental data on the joint shear force vs. shear strain relationship was not collected, only the lateral load vs. story drift curves are compared.

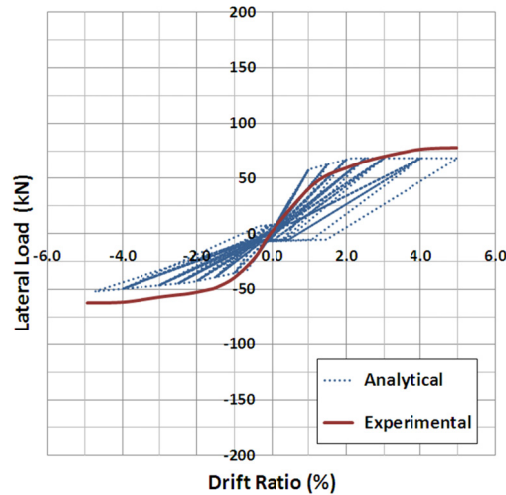


**Figure 5.13: Burak and Wight, Specimen 1-N**

The most important observation from both the analytical and experimental lateral load vs. story drift relationships is the asymmetry of the response curve. Since the bottom and top beam longitudinal reinforcement are different for the normal beam in addition to the effect of floor slab included in the test setup, the response of the connection differ considerably in positive and negative loading directions.

Although the stiffness of the curve in the positive loading direction is over estimated most probably because of disregarding the effect of prior loading, the general representation of the lateral load vs. story drift response of the connection in terms of maximum magnitudes of lateral load and drift is accurate.

#### Specimen 2, Normal Beam Direction (2-N)

The beam in the normal direction of Specimen 2 frames into the strong direction of the rectangular column. As mentioned for the first specimen, this connection is also an exterior one with asymmetrical beam reinforcement and floor slab with prior loading in the spandrel beam direction.

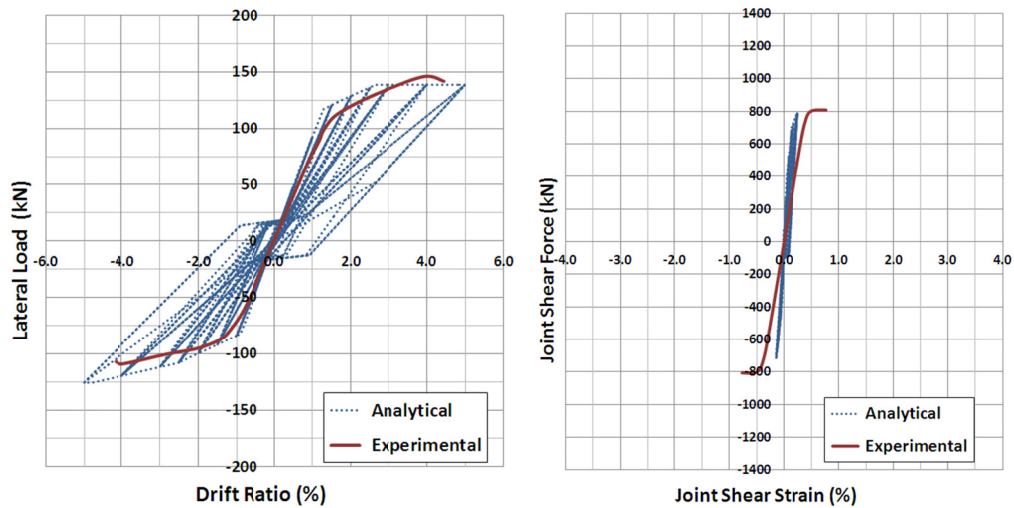


**Figure 5.14: Burak and Wight, Specimen 2-N**

Also the second specimen, when loaded in the normal beam direction, behaves asymmetrically in terms of lateral load vs. story drift response (**Figure 5.14**). Since the area of top beam reinforcement is higher than that of the bottom bars, especially when the slab bars located in the effective flange width are considered, the connection is forced to sustain higher strains in the positive direction due to the relatively higher imposed shear forces from the beam. On the contrary, since the beam can rotate more in the negative direction, the connection experiences lower strains.

The general behavior of the specimen with limited shear deformation and lateral load vs. story drift relationship governed by the beam response is satisfactorily represented by the analytical model.

#### Specimen 3, Normal Beam Direction (3-N)

The response of Specimen 3 loaded in the normal beam direction resembles the response of Specimen 2. As indicated in **Figure 5.15**, the connection deforms asymmetrically due to unequal beam reinforcement areas and the lateral load vs. story drift behavior of the subassembly is governed by the beam properties.

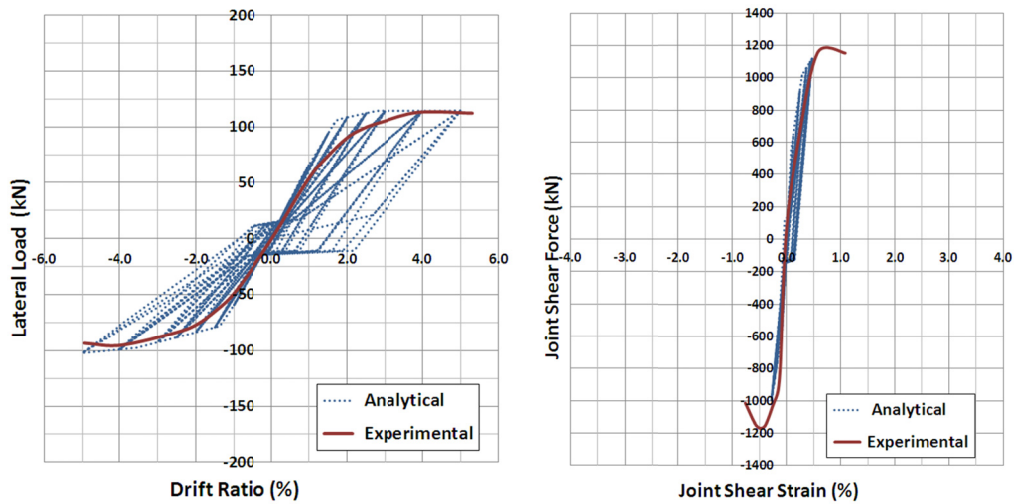


**Figure 5.15: Burak and Wight, Specimen 3-N**

As for the first two specimens of Burak and Wight [14], which are loaded in the normal beam direction, the stiffness of the joint shear force vs. shear strain response of the connection is over estimated, since prior loading is not included in the analysis. Even so, the lateral load vs. story drift relationship of the third specimen is estimated in with a considerable accuracy.

#### **5.4.2 Specimens of Raffaele and Wight**

Raffaele and Wight [24] experimentally investigated the effect of eccentricity on the response of reinforced concrete beam-to-column connections. 4 eccentric interior connections with varying geometric and reinforcement properties of the beam in the loading direction are constructed, while the column properties were kept the same. Neither of the connections had transverse beams or floor slab.

##### Specimen 1

The first specimen of the experimental investigation had an eccentricity of 50.8 mm (2 inches) in the direction of loading. The dimensions of the beam were 254 mm x 381 mm (10" x 15") with 3  $\phi$ 19 (3 #6) and 3  $\phi$ 16 (3 #5) bars used as top and bottom longitudinal reinforcement, respectively.

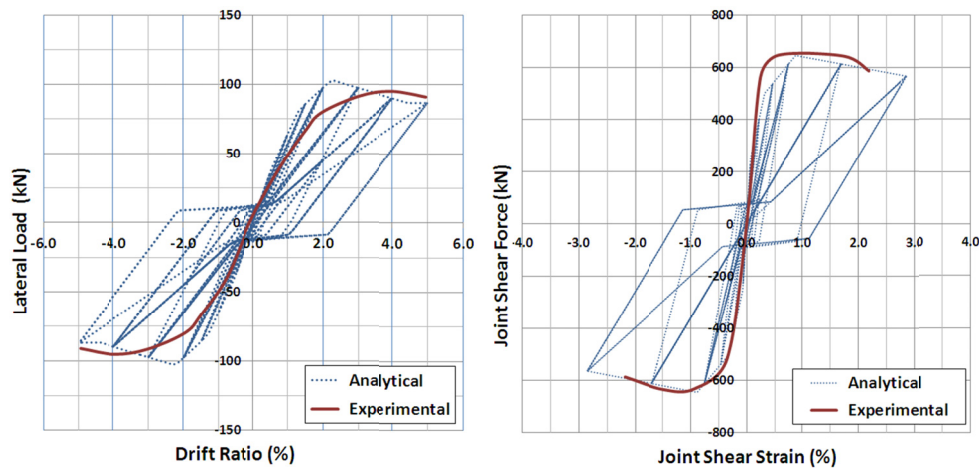


**Figure 5.16: Raffaele and Wight, Specimen 1**

As can be inferred from the lateral load vs. story drift graph presented in **Figure 5.16**, the model estimates a stiffer response of the beam-to-column connection subassembly. Also the lateral load capacity of the connection is slightly over estimated. However, the analytical joint shear force vs. shear strain behaviour of the connection shows a close match with the experimental behavior which indicates that the over prediction of the stiffness and lateral load capacity of the connection is not related to the connection region, but other members. The deviation of beams from the experimental moment vs. rotation relationship may cause the over estimation of lateral load response of Specimen 1, however since the experimental data on beam moment vs. rotation response is not available for this test series, a comparison cannot be performed.

### Specimen 2

A narrow beam with dimensions of 177.8 mm x 381 mm (7" x 15") and 2  $\phi$ 19 (2 #6) and 2  $\phi$ 16 (2 #5) bars were used in the construction of Specimen 2, which was the only difference from Specimen 1. Since the beam face is flush with the face of the column, an eccentricity of 88.9 mm (3.5 inches) was present.

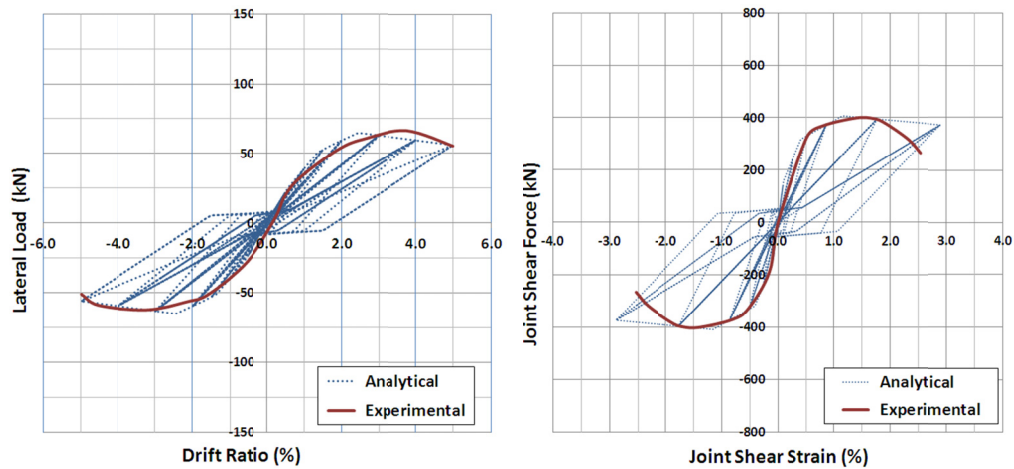


**Figure 5.17: Raffaele and Wight, Specimen 2**

The response obtained from OpenSees analyses of the second specimen of test series shows a close match with experimental results. Especially for the results of loading in the negative direction, the stiffness and strength characteristics of the beam-to-column connection is represented precisely, for increasing strength branch of the connection response. Although a slight stiffness deviation from the experimental curve can be noticed, the general behavior of the connection is represented successfully, except for the fact that the joint shear strength degradation at high strain values is predicted to be lower than the experimental ones.

### Specimen 3

The dimensions of the beam is slightly altered from the beam of the second specimen by increasing the width of the beam to 190.5 mm (7.5"), 3  $\phi$ 16 (3 #5) and 2  $\phi$ 16 (2 #5) bars are used as top and bottom reinforcement. The eccentricity of the connection is reduced to 82.55 mm (3.25"). Comparison of the experimental and analytical results is given in **Figure 5.18**.

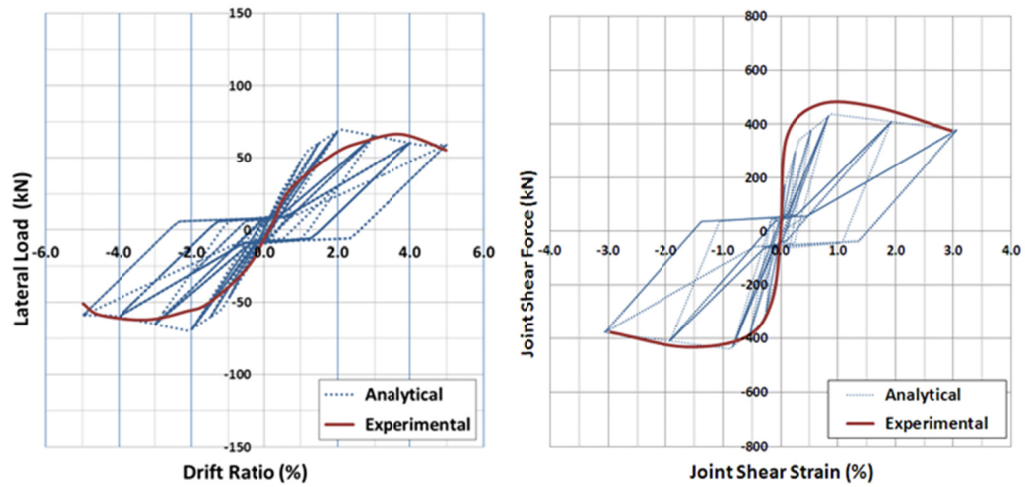


**Figure 5.18: Raffaele and Wight, Specimen 3**

The comparison of the analytical and experimental results of Specimen 3 leads to similar conclusions for the case of Specimen 1. Although the analytical joint shear stress vs. strain curve represents the experimental behavior with high accuracy, a stiffer response of the specimen is observed in the evaluation of lateral load vs. story drift comparison. As mentioned earlier, this indicates the deviation of the experimental behavior of the beam from the analytical moment vs. rotation response.

#### Specimen 4

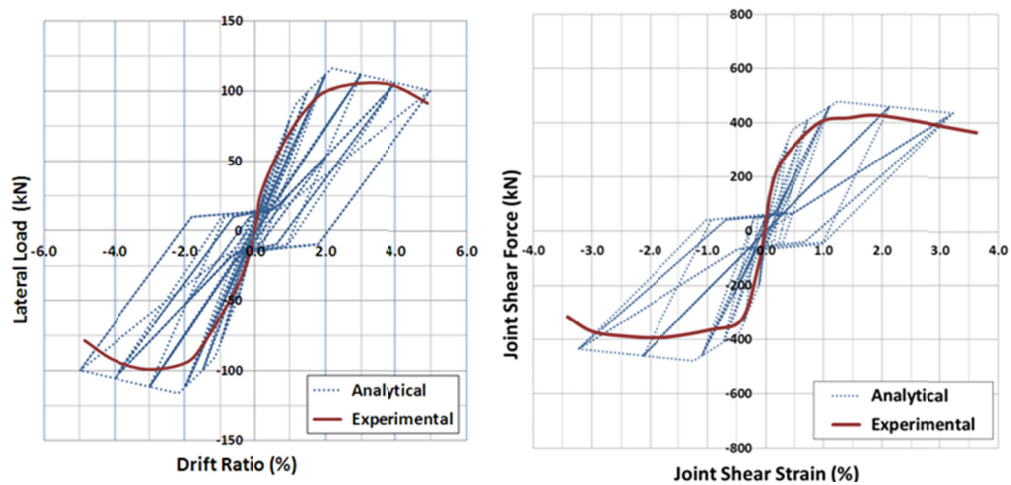


**Figure 5.19: Raffaele and Wight, Specimen 4**

The last specimen is very similar to Specimen 3 as only the height of the beam is increased to 558.8 mm (22"), whereas the longitudinal reinforcement and eccentricity ratios were kept constant. An important difference of Specimen 4 is the placement of 6 layers of transverse reinforcement in the joint region, instead of 3, which was the case for other specimens in this test series.

As can be seen in **Figure 5.19**, the overestimation of joint shear strength vs. strain relationship for the connection leads to a relatively higher estimation of lateral load vs. story drift response of the specimen. Although the general behavior of the specimen is presented with the connection model, the shear strength response of the connection could not be predicted as accurately as for the prior specimens.

An important property of the beam in the loading direction is its narrow shape with a beam depth to beam width ( $h_b/b_b$ ) ratio of 2.93. Since the number of specimens with high  $h_b/b_b$  ratios is limited, the effect of this parameter could not be considered in the joint shear strength prediction model. The effect of the inadequate confinement provided by the narrow beams on the response of beam-to-column connections is one of the areas that need further experimental and analytical research.

### **5.4.3 Specimens of Kurose et al.**

In the experimental research program carried out by Kurose et al. [41], three reinforced concrete beam-to-column connections with floor slabs were tested under bidirectional reversed cyclic loading. The main parameters investigated were the presence of transverse beam and variation of slab reinforcement. From the 5 analyses performed, 1 is for exterior beam-to-column connections, whereas the rest are for interior connections.

In the comparison of analytical and experimental shear strength vs. shear strain data of Specimens of Kurose, it should be noted that the experimental shear response data provided was highly pinched and irregular. Accordingly, the main point considered in the evaluation of analytical joint shear response is the accuracy of general behavior of the connection, rather than the descending portion of the response

curves. Some of the experimental shear stress vs. shear strain data is presented in **Section 5.4.5**.

### Specimen J1

Specimen J1 is the only specimen of the test series which does not include a transverse beam in the direction orthogonal to the loading direction. The comparison of experimental and analytical results is given in **Figure 5.20**.

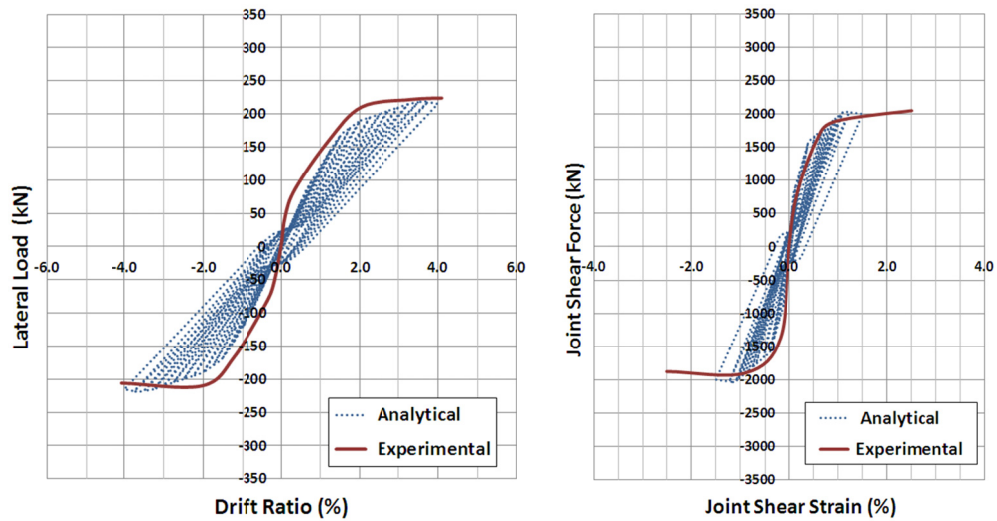


**Figure 5.20: Kurose et al., Specimen J1**

The joint shear strength vs. shear strain response of Specimen J1 obtained from analytical model possesses considerable accuracy when compared to the experimental results. However joint shear strain levels are predicted to be lower than experimental values for high drift levels. Generally, reinforced concrete frame structures are designed for 2 % story drift, so the prediction of shear strains at this drift level is the major concern of this study, which was satisfactorily performed as described in **Section 5.4.5**. Both the initial stiffness and strength of the connection shear response for positive and negative directions conforms to the experimental curve, resulting in an adequate lateral load vs. story drift response prediction.

### Specimen J2, East-West Direction

The second specimen of this experimental study included both floor slab and transverse beam in the direction orthogonal to the loading. Analytical and experimental results of the analyses are presented in **Figure 5.21**.

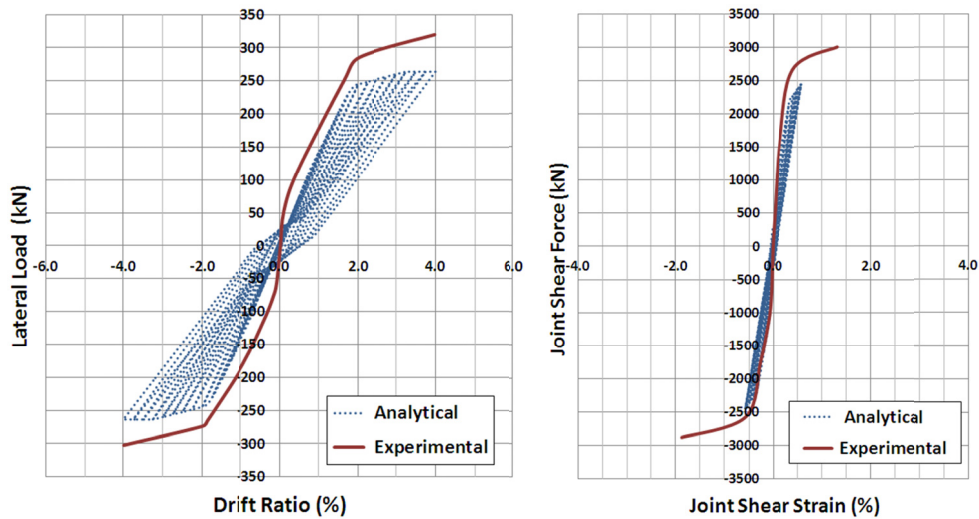


**Figure 5.21: Kurose et al., Specimen J2, E-W Direction**

The first point to underline in the graphs presented in **Figure 5.21** is the lower stiffness of the analytical lateral load vs. story drift response when compared to the stiffness accurately predicted for the joint shear strength vs. strain graph. Under these circumstances, the reduced stiffness and strength of the lateral load vs. story drift response of the beam-to-column connection specimen indicates the inaccuracy of the stiffness of the beam modeled. In addition, the inconsistency of analytical beam response results in the beam-to-column connection not being able to reach its capacity, as can be seen in the joint shear force vs. shear strain response.

### Specimen J2, North-South Direction

In the third analysis, Specimen J2 was loaded in the direction orthogonal to the prior loading direction. A comparison of the analytical and experimental results is presented in **Figure 5.22**.

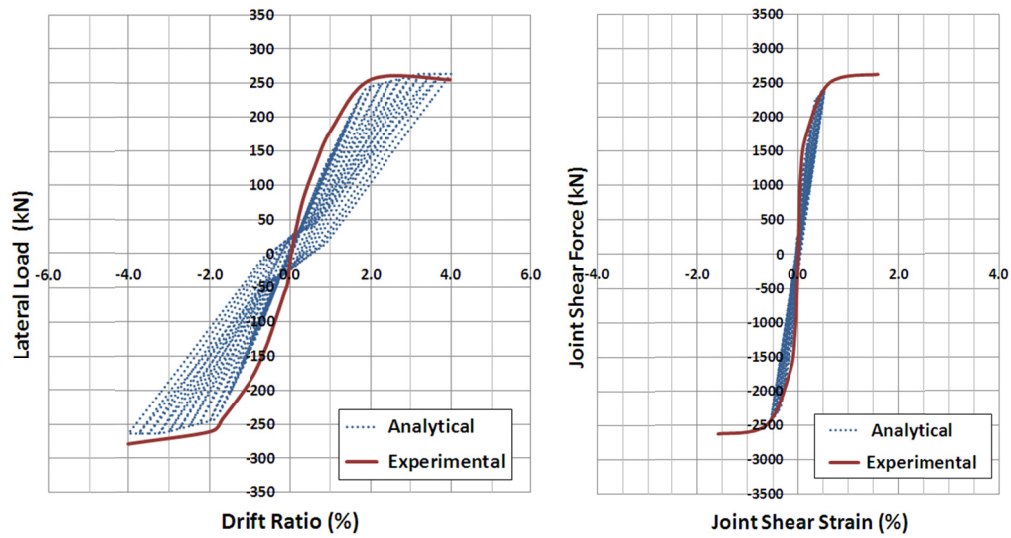


**Figure 5.22: Kurose et al., Specimen J2, N-S Direction**

Analytical results of the north-south direction loading of the Specimen J2 matches with the experimental results with adequate accuracy. As the stiffness and strength of the joint shear strength vs. strain response of the analytical model follows the experimental curve, the lateral load vs. story drift ratio behavior of the beam-to-column connection model represents the actual behavior closely.

### Specimen J3, East-West Direction

Specimen J3 loaded in the east-west direction was the only exterior connection tested in the experimental study. The specimen differs from Specimens J1 and J2 since the three beams are framing into the connection.

The analytical response of Specimen J3 when loaded in east-west direction is presented in **Figure 5.23**.

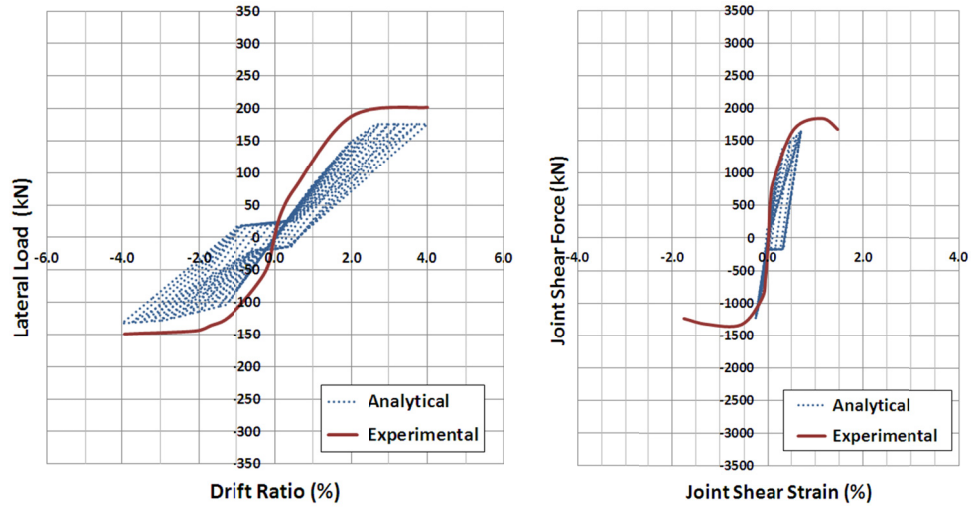


**Figure 5.23: Kurose et al., Specimen J3, E-W Direction**

Although the initial stiffness of the beam-to-column connection of Specimen J3 is represented accurately, the low stiffness and strength of beam members prevented the joint to reach its shear capacity, similar to the east-west loading of Specimen J2. Since the beam-to-column connection of the model could not attain its capacity, the lateral load vs. story drift response of Specimen J3 is predicted below its actual strength, despite following a similar path with the experimental curve.

Specimen J3, North-South Direction

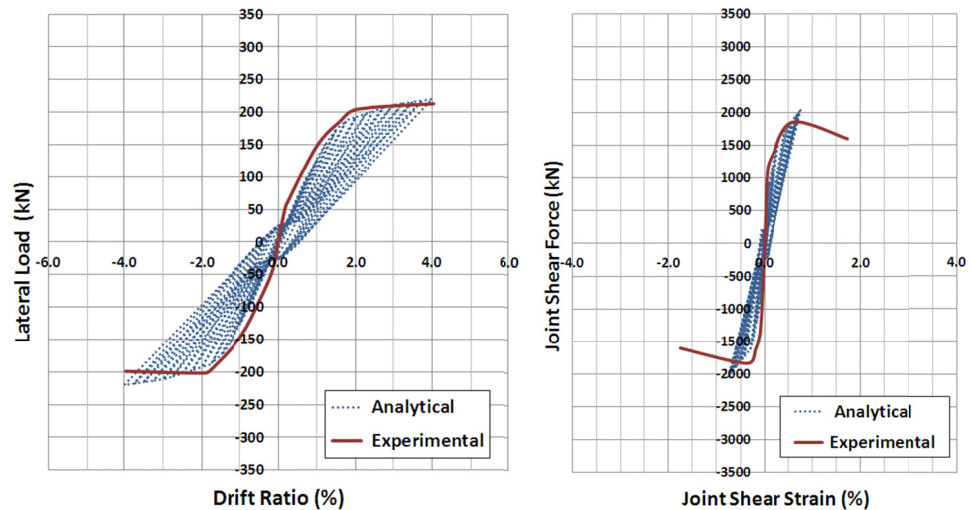


**Figure 5.24: Kurose et al., Specimen J3, N-S Direction**

The last analysis of this test series is performed in the north-south direction, using Specimen J3. As can be observed in **Figure 5.24**, the initial stiffness prediction of the beam-to-column connection is performed with considerable accuracy, although the shear capacity of the joint is slightly overestimated.

The accuracy of the model in representing the general behavior of the subassembly can be identified from the lateral load vs. story drift graph, with the only deviation of analytical response from experimental curve after concentration of inelastic activity, in relation with the overestimation of the joint shear strength.

#### 5.4.4 Specimens of Chen and Chen

In their experimental research on beam-to-column connections, Chen and Chen [42] tested 6 full scale specimens, mainly investigating the effect of eccentricity on the response of connections. One of the specimens (JC) was concentric, another one (JE) was eccentric, remaining 4 (JS1-JS4) were tested in order to evaluate the influence of spread ended beams on eccentric beam-to-column connections. None of the specimens included transverse beams or floor slab. Unfortunately, only the results of JC, JE, JS1 and JS4 were discussed in the final report of the research project and are available for comparison.

The spread end connection detail of JS series specimens is provided in **Figure 5.25**.

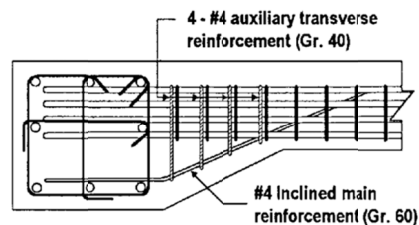


**Figure 5.25: Connection Detail of Spread Ended Beams, Chen and Chen [11]**

The joint response comparison of analytical and experimental results are presented on joint moment vs. joint shear strain curves, different from the previous specimens, to be compatible with the data presented in experimental research report.

### Specimen JC

As stated above, JC was the only concentric specimen in the test series. Comparison of the analytical and experimental results is presented in **Figure 5.26**. It should be noted that the shear response of the connection was presented as joint moment vs. joint strain hysteresis curve instead of joint shear strength vs. strain relationship. Therefore, in this report the joint shear response comparisons for all the specimens of Chen and Chen is presented as joint moment vs. joint strain relationships.

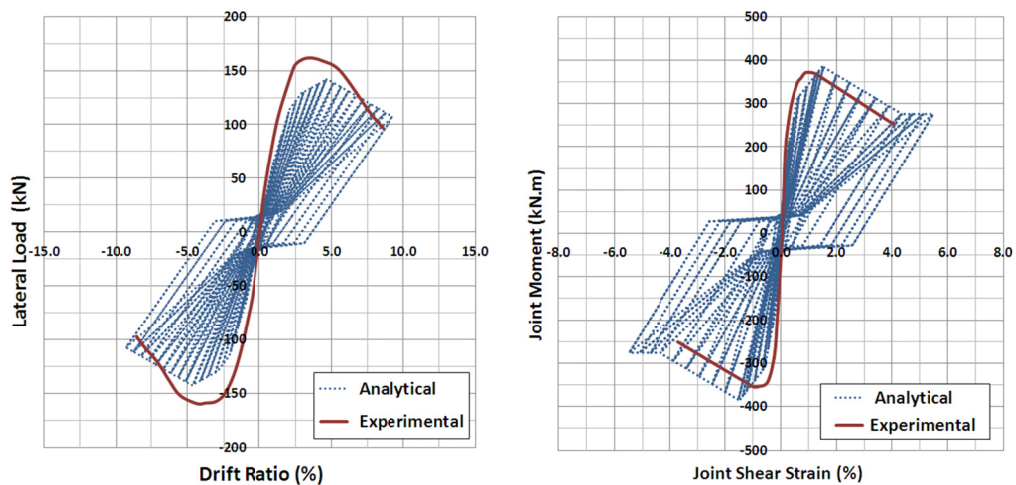


**Figure 5.26: Chen and Chen, Specimen JC**

On the positive direction of the joint moment vs. joint shear strain response, the maximum strength of the analytical model matches the strength of experimental value, which is one of the primary goals of this analytical study, however, the lower stiffness of the connection model leads to a shift in the moment response.

The lateral load vs. story shear prediction of the model is conservative from the point of maximum strength, while the general response of the subassembly is followed closely.

### Specimen JE

Specimen JE had an eccentricity of 100 mm, corresponding to 20% of the column width. It was the only specimen with eccentricity, but without spread ended beams.

Experimental and analytical results are compared with respect to lateral load vs. story drift and joint moment vs. joint shear strain relationships in **Figure 5.27**.

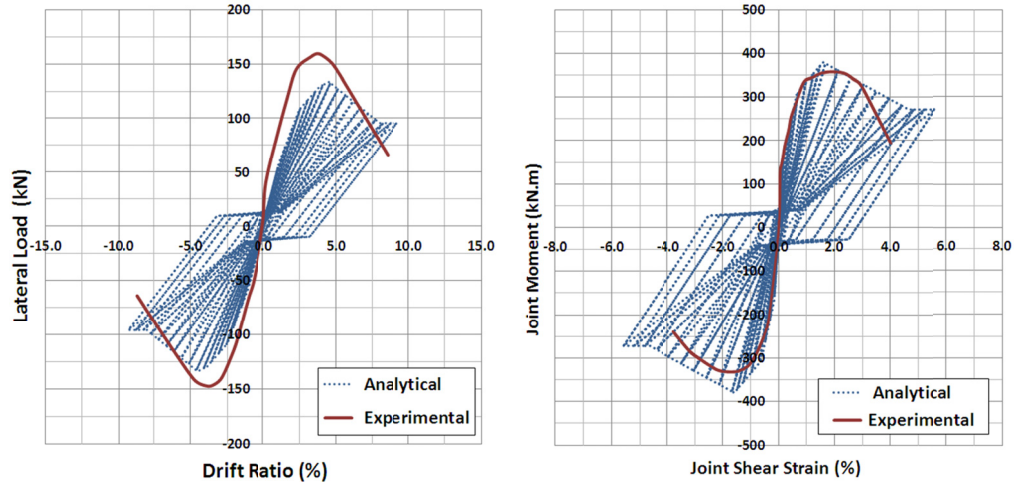


**Figure 5.27: Chen and Chen, Specimen JE**

As can be realized from **Figure 5.27**, the analytical model of Specimen JE adequately represents the joint response under imposed loading. The initial stiffness of the joint moment curve, the peak point and the points of stiffness change are closely predicted. Also the lateral load vs. story drift of the subassembly follows the same trend with experimental results.

### Specimen JS1

The geometric and material properties of Specimen JS1 were the same with Specimen JE, except for the connection detail in between the beam in the loading direction and the connection region. Within a 400 mm long segment, the width of the beam is enlarged from 300 mm to 500 mm, in order to decrease the degrading effect of eccentricity. Although no additional parameter is specified for the spread ended beams framing into the connection, the accuracy of the model is also examined comparing the experimental and analytical results of Specimens JS1 and JS4, which is presented in **Figure 5.28**.

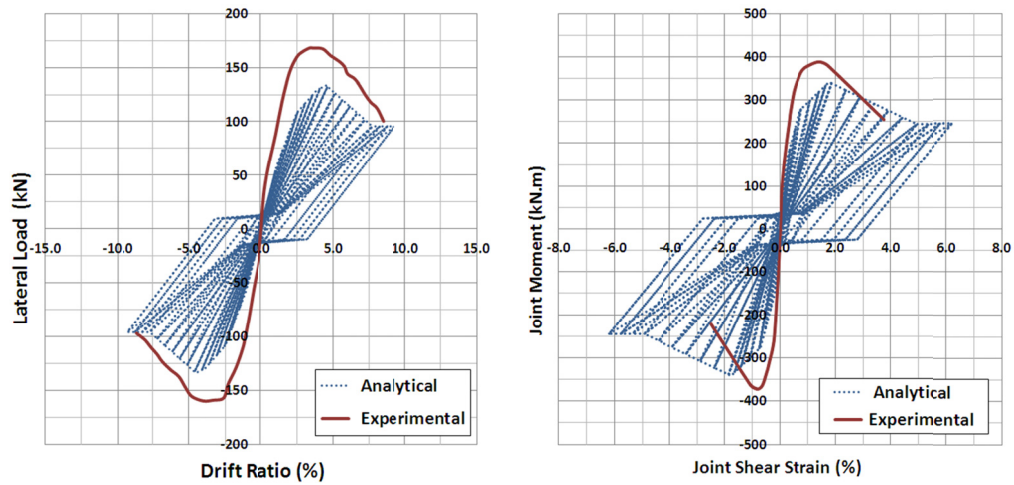


**Figure 5.28: Chen and Chen, Specimen JS1**

As expected, the accuracy of the joint model for Specimen JS1 is not as satisfactory as for the prior specimens of the test series. Both joint moment vs. joint shear strain and lateral load vs. story drift ratio response of the analytical model have lower stiffness and strength than the experimental setup with a spread ended beam.

#### Specimen JS4

Although Specimen JS4 had the same geometric dimensions and similar material properties, it was different from Specimen JS1 in terms of the orientation of longitudinal beam bars in the spread end region of the beam. The number of  $\phi 13$  (#4) bars located at the end region of JS4 was 8, whereas it was only 2 for JS1. The comparison of results is presented in **Figure 5.29**.

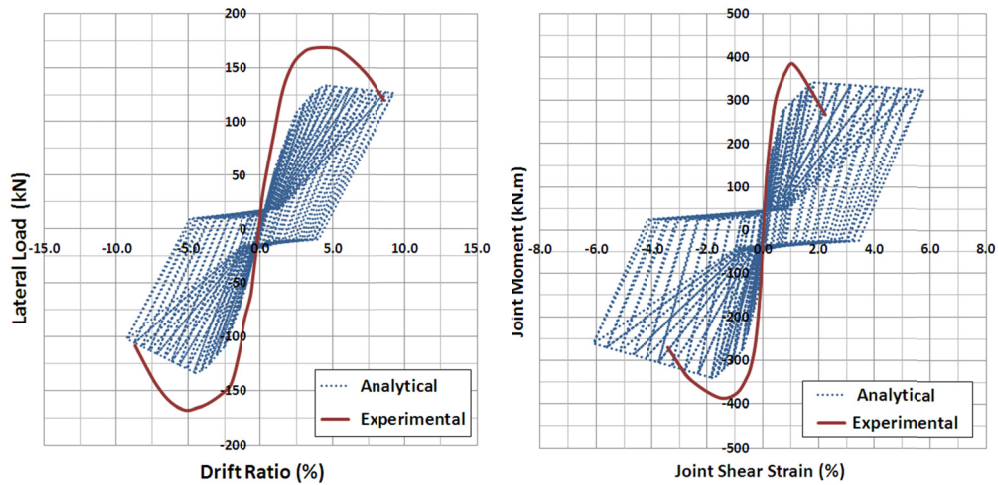


**Figure 5.29: Chen and Chen, Specimen JS4**

The experimental results of Specimen JS4 reveal that the inclusion of additional bars at the spread end section of beams increases the shear strength of beam-to-column connections. Additionally, the stiffness of the connection is preserved until high lateral load levels. The deviation of the analytical model from the experimental data, which was an expected result, indicates that in order to use the model for these types of connections, further investigation of specimens with spread ends is required.

#### 5.4.5 Evaluation of Pinching Response

One of the main reasons for this study to be carried out using OpenSees is the availability of a 4 point hysteretic material, capable of representing the pinching characteristics of the cyclic response. In this section, the accuracy of the analytical model in representing the pinched behavior of beam-to-column connections is evaluated.

In **Figures 5.30**, the joint moment vs. joint strain response of the first and second specimens of Chen and Chen are compared with the analytically obtained curves. It can be concluded from these graphs that the highly pinched behavior is represented successfully by the joint model.

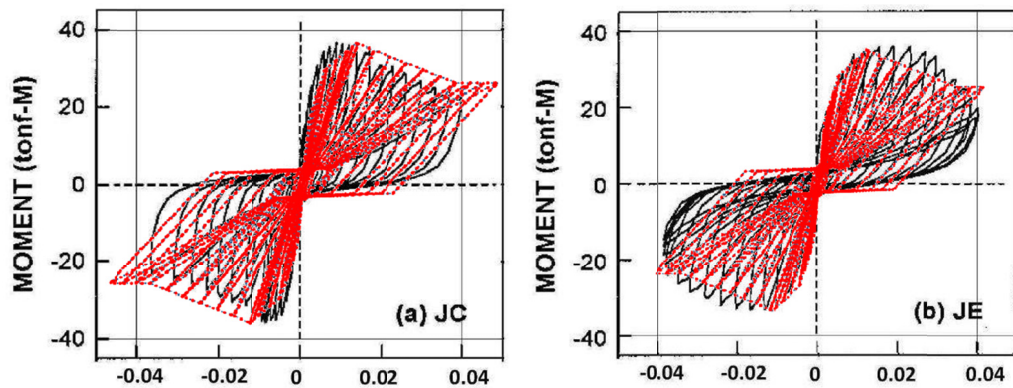


**Figure 5.30: Joint Response of Specimens JC and JE, Chen and Chen [42]**

In addition, the specimens of Raffaele and Wight [24] have highly pinched shear force vs. shear strain behavior. Although the response curves of the specimens in **Figure 5.31** are not as smooth as the ones for Chen and Chen [42], the pinching characteristics of these specimens are also represented with considerable accuracy. The reason for the difference in results is that the experimental data presented in **Figure 5.31** is measured on the flush (outer) face of the connection region. The inner face strains are lower and the joint model predicts the average behavior.

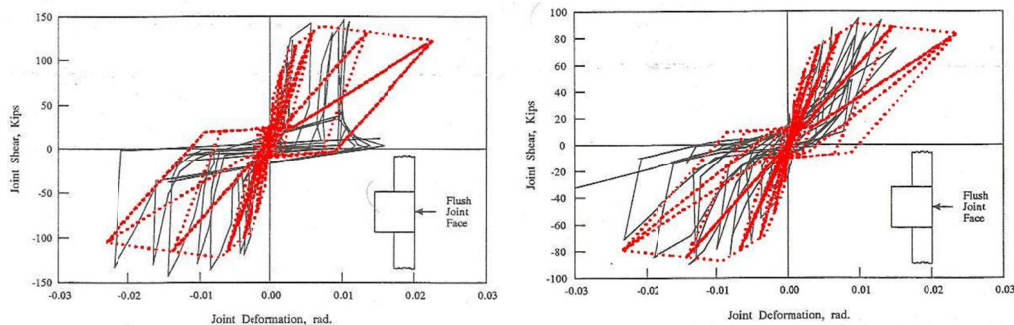


**Figure 5.31: Joint Response of Specimens 1 and 2, Raffaele and Wight [24]**

The most problematic pinching responses are observed in the analyses of specimens tested by Kurose et al. As the experimental response curves possess high irregularity, the resultant analytical shear force vs. shear strain responses failed to reach their experimental maximum drift ratios. The analytical and experimental joint shear

strength vs. strain response of Specimen J1 is compared in **Figure 5.32**. Although the response is representative for the earlier cycles, the analytical response fails to predict the high shear distortion values observed in the last two cycles.

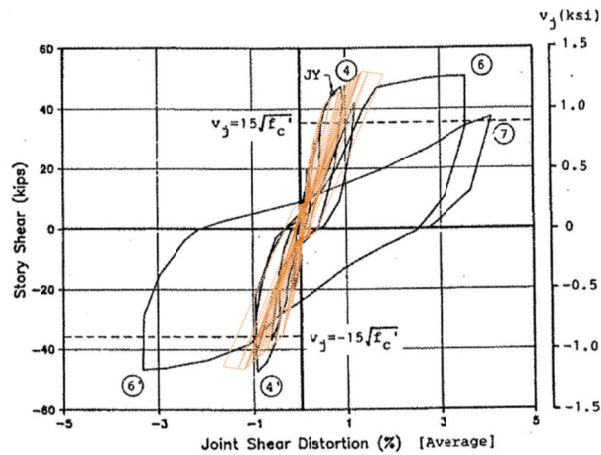


**Figure 5.32: Joint Response of Specimen J1, Kurose et al. [41]**

#### 5.4.6 Contribution of Joint Shear Strain to the Total Story Drift

In order to determine the effect of the joint shear distortions on the total behavior of the structure, its contribution to the story drift is computed. The contributions are calculated at 2 % story drift, which is the drift limit for reinforced concrete structures considered in many of the design codes (ACI 318-R08, TEC 2007). The maximum story drift is not utilized in the computations, because most of the specimens are tested up to different maximum story drift levels imposed in different experimental studies.

The contribution of the joint shear distortion to the total story drift is determined using the following equation:

$$\Delta_j = H\gamma\left(1 - \frac{h_b}{H} - \frac{h_c}{L_b}\right) \quad (5.14)$$

where, H = height of the specimen,

$\gamma$  = joint shear strain,

$h_b$  = beam height,

$h_c$  = column height,

$L_b$  = total beam length.

The contribution of the joint shear strain for the specimens of Burak and Wight [14], Raffaele and Wight [24] and Shin and LaFave [27] are computed using both the strain values determined experimentally and analytically. Determined story drift contributions are presented in **Table 5.1**.

**Table 5.1: Comparison of Story Drift Contributions at 2% Story Drift**

Researcher	Specimen	$\Delta_{j,pre.}$	$\Delta_{j,exp.}$	$\Delta_{j,pre.} / \Delta_{j,exp.}$	$\Delta_T$	% Error
		(mm)	(mm)	(%)	(mm)	
<i>B. Burak, J. K. Wight</i>	1-S	7.69	10.30	74.7	51.80	-25.30
	1-S	13.29	13.58	97.9	51.80	-2.10
	1-S	14.17	10.63	133.3	51.80	33.33
	2-N	3.86	10.70	36.1	51.80	-63.94
	3-N	6.90	6.16	112.1	51.80	12.11
<i>G. S. Raffaele, J. K. Wight</i>	1	12.93	7.92	163.1	44.72	63.15
	2	14.11	8.16	172.9	44.72	72.88
	3	12.14	12.03	100.9	44.72	0.89
	4	20.81	18.90	110.1	44.72	10.08
<i>M. Shin, J. La Fave</i>	SL1	16.04	23.39	68.6	58.94	-31.40
	SL2	14.07	20.38	69.1	58.94	-30.94
	SL3	12.74	8.18	155.8	58.94	55.76
	SL4	16.83	23.41	71.9	58.94	-28.08

where,  $\Delta_{j,pre}$  = Story drift contribution of predicted joint distortion,

$\Delta_{j,exp}$  = Story drift contribution of experimental joint distortion,

$$\% \text{ Error} = \frac{\Delta_{j,pre} - \Delta_{j,exp}}{\Delta_{j,exp}}$$

$\Delta_{j,pre} / \Delta_{j,exp}$  = Ratio of predicted story drift contribution to experimental story drift contribution.

### 5.4.7 Comparison of Response with and without the Connection Model

In this section, the specimen behavior when the analysis is carried out by utilizing the connection model and when connection regions are assumed to be rigid are compared. Experimental results are also presented in the comparison graphs to enable the evaluation of the accuracies of the two approaches.

In order to determine the response of specimens with rigid connection regions under the same loading conditions as the ones with the connection model, the loading histories obtained from the displacement controlled reversed cyclic loading analyses of subassemblies with inelastic beam-to-column connections are applied to subassemblies with rigid beam-to-column connections. Specimens of Burak and Wight [14], loaded in the spandrel beam direction, are utilized for comparison. The following graphs illustrate the lateral load vs. story drift responses of rigid connections and inelastic models as well as the experimental results.

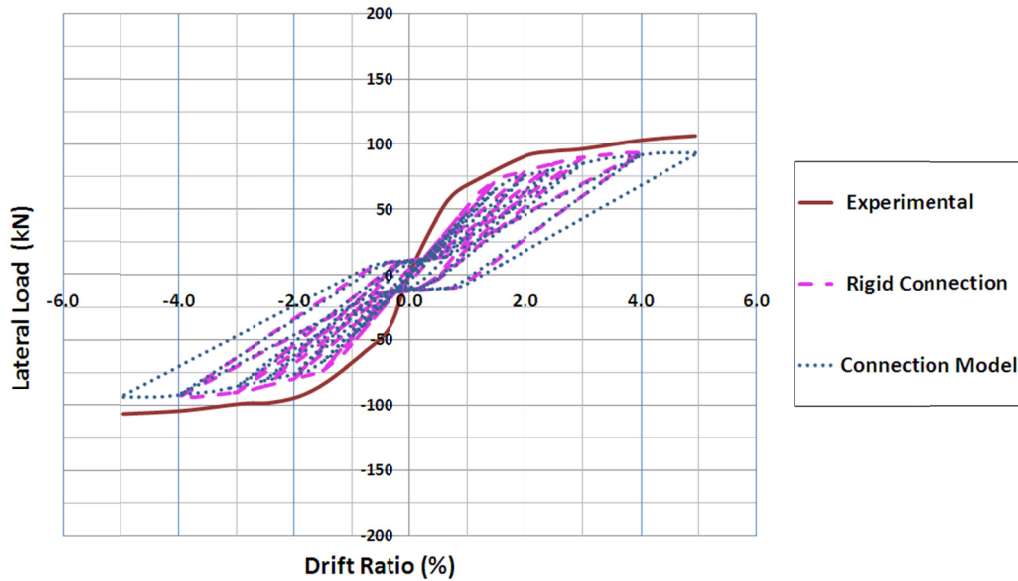
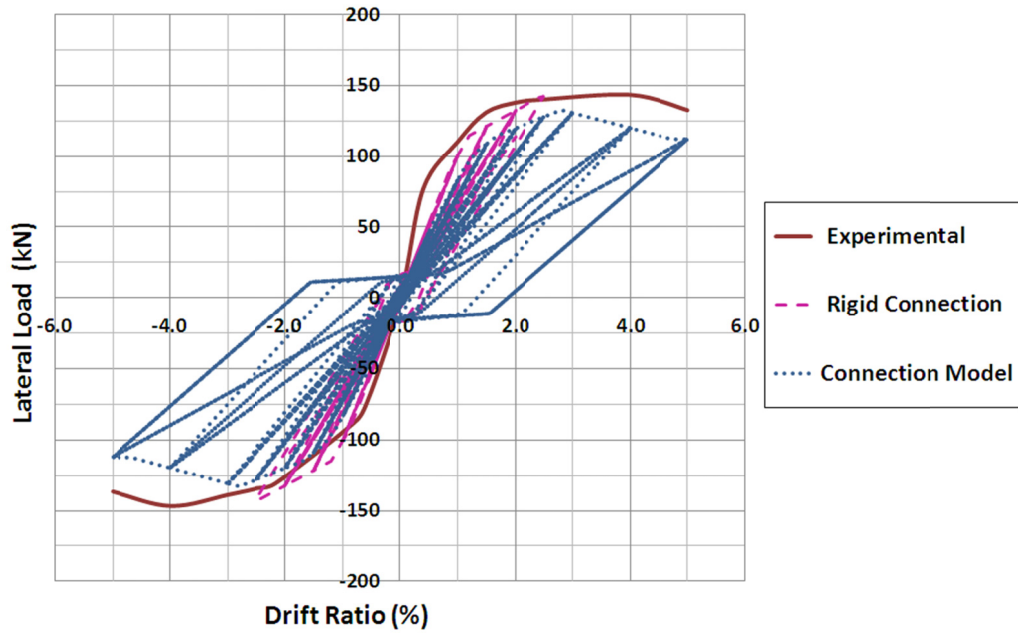
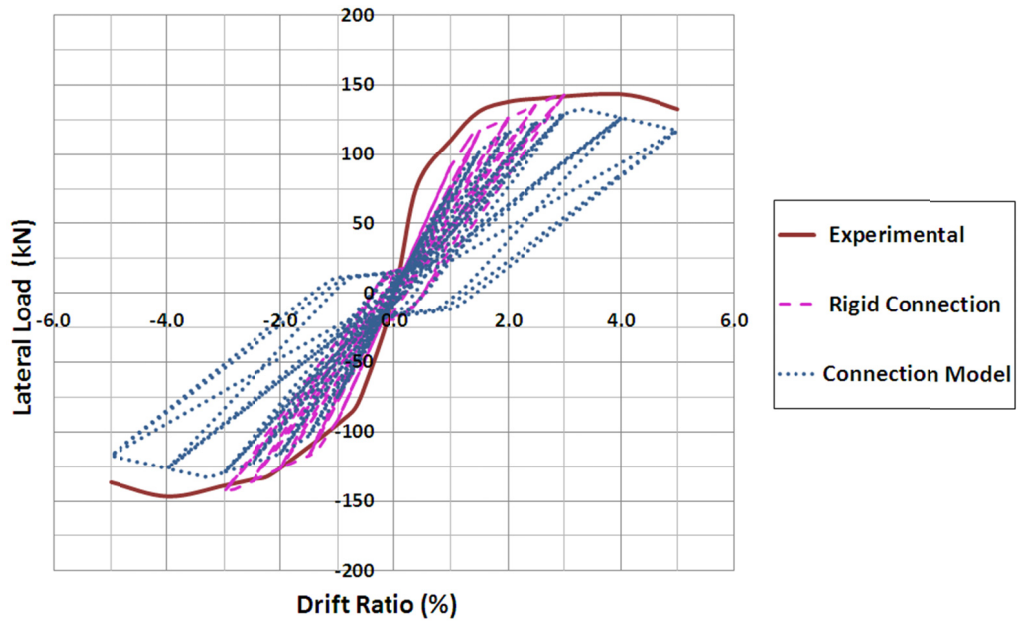


Figure 5.33: Rigid Connection vs. Connection Model, Burak and Wight, Sp. 1-S



**Figure 5.34: Rigid Connection vs. Connection Model, Burak and Wight, Sp. 2-S**



**Figure 5.35: Rigid Connection vs. Connection Model, Burak and Wight, Sp. 3-S**

As can be inferred from the graphs, the proposed connection model represents the joint response and consequently the structural behavior more precisely than the assumption of rigid connection regions.

For specimens with low joint shear strain values, as for the specimen 1-S, the rigid connection response results in a relatively close lateral load vs. story drift curve with the connection model. However, for specimens with high joint shear deformations, the assumption of rigid beam-to-column connections clearly leads to an extensive underestimation of total story drift. For both specimens 2-S and 3-S, the connection model represents the structural behavior much more accurately and realistically.

**Figures 5.33, 5.34 and 5.35** clearly indicate that the assumption of rigid connection regions leads to underestimation of story drifts and should not be used in design and analysis. The use of inelastic beam-to-column connection models results in more conservative story drift estimations and more accurate assessment of the load vs. deformation behavior for the whole structure and each member.

## CHAPTER 6

### SUMMARY AND CONCLUSIONS

#### 6.1 SUMMARY

The purpose of this thesis was to develop an analytical model that defines the shear response of beam-to-column connections subjected to cyclic loading. The proposed model is intended to be applicable for a wide variety of connections yet simple enough to be convenient for practical use.

Primarily, a comprehensive database of experimental research on beam-to-column connection specimens is generated, including different types of connections with a wide range of geometric and material properties. After the construction of the database, the properties of the selected specimens are evaluated in order to define a joint shear strength prediction procedure considering the key properties of beam-to-column connections.

The generation of the shear strength prediction model begins with a basic joint shear strength definition based on the imposed loads on the connections from the beams in the loading direction. The proposed basic joint shear strength of the connections is later improved by adjustment factors, which are specified with respect to the geometric and material properties of the connections. After evaluation of the influence of key parameters on the shear strength capacity of the connections in the light of prior experimental and analytical research, a detailed shear strength prediction model is developed which is applicable to a wide variety of connections.

The following step in construction of a response model for beam-to-column connections under reversed cyclic loading is the determination of basic shear strain and shear strength performance points. For that purpose, major performance points

for the shear response,  $P_{cr}$ ,  $P_{inel}$ ,  $P_{max}$  and  $P_{final}$  are specified using the experimental joint shear force vs. shear strain data. Since  $P_{inel}$  is the point that can be determined accurately among the four performance points, a prediction procedure, based on the basic joint shear strength is proposed to define  $P_{inel}$ . Shear force and shear strain values of the other performance points are determined relative to  $P_{inel}$  and the performance curves defining the shear force vs. shear strain relationship for exterior and interior beam-to-column connections are generated.

The verification of the proposed performance curves are carried out using OpenSees software. Beam-to-column connection element proposed by Alath and Kunnath [31] is used in the analytical verification process along with the hysteretic material *Pinching4* to define the previously generated shear force vs. shear strain relationships of the specimens. The results of the reversed cyclic loading analyses of beam-to-column connections are compared with experimental data in order to verify the analytical model.

## 6.2 CONCLUSIONS

As a result of this analytical study, the conclusions presented in the following paragraphs are drawn:

1. Since the contribution of a beam-to-column connection distortion on the story drift can be in the range of 40%, assuming the connections as elastic or rigid zones can lead to analytical story drifts much below the actual value, which may even result in the collapse of the structure.
2. In order to achieve a reliable structural behavior, the response of beam-to-column connections should be considered carefully in the analysis and design of reinforced concrete structures, especially for seismic design. The proposed beam-to-column connection performance models constitute a simple and accurate approach to estimate the joint behaviour under cyclic loading.
3. Although providing extensive information on the detailing of beam-to-column connections, the shear strength determination equations presented in

ACI 352R-02 may lead to an improper assessment of the joint shear capacity as a result of using predefined coefficients for certain connection types.

4. The basic equations presented in TEC2007 significantly overestimate the shear capacity of beam-to-column connections and therefore, they cannot be conservatively used in seismic design applications.
5. Shear strength capacity of beam-to-column connections are strongly related to the shear demand imposed by the beams in the loading direction.
6. Although the use of steel reinforcement with high yield strengths as longitudinal beam reinforcement increases the shear capacity of a beam-to-column connection, using bars with yield strength higher than 500 MPa does not improve the capacity further.
7. On the other hand, use of high strength transverse shear reinforcement delays the deterioration of confinement in the connection region, leading to higher joint shear force capacities.
8. Bond properties of the longitudinal beam reinforcement in the loading direction considerably affect the shear strength capacity of connections. The recommendations presented in ACI 352-R02 are adequate in specifying bond properties and minimizing bar slip.
9. Confinement provided by surrounding members and transverse shear reinforcement significantly affects the shear strain characteristics of connections under cyclic loading.
10. The proposed stiffness model in 'Update to ASCE/SEI 41 Concrete Provisions (2007)' estimates the cracked stiffness of the members in the elastic range with considerable accuracy.
11. In order for the Pinching4 material model defined in OpenSees to be more reliable, a procedure to determine the damage and pinching parameters for different geometric, material and loading conditions should be described.
12. Also for the Pinching4 material to be used more accurately in the prediction of the contribution of joint shear distortions to the total story drift, the problem of rapid strain increase for the descending portion of the shear strength vs. strain response should be resolved.

### **6.3 RECOMMENDATIONS FOR FUTURE RESEARCH**

Although the presented joint shear behavior model leads to satisfactory results for a wide variety of beam-to-column connections and presents a simple approach for the understanding of the joint behavior, some important subjects in need of further research should be underlined.

1. In order to reach more accurate results, especially for generating joint shear strain performance points, more experimental research should be conducted that measures the shear strain vs. shear stress response of connections.
2. Additionally, to provide a thorough understanding of the response of connections after maximum strength has been reached, the specimens should be tested to higher drift levels.
3. The confining effect of beams with varying beam depth to beam width ratios, both high and low, and spread end zones on connection behavior should be examined.
4. The effect of aspect ratio of columns with high column depth to column width ratios should be evaluated.

## REFERENCES

- [1] Hanson, N.W, Conner, H.W., 1967, “Seismic Resistance of Reinforced Concrete Beam-Column Joints”, Journal of the Structural Division, Proceedings of the American Society of Civil Engineers, p.533.
- [2] ACI Committee 318, 2008, “Building Code Requirements for Structural Concrete, 318-08”, American Concrete Institute, Farmington Hills, Michigan.
- [3] ACI-ASCE Committee 352, 2002, “Recommendations for Design of Beam-Column Connections in Monolithic Reinforced Concrete Structures”, American Concrete Institute, Farmington Hills, Michigan.
- [4] European Committee for Standardization, 2004, “Eurocode 8: Design of Structures for Earthquake Resistance - Part 1: General rules, Seismic Actions and Rules for Buildings, European Standard EN 1998-1”, Comité Européen de Normalisation, Bruxelles.
- [5] Ministry of Public Works and Settlement, 2007, “Turkish Earthquake Code: Specifications for the Buildings to be Constructed in Disaster Areas”, Ankara, Turkey.
- [6] Architectural Institute of Japan, 1999, “Design Guidelines for Earthquake Resistant Reinforced Concrete Buildings Based on Inelastic Displacement Concept”, AIJ.
- [7] Bonacci, J., and Pantazopoulou, S., 1993, “Parametric Investigation of Joint Mechanics”, Technical Paper, ACI Structural Journal, Title no. 90-S8, pp. 61-91.

- [8] Alameddine, F. and Ehsani, M. R., 1990, "Seismic Design Recommendations For High Strength Concrete Beam-to-Column Connections.", Ph.D. Thesis, The University of Arizona, Tucson.
- [9] Ehsani, M.R. and Wight, J.K., 1985, "Effect of Transverse Beams and Slab on Behavior of Reinforced Concrete Beam-to-Column Connections", Technical Paper, ACI Structural Journal, Title no. 82-17, pp. 188-195.
- [10] Durrani, A.J. and Zerbe, H.E., 1987, "Seismic Resistance of RC Exterior Connections with Floor Slab", ASCE Journal of Structural Engineering, Vol.113, No.8, pp. 1850-1864.
- [11] French, C.W. and Boroojerdi, A., 1989, "Contribution of RC Floor Slab in Resisting Lateral Loads", ASCE Journal of Structural Engineering, Vol.113, No.8, pp. 1850-1864.
- [12] Cheung, P.C., Paulay, T. and Park, R., 1991, "New Zealand Tests on Full-Scale Reinforced Concrete Beam-Column-Slab Subassemblages Designed for Earthquake Resistance", Design of Beam-Column Joints for Seismic Resistance-ACI SP123, pp. 1-37.
- [13] LaFave, J.M., and Wight, J.K., 1997, "Behavior of Reinforced Concrete Exterior Wide Beam-Column-Slab Connections Subjected to Lateral Earthquake Loading", Ph.D. Thesis, The University of Michigan, Ann Arbor.
- [14] Burak, B. 2005, "Seismic Behavior of Eccentric Reinforced Concrete Beam-Column-Slab Connections", Ph.D. Thesis, The University of Michigan, Ann Arbor.
- [15] Turkish Standards Institute, 2000, "TS-500, Requirements for Design and Construction of Reinforced Concrete Structures", Ankara, Turkey.

- [16] Quintero-Febres, C.G. and Wight, J.K., 1997, "Investigation on the Seismic Behavior of RC Interior Wide-Beam Connections", Ph.D. Thesis, The University of Michigan, Ann Arbor.
- [17] Leon, R.T., 1990, "Shear Strength and Hysteretic Behavior of Interior Beam-Column Joints", Technical Paper, ACI Structural Journal, Title no. 87-S1, pp. 3-11.
- [18] Durrani, A.J. and Wight, J.K., 1982, "Experimental and Analytical Study of Internal Beam to Column Connections Subjected to Reversed Cyclic Loading", Ph.D. Thesis, The University of Michigan, Ann Arbor.
- [19] Paulay, T., 1986, "A Critique of the Special Provisions for Seismic Design of the Building Code Requirements for Reinforced Concrete (ACI 318-83)", Technical Paper, ACI Structural Journal, Title no. 83-29, pp. 274-283.
- [20] Kaku, T. and Asakusa, H., 1991, "Bond and Anchorage of Bars in Reinforced Concrete Beam-Column Joints", Design of Beam-Column Joints for Seismic Resistance – ACI SP-123, pp. 401-424.
- [21] Meinheit, D. F. and Jirsa, J. O., "Shear Strength of Reinforced Concrete Beam-Column Connections", Journal of the Structural Division, Vol.107, No.11, pp. 2227-2244.
- [22] Fujii, S. and Morita, S., 1991, "Comparison between Interior and Exterior RC Beam-Column Joint Behavior", Design of Beam-Column Joints for Seismic Resistance-ACI SP-123, pp. 145-165.
- [23] Li, B, and Kulkarni, A.S., 2010, "Seismic Behavior of Reinforced Concrete Exterior Wide Beam-Column Joints", ASCE Journal of Structural Engineering, Vol.136, No.1, pp. 26-36.

- [24] Raffaele, G.S., and Wight, J.K., 1995, “Reinforced Concrete Eccentric Beam-Column Connections Subjected to Earthquake-Type Loading”, Ph.D. Thesis, The University of Michigan, Ann Arbor.
- [25] Kusahara, F., Azukawa, K., Shiohara, H., and Otani, S., 2004, “Tests of Reinforced Concrete Interior Beam-Column Joint Subassembly with Eccentric Beams”, 13th World Conference on Earthquake Engineering, Paper No. 185, August 1-6, Vancouver, B.C., Canada.
- [26] Goto, Y., Joh, O., 2004, “Shear Resistance of RC Interior Eccentric Beam to Column Joints”, 13th World Conference on Earthquake Engineering, Paper No. 649, August 1-6, Vancouver, B.C., Canada.
- [27] Shin, M. and LaFave, J., 2004, “Performance of Reinforced Concrete Edge Beam-Column-Slab Connections Subjected to Earthquake Loading”, Ph.D. Thesis, The University of Illinois, Urbana-Campaign.
- [28] Gentry, T.R. and Wight, J.K., 1992, “Reinforced Concrete Wide Beam-Column Connections under Earthquake-Type Loading”, Ph.D. Thesis, The University of Michigan, Ann Arbor.
- [29] Anderson, J.C. and Townsend, W.H., 1977, “Models for RC Frames with Degrading Stiffness”, Journal of Structural Division, Vol.103, No.12, pp. 2361-2376.
- [30] El-Metwally, S.E., and Chen, W.F., 1988, “Moment-Rotation Modeling of Reinforced Concrete Beam-Column Connections”, Technical Paper, ACI Structural Journal, Title no. 85-S36, pp. 384-394.

- [31] Alath, S. and Kunnath, S.K., 1995, "Modeling Inelastic Shear Deformation in Reinforced-Concrete Beam-Column Joints." Engineering Mechanics, Proceedings of 10th Conference. University of Colorado at Boulder, Boulder, Colorado, Vol. 2, pp. 822-825, May 21-24, American Society of Civil Engineers, New York,
- [32] Elmorsi, M., Kianoush, R.M. and Tso, W.K., 1998, "Nonlinear Analysis of Cyclically Loaded Reinforced Concrete Structures", Technical Paper, ACI Structural Journal, Title no. 95-S66, pp. 725-739.
- [33] Fleury, F., Reynouard, J.M., and Merabet, O., 2000, "Multicomponent Model of Reinforced Concrete Joints for Cyclic Loading", Journal of Engineering Mechanics, Vol.126, No. 8, pp. 804-811.
- [34] Lowes, L. and Altoontash, A., 2003, "Modeling Reinforced-Concrete Beam-Column Joints Subjected to Cyclic Loading", ASCE Journal of Structural Engineering, Vol.129, No.12, pp. 1686-1697.
- [35] Mitra, N. and Lowes, L.N., 2004, "Evaluation and Advancement of a Reinforced Concrete Beam-Column Joint Model", 13th World Conference on Earthquake Engineering, Paper No. 1001, August 1-6, Vancouver, B.C., Canada.
- [36] Shin, M., and LaFave, J.M., 2004, "Modeling of Cyclic Joint Shear Deformation Contributions in RC Beam-Column Connections to Overall Frame Behavior", Structural Engineering and Mechanics, Vol. 18, No. 5, pp.645-669.
- [37] Kim, J., LaFave, J.M., Song, J., 2007, "A New Statistical Approach for Joint Shear Strength Determination of RC Beam-Column Connections Subjected to Lateral Earthquake Loading", Structural Engineering and Mechanics, Vol.27, No.4, pp 439-456.

- [38] Burak., B., 2008, “Structural Applications of a Reinforced Concrete Beam-Column-Slab Connection Model For Earthquake Loading”, 14th World Conference on Earthquake Engineering, October 12-17, Beijing, China.
- [39] Unal, M. and Burak, B., 2010, “Analytical Modeling of Reinforced Concrete Beam-To-Column Connections”, M.Sc. Thesis, Middle East Technical University, Ankara.
- [40] Computers and Structures Inc. (CSI), 2006, “User Manual for PERFORM-3D v4.0”, Berkeley, California, USA, August 2006.
- [41] Kurose, Y., Guimaraes, G.N., Liu, Z., Kreger, M.E., and Jirsa, J.O, 1988, “Study of Reinforced Concrete Beam-Column Joints Under Uniaxial and Biaxial Loading”, PMFSEL Report, No. 88-2, The University of Texas, Austin.
- [42] Chen, C.C. and Chen, G., 1999, ”Cyclic Behavior of Reinforced Concrete Eccentric Beam-Column Corner Joints Connecting Spread-Ended Beams”, Technical Paper, ACI Structural Journal, Title no. 96-S50, pp. 443-450.
- [43] Teng, S., and Zhou, H., 2003, “Eccentric Reinforced Concrete Beam-Column Joints Subjected to Cyclic Loading”, Technical Paper, ACI Structural Journal, Title no. 100-S15, pp. 139-148.
- [44] Hwang, S.J., Lee H.J. and Wang K., 2004, “Seismic Detailing of Exterior Reinforced Concrete Beam-Column Joints”, 13th World Conference on Earthquake Engineering, Paper No. 397, August 1-6, Vancouver, B.C., Canada.
- [45] Wong, H.F., 2005, “Shear Strength and Seismic Performance of Non-Seismically Designed Reinforced Concrete Beam-Column Joints”, Ph.D. Thesis, The Hong Kong University of Science and Technology.

- [46] Shiohara, H. And Kusahara F., 2006, "Proposed Benchmark Problem for Blind Analysis: Tests for Validation of Mathematical Models on R/C Beam-Column Joints", Technical Paper, University of Tokyo, Department of Architecture.
- [47] Lee, H., and Ko, J., 2007, "Eccentric Reinforced Concrete Beam-Column Connections Subjected to Cyclic Loading in Principal Directions", Technical Paper, ACI Structural Journal, Title no. 104-S44, pp. 459-467.
- [48] Joh, O.; Goto, J. and Shibata, T., 1991, "Influence of Transverse Joint and Beam Reinforcement and Relocation of Plastic Hinge Region on Beam-Column Joint Stiffness Deterioration" Design of Beam-Column Joints for Seismic Resistance-ACI SP-123, pp. 187-223.
- [49] Manzoni, S., McKenna, F, Scott, M.H., Fenves, G.L., 2009, "Open System for Earthquake Engineering Simulation User Command-Language Manual", Pacific Earthquake Engineering Research Center University of California, Berkeley.
- [50] Bentz, E.C., Collins, M.P., 2000, "Response-2000, Reinforced Concrete Sectional Analysis using the Modified Compression Field Theory", University of Toronto
- [51] Bae, S., Bayrak, O., 2008, "A Plastic Hinge Length of Reinforced Concrete Columns", Technical Paper, ACI Structural Journal, Title no. 105-S28, pp. 290-300.
- [52] Stevens, N.J., Uzumeri, S.M., Collins, M.P., 1991, "Reinforced Concrete Subjected to Reversed Cyclic Shear-Experiments and Constitutive Model", Technical Paper, ACI Structural Journal, Title no. 88-16, pp. 135-147.

- [53] Çelik, O.C. and Ellingwood, B.R., “Modeling Beam-Column Joints in Fragility Assessment of Gravity Load Designed Reinforced Concrete Frames”, *Journal of Earthquake Engineering*, 12:3, pp. 357-381.

# APPENDICES

## APPENDIX A: SELECTED EXPERIMENTS

### A.1 TEST SETUP

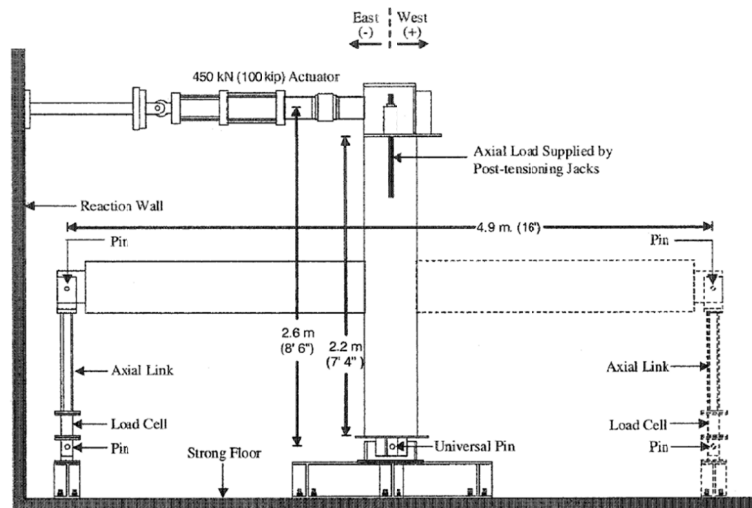


Figure A1.1: Test Setup of Burak and Wight

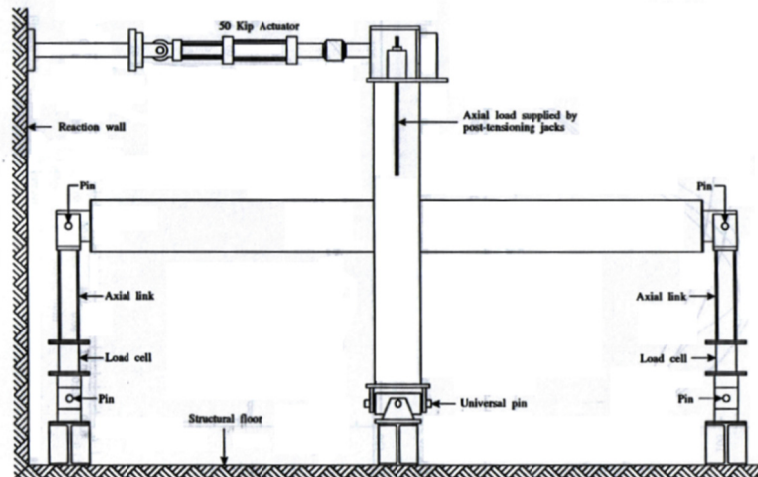


Figure A1.2: Test Setup of Raffaele and Wight

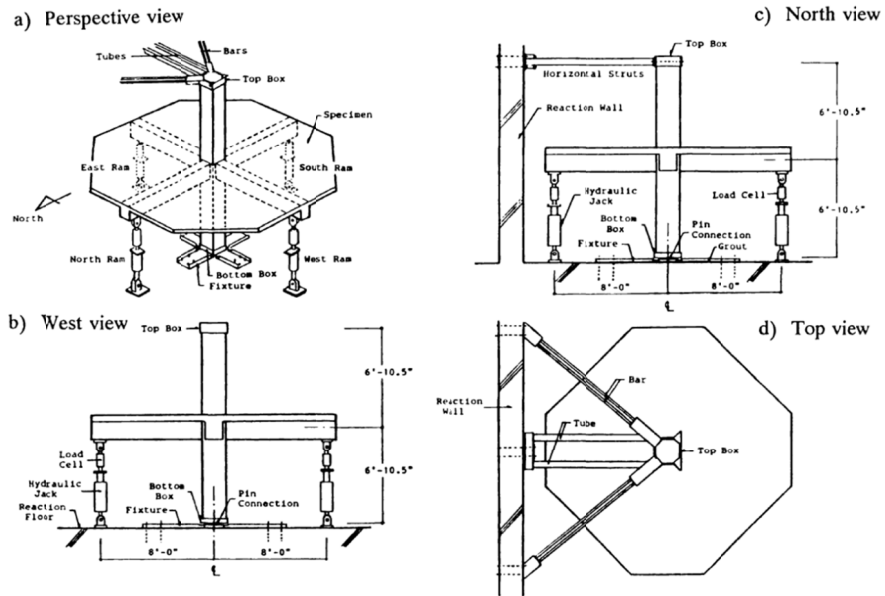


Figure A1.3: Test Setup of Kurose et al.

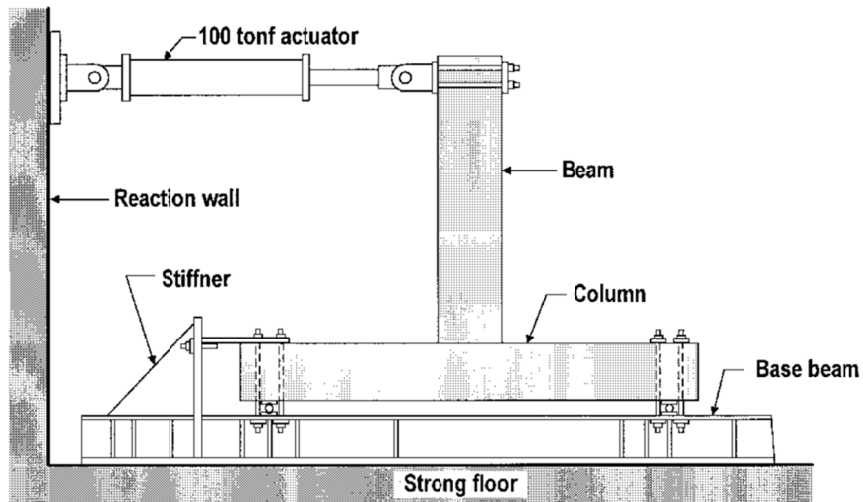


Figure A1.4: Test Setup of Chen and Chen

## A.2 IMPOSED DISPLACEMENT HISTORIES

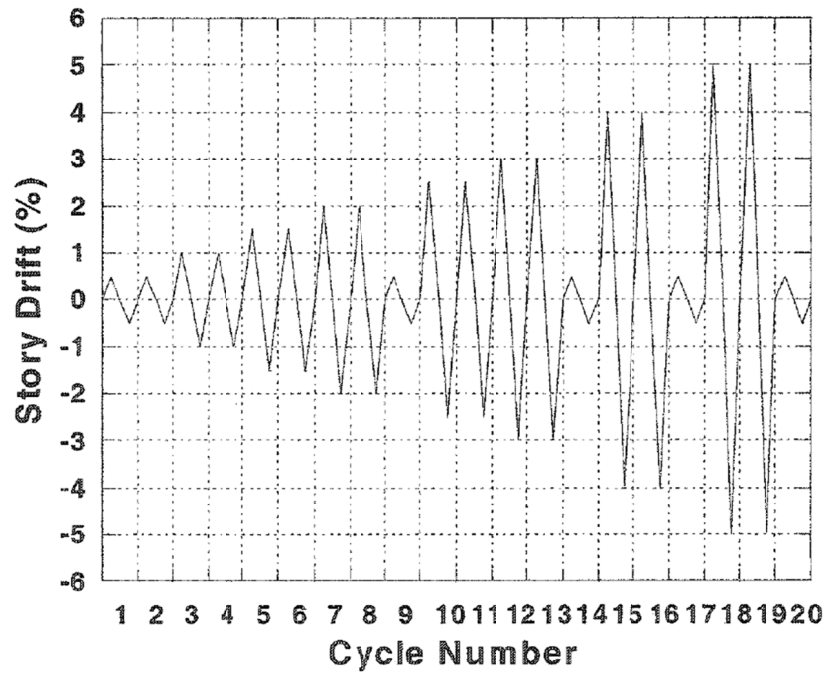


Figure A2.1: Displacement History of Burak and Wight

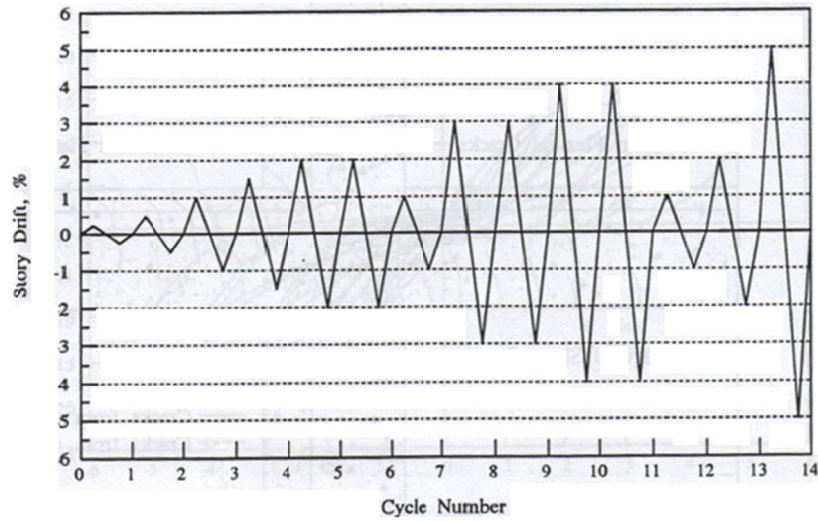


Figure A2.2: Displacement History of Raffaele and Wight

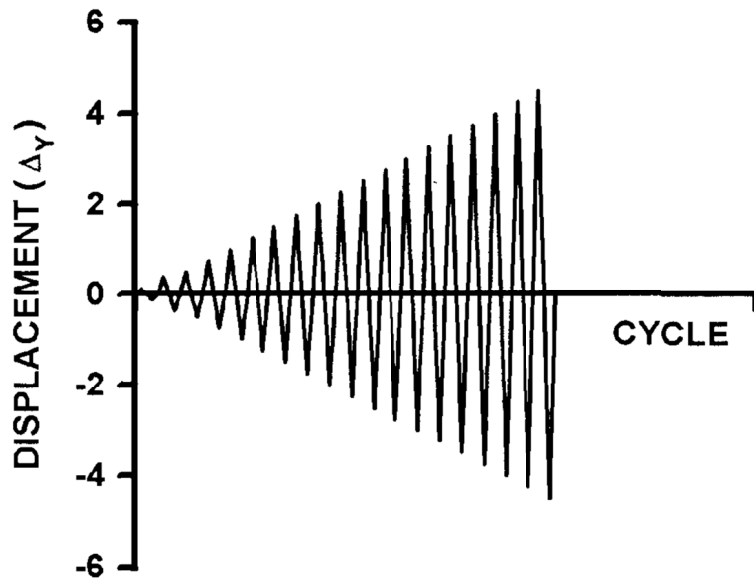
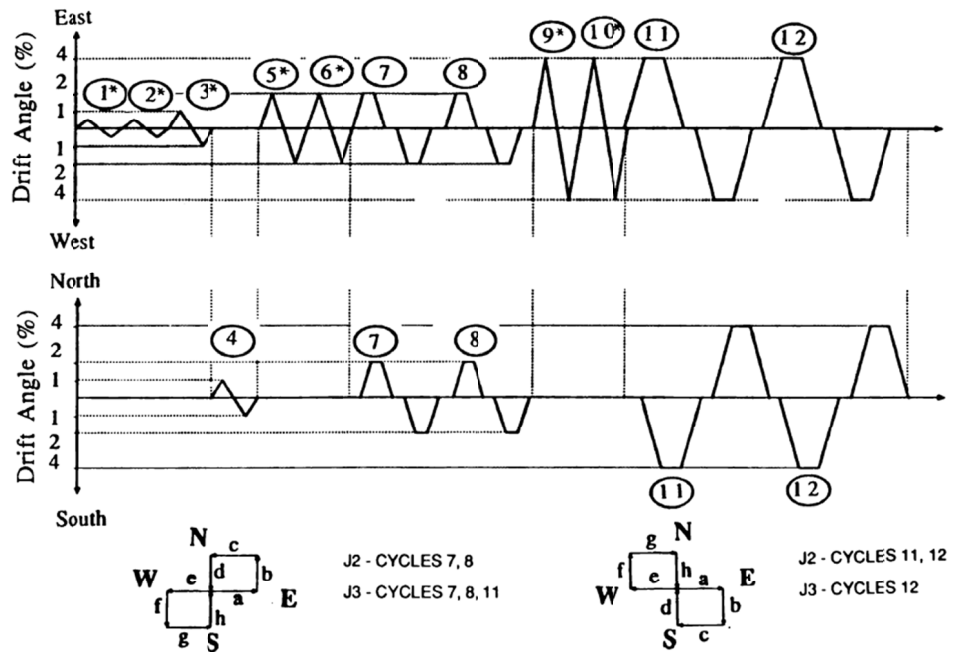


Figure A2.3: Displacement History of Chen and Chen

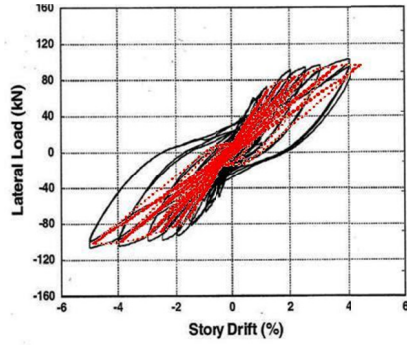


Note: For J1, only EW loading applied  
 \*Cycles for J1 are renumbered consecutively.

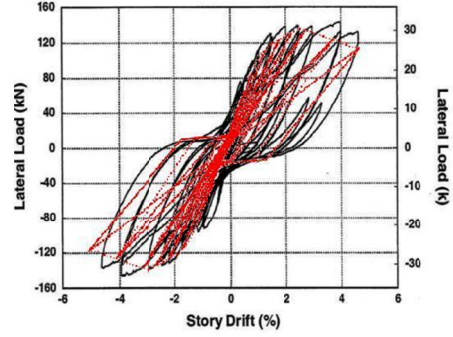
Figure A2.4: Displacement Histories of Kurose et al.

## APPENDIX B: COMPARISON OF GRAPHS

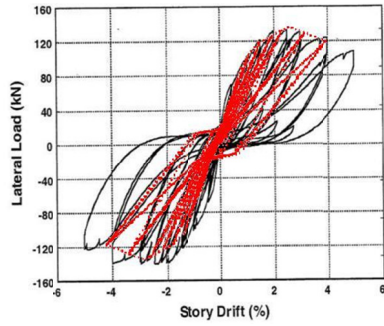
### B.1 LATERAL LOAD vs. STORY DRIFT (or DEFORMATION)



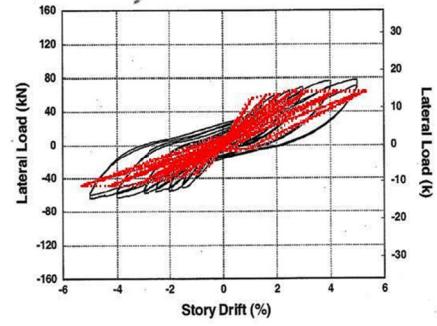
Specimen 1-S



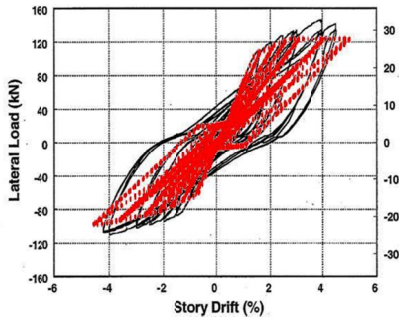
Specimen 2-S



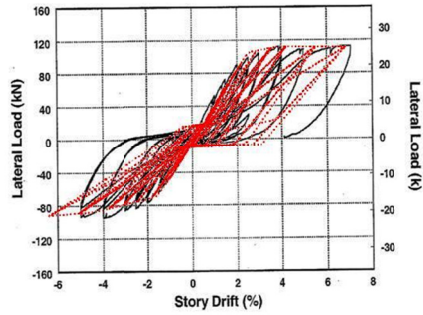
Specimen 3-S



Specimen 1-N

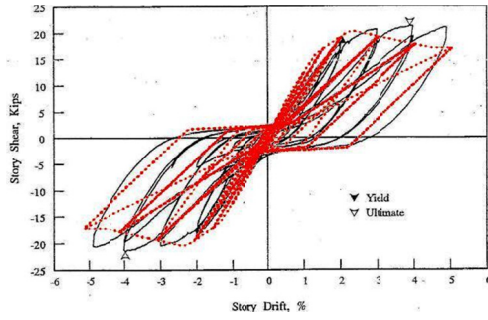


Specimen 2-N

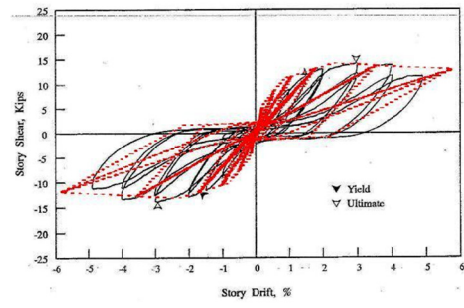


Specimen 3-N

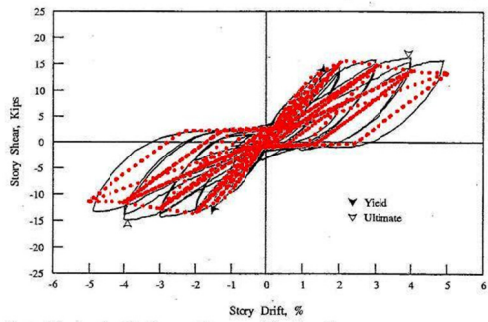
Figure B1.1: Specimens of Burak and Wight



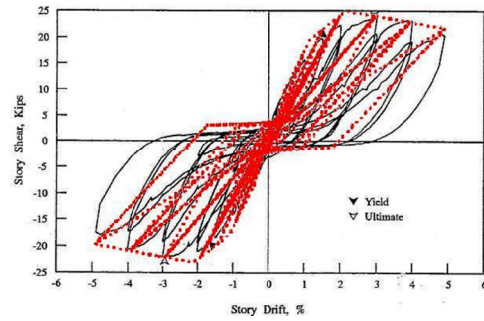
Specimen 1



Specimen 2

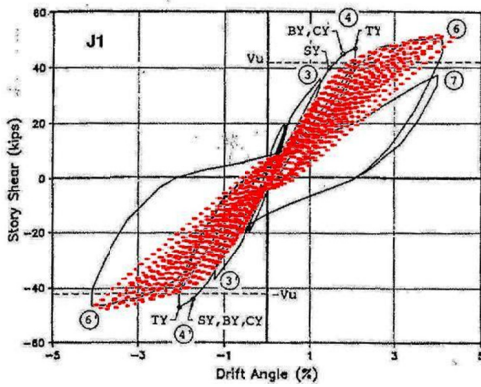


Specimen 3

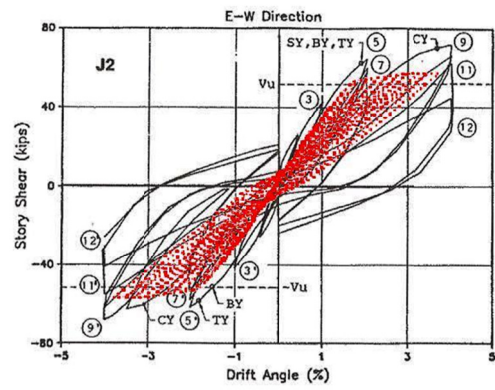


Specimen 4

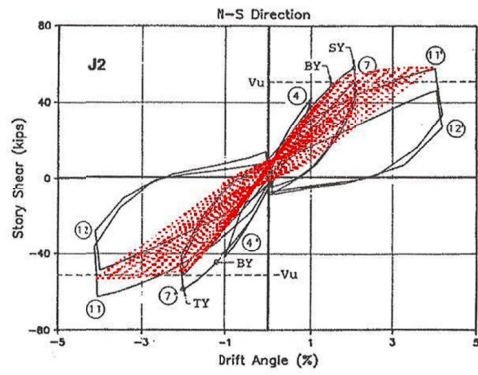
Figure B1.2: Specimens of Raffaele and Wight



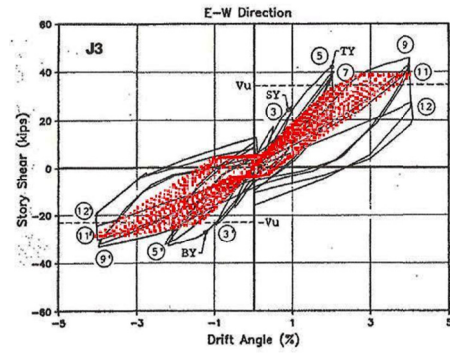
Specimen J1



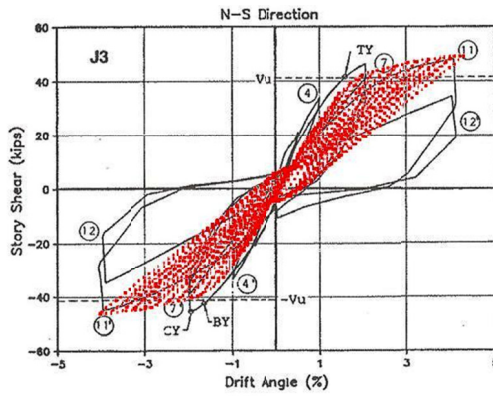
Specimen J2-EW



Specimen J2-NS

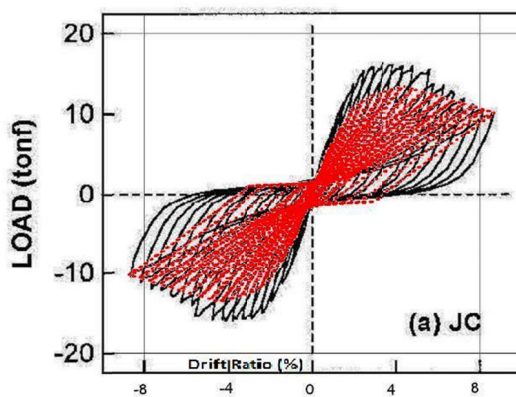


Specimen J3-EW

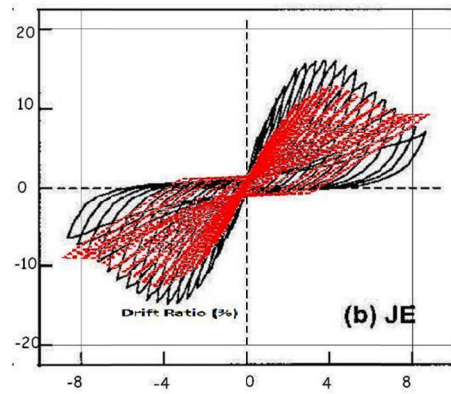


Specimen J3-NS

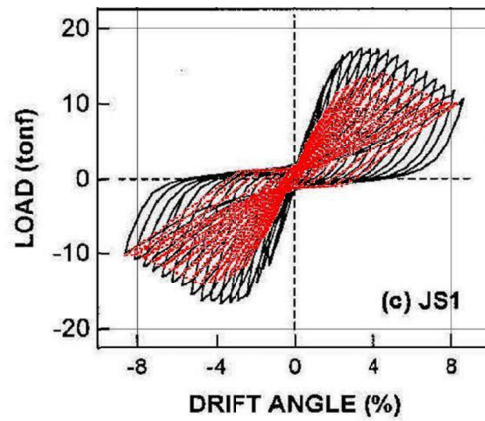
Figure B1.3: Specimens of Kurose et al.



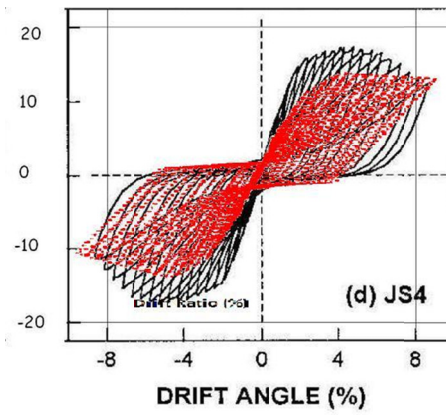
Specimen JC



Specimen JE



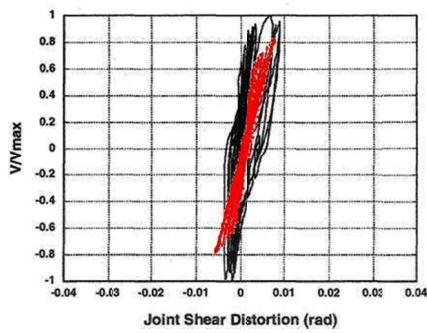
Specimen JS1



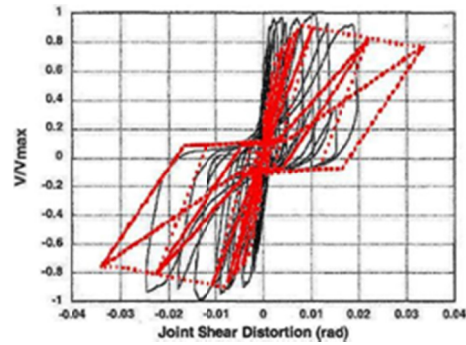
Specimen JS4

Figure B1.4: Specimens of Chen and Chen

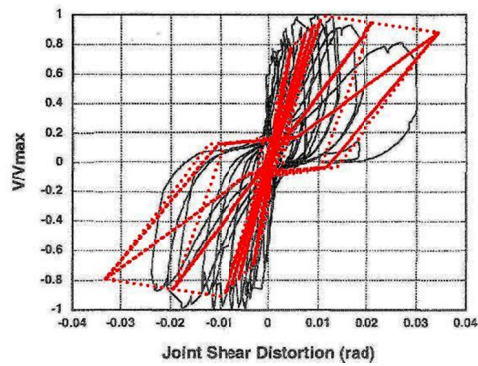
## B.2 JOINT SHEAR FORCE vs. JOINT DEFORMATION



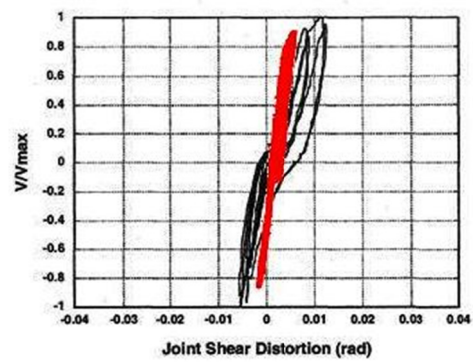
Specimen 1-S



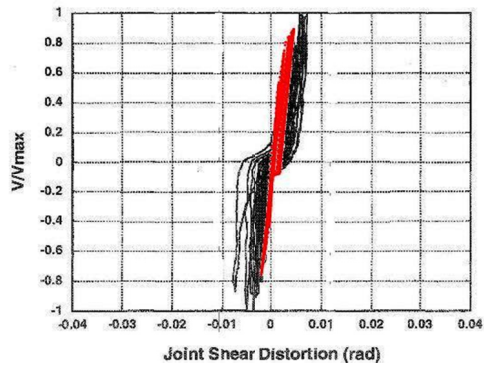
Specimen 2-S



Specimen 3-S

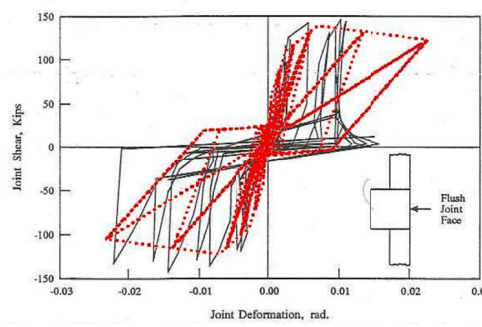


Specimen 2-N

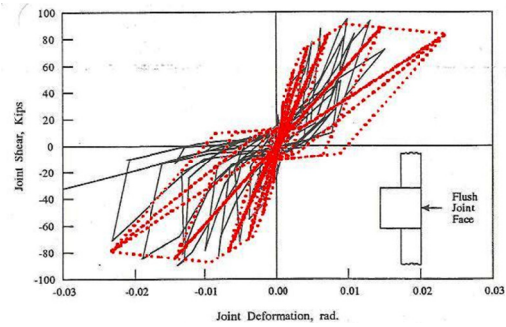


Specimen 3-N

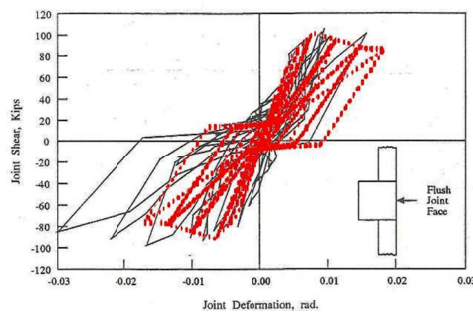
Figure B2.1: Specimens of Burak and Wight



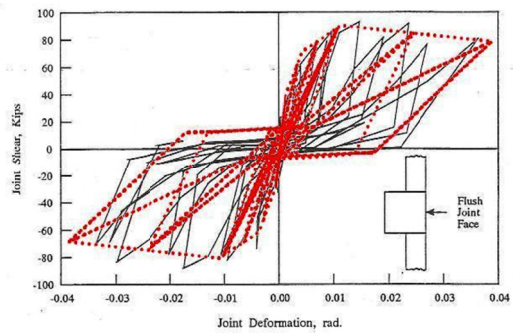
Specimen 1



Specimen 2



Specimen 3



Specimen 4

Figure B2.2: Specimens of Raffaele and Wight